

**HIGH RESOLUTION LASER STUDIES OF PHOTOINDUCED  
CHANGES IN MOLECULAR CHARGE DISTRIBUTIONS  
USING THE STARK EFFECT**

by

**Justin William Young**

B. S., Chemistry, Stevenson University, 2006

Submitted to the Graduate Faculty of the Kenneth P.  
Dietrich School of Arts & Sciences in partial fulfillment  
of the requirements for the degree of  
Doctor of Philosophy

University of Pittsburgh

2011

UNIVERSITY OF PITTSBURGH  
DIETRICH SCHOOL OF ARTS & SCIENCES

This dissertation was presented

by

Justin William Young

It was defended on

December 1, 2011

and approved by

Dr. Renã A. S. Robinson, Assistant Professor,  
Department of Chemistry, University of Pittsburgh

Dr. Hrvoje Petek, Professor,  
Department of Physics & Astronomy, University of Pittsburgh

Dr. David H. Waldeck, Professor,  
Department of Chemistry, University of Pittsburgh

Dissertation Advisor:  
Dr. David W. Pratt, Professor,  
Department of Chemistry, University of Pittsburgh

Copyright © by Justin William Young

2011

**HIGH RESOLUTION LASER STUDIES OF PHOTOINDUCED  
CHANGES IN MOLECULAR CHARGE DISTRIBUTIONS  
USING THE STARK EFFECT**

Justin William Young, PhD

University of Pittsburgh, 2011

Electronic excitation can lead to numerous subtle and dramatic changes in molecular systems. Such photoinduced events have been incorporated into many biological systems through evolutionary means. However, despite this fact, many of the intricacies of photoinduced phenomena are not well understood. In part, this is because of the nature of electronically excited states, which generally exist for only nanoseconds, and typically return the system to its original state causing no permanent changes to the system.

This dissertation presents results concerning photoinduced phenomena observed with high resolution electronic spectroscopy. The high resolution results provide detailed structural information about isolated molecules and complexes in both the ground and excited electronic states. By also performing the experiment in the presence of an electric field (the Stark-effect), we can determine how the distribution of electronic charge changes upon photoexcitation. This proves to be a useful tool to detect phenomena such as charge transfer and electronic state mixing.

Themes and systems presented in this dissertation include excited state intramolecular proton transfer in 5-fluorosalicylic acid, solvent-induced charge transfer in 7-azaindole( $\text{H}_2\text{O}$ ),

electronic state mixing in 7-azaindole, and the role of torsional angles in the conjugation of N-phenylcarbazole and 2-phenylindole.

## TABLE OF CONTENTS

<b>PREFACE .....</b>	<b>XVII</b>
<b>1.0 INTRODUCTION.....</b>	<b>1</b>
<b>1.1 WORKS CITED .....</b>	<b>6</b>
<b>2.0 EXPLORING SINGLE AND DOUBLE PROTON TRANSFER PROCESSES IN THE GAS PHASE. A HIGH RESOLUTION ELECTRONIC SPECTROSCOPY STUDY OF 5-FLUOROSALICYLIC ACID .....</b>	<b>8</b>
<b>2.1 ABSTRACT .....</b>	<b>9</b>
<b>2.2 INTRODUCTION.....</b>	<b>9</b>
<b>2.3 EXPERIMENTAL.....</b>	<b>12</b>
<b>2.4 RESULTS.....</b>	<b>14</b>
<b>2.5 DISCUSSION.....</b>	<b>23</b>
<b>2.5.1 Identification of the carriers of the spectra.....</b>	<b>23</b>
<b>2.5.2 Dynamics in the FSA monomer.....</b>	<b>27</b>
<b>2.5.3 Dynamics in the FSA dimer.....</b>	<b>34</b>
<b>2.6 CONCLUSIONS .....</b>	<b>35</b>
<b>2.7 ACKNOWLEDGEMENTS .....</b>	<b>36</b>
<b>2.8 WORKS CITED .....</b>	<b>37</b>

<b>3.0</b>	<b>EXCITED STATE ELECTRON TRANSFER PRECEDES PROTON TRANSFER FOLLOWING IRRADIATION OF THE HYDROGEN-BONDED SINGLE WATER COMPLEX OF 7-AZAINDOLE WITH UV LIGHT.....</b>	<b>40</b>
3.1	ABSTRACT .....	41
3.2	INTRODUCTION .....	41
3.3	EXPERIMENTAL.....	44
3.4	RESULTS.....	46
3.5	DISCUSSION.....	55
3.5.1	Structure of 7AIW in the ground and excited electronic states .....	55
3.5.2	$S_1$ - $S_0$ ETM orientation in 7AI.....	59
3.5.3	Charge redistribution in 7AI on complex formation.....	62
3.6	SUMMARY .....	69
3.7	ACKNOWLEDGEMENTS.....	70
3.8	WORKS CITED .....	71
<b>4.0</b>	<b>EXCITED ELECTRONIC STATE MIXING IN 7-AZAINDOLE. QUANTITATIVE MEASUREMENTS USING THE STARK EFFECT .....</b>	<b>75</b>
4.1	ABSTRACT .....	76
4.2	INTRODUCTION .....	76
4.3	EXPERIMENTAL.....	78
4.4	RESULTS.....	79
4.5	DISCUSSION.....	85
4.6	SUMMARY .....	88
4.7	ACKNOWLEDGEMENTS.....	89

4.8	WORKS CITED .....	90
5.0	USING HIGH RESOLUTION ELECTRONIC SPECTROSCOPY TO PROBE THE EFFECTS OF RING TWIST ON CONJUGATION AND ELECTRON TRANSFER IN 2-PHENYLINDOLE AND N-PHENYLCARBAZOLE .....	92
5.1	ABSTRACT .....	93
5.2	INTRODUCTION .....	93
5.3	METHODS.....	94
5.4	RESULTS.....	97
5.5	DISCUSSION.....	104
5.5.1	Structures of PI and PC in the $S_1$ state .....	104
5.5.2	Effects of ring substitution.....	107
5.6	ACKNOWLEDGEMENTS .....	109
5.7	WORKS CITED .....	110
6.0	SUMMARY.....	112
	APPENDIX A.....	114
	APPENDIX B .....	119
	APPENDIX C .....	121



## LIST OF TABLES

Table 2-I. Experimentally measured inertial parameters of four bands that appear in the gas phase $S_1$ - $S_0$ fluorescence excitation spectrum of 5-fluorosalicylic acid (FSA).....	18
Table 2-II. Experimentally measured permanent electric dipole moments of FSA in its two electronic states.....	18
Table 2-III. Theoretical inertial parameters and permanent electric dipole moments of two rotamers of FSA and the symmetric dimer, (FSA) <sub>2</sub> , in their ground electronic states. <sup>a</sup> .....	25
Table 2-IV. Relative frequencies and intensities of the monomer transitions in the $S_1$ - $S_0$ fluorescence excitation spectrum of 5-fluorosalicylic acid.....	28
Table 2-V. Relative frequencies and intensities of the dimer transitions in the $S_1$ - $S_0$ fluorescence excitation spectrum of 5-fluorosalicylic acid. ....	29
Table 2-VI. Comparison of theoretical electric dipole moments (and O-O bond distances) of different possible excited state structures of FSA with experiment. ....	33
Table 3-I. Measured inertial parameters of 7-azaindole- $H_2O$ (7AIW) and 1-deutero-7-azaindole- $D_2O$ (7-AIW- $d_3$ ) in their $S_0$ and $S_1$ electronic states, compared to selected theoretical values....	49
Table 3-II. Absolute positions of $H_2O$ (approximated as a point mass) in the single water complex of 7-azaindole in its $S_0$ and $S_1$ electronic states.....	51

Table 3-III. Experimental and theoretical permanent electric dipole moments of 7-azaindole-H <sub>2</sub> O in its S <sub>0</sub> and S <sub>1</sub> electronic states. ....	54
Table 4-I. Experimental inertial parameters of the 7AI S <sub>1</sub> ← S <sub>0</sub> origin band and the +280 cm <sup>-1</sup> band. ....	81
Table 4-II. Measured and calculated permanent electric dipole moments of 7AI in its ground and excited electronic states. ....	84
Table 5-I. Inertial parameters of PI, carbazole and PC in their ground and excited electronic states. ....	100
Table 5-II. Permanent electric dipole moments of indole, PI, carbazole, and PC in their ground and electronically excited states. ....	103

## LIST OF FIGURES

Figure 2-1. $S_1$ - $S_0$ fluorescence excitation spectrum of 5-fluorosalicylic acid (FSA) viewing a.) total fluorescence (top) and b.) visible ( $> 480$ nm) fluorescence only (bottom). Arrows denote transitions recorded in the high resolution apparatus. As will be shown, the strong lines in b.) belong to a FSA dimer species. ....	15
Figure 2-2 High resolution $S_1$ - $S_0$ fluorescence excitation spectrum of the $29147\text{ cm}^{-1}$ band of FSA with a simulated spectrum underneath. ....	16
Figure 2-3. High resolution $S_1$ - $S_0$ fluorescence excitation spectrum of the $29402\text{ cm}^{-1}$ band of FSA with a simulated spectrum underneath. Note the significant increase in linewidth compared to Fig 2-2. ....	16
Figure 2-4. High resolution $S_1$ - $S_0$ fluorescence excitation spectrum of three bands of FSA at $29393\text{ cm}^{-1}$ . The lower panels show a small portion of the experimental spectrum (black), with two simulated spectra (blue), one with and one without a convoluted lineshape function. ....	19
Figure 2-5. High resolution $S_1$ - $S_0$ fluorescence excitation spectra of three bands of FSA at $29508\text{ cm}^{-1}$ . ....	19
Figure 2-6. High resolution $S_1$ - $S_0$ fluorescence excitation spectra of three bands of FSA at $29542\text{ cm}^{-1}$ . ....	20

Figure 2-7. Stark spectra of the 29393 cm<sup>-1</sup> band in FSA, at zero field (middle) and a 422 V/cm electric field (bottom). As before, the lower panels show a black experimental trace as well as blue simulated spectra with and without a lineshape function. ....22

Figure 3-1. Structure of 7-azaindole-H<sub>2</sub>O (7AIW). ....43

Figure 3-2. High resolution S<sub>1</sub>-S<sub>0</sub> fluorescence excitation spectrum of 7AIW in a molecular beam. Below is a close up view of the spectrum (black) with a simulated spectrum underneath (blue). ....47

Figure 3-3. Portion of the S<sub>1</sub>-S<sub>0</sub> fluorescence excitation spectrum of 7AIW, illustrating the axis tilting observed at full experimental resolution. The *a/b* character of the simulations in the bottom panels were normalized to the pure *a* and *b* transitions shown. The blue spectrum shows the result without including axis tilt, while the red spectrum includes an axis tilt of -8°. The star highlights a particularly affected transition. ....48

Figure 3-4. S<sub>1</sub>-S<sub>0</sub> fluorescence excitation spectrum of 7AIW-*d*<sub>3</sub>. The lower panel shows a close up view of the spectrum (black) with a simulated spectrum underneath (blue). ....51

Figure 3-5. Stark spectra of 7AIW. The bottom panel shows a detailed view of the spectra (black) and simulations (blue) at various electric fields. ....53

Figure 3-6. Position of the water molecule (when treated as a point mass of 18 amu) determined from a Kraitchman's analysis of the ground state rotational constants of 7AI and 7AIW. ....54

Figure 3-7. Potential energy for water motion. The points were calculated at the M05-2X/6-31+G\* level of theory. The red line shows a functional fit to the torsional terms, with V<sub>1</sub>=7592, V<sub>2</sub>=-5313, V<sub>3</sub>=2965, V<sub>4</sub>=-1341, V<sub>5</sub>=410, and V<sub>6</sub>=-72 cm<sup>-1</sup>. The blue curve is the real part of the ground state wavefunction along this coordinate. ....58

Figure 3-8. Possible S<sub>1</sub>-S<sub>0</sub> ETM alignments of 7AI (left) and 7AIW (right). ....60

Figure 3-9. The top panels show the experimentally measured EDMs, in the ground (left) and excited states (right). The bottom left panel shows the ground state EDM's of water (red), 7AI (blue) and their sum (orange),  $\mu_{7AI} + \langle \mu_{H_2O} \rangle$ . The bottom right panel shows the component EDMs of water (red) and 7AI\* (blue), as well as a difference dipole (green) between the measured EDM and the vector sum of its components. ....63

Figure 3-10. Calculated electrostatic interactions between ground and excited state 7AI and the water molecule at different values of the inversion angle  $\tau$ , left. On the right are shown functions that were fit to each of the calculated curves.....68

Figure 4-1. Rotationally resolved fluorescence excitation spectrum of the  $+280 \text{ cm}^{-1}$  band in the  $S_1-S_0$  electronic transition of 7-azaindole in a molecular beam. The upper panel shows an overview of the entire spectrum. The lower panel shows a portion of the spectrum at full resolution (black) with the simulated spectrum underneath, with and without a Voigt profile.....80

Figure 4-2. Stark-effect spectra of the  $+280 \text{ cm}^{-1}$  band in the  $S_1-S_0$  electronic transition of 7AI, measured at the designated electric field values. ....83

Figure 5-1. Jet-cooled fluorescence excitation spectrum of 2-phenylindole (PI). An arrow denotes the band recorded at high resolution. ....98

Figure 5-2. Rotationally resolved electronic spectrum of PI. The upper panel shows (from top to bottom) the frequency markers, the iodine spectrum, the experimental spectrum (black) and the simulated spectrum. ....99

Figure 5-3. Stark effect on the rotationally resolved spectra of carbazole, PC and PI, from left to right, showing both the experimental (black) and simulated (blue) spectra. The bottom panels show expanded views of portions of the spectra, in the absence and presence of an applied electric field. ....102

Figure 5-4. A plot showing the inertial defect of PI as a function of the torsional angle.. Data points were calculated using M05-2X/6-31+G\*. Tie lines indicated likely values of the vibrationally averaged value of the torsional angle in the S<sub>0</sub> and S<sub>1</sub> electronic states.....106

Figure 6-1. Permanent electric dipole moments of 7-azaindole in the ground state, S<sub>1</sub> origin and the +280 cm<sup>-1</sup> vibronic band. The ground state and S<sub>1</sub> dipole moment were taken from Ref 1..119

## LIST OF SCHEMES

Scheme 1-1 .....	4
Scheme 2-1 .....	23
Scheme 2-2 .....	26
Scheme 2-3 .....	31
Scheme 4-1 .....	85
Scheme 5-1 .....	107

## LIST OF EQUATIONS

Equation 1-1 .....	3
Equation 3-1 .....	56
Equation 3-2 .....	57
Equation 3-3 .....	57
Equation 3-4 .....	59
Equation 3-5 .....	65
Equation 3-6 .....	66
Equation 3-7 .....	66
Equation 3-8 .....	66
Equation 3-9 .....	67
Equation 3-10.....	67
Equation 4-1 .....	88
Equation 4-2 .....	88
Equation 5-1 .....	108



## PREFACE

Scientific research is surrounded with uncertainty. This nature of scientific research nurtures great rewards, as well as challenges and disappointments. During this time working on my dissertation I have certainly encountered all three events. However, I have made it through the challenges and obtained great rewards with the help of fantastic people to whom I owe thanks.

Foremost, I would like to thank my advisor Professor David W. Pratt. Dr. Pratt has been an excellent advisor through the years. To those that know him, perhaps it is clear that he is deeply interested and devoted to science. However, his goals in science are matched if not surpassed by his goal to see his students succeed and learn. The atmosphere in Dr. Pratt's laboratory was a learning atmosphere. I believe that it is his focus and desire to see his students succeed that has made Dr. Pratt's support, encouragement, and temperament unmatched during my time I spent in his laboratory.

The challenging reputation of the laser equipment has not deviated through its years of use. However, my introduction to the equipment was mentored by a number of colleagues, Dr. Leonardo Alvarez-Valtierra, Dr. John T. Yi, Dr. Diane Miller and Dr. Phillip J. Morgan, to whom I have to credit and thank. Particularly, I would like to acknowledge Dr. Morgan for his encouragement and help.

I have had successful collaborations with my colleagues including Dr. Ryan Bird, Casey Clements, M.S., and Dr. Jessica Thomas. I am thankful for their help, discussions and friendships through the years.

I have shared many of my most triumphant moments with Dr. Adam J. Fleisher. He has been a good companion through the years, and showed great devotion to helping and working with me even when projects required remaining in the laboratory overnight. I have enjoyed working with such a devoted young scientist, and fondly remember working with him. I will particularly enjoy memories of building and sharing our proud Mathcad “programs.”

The help I have received from the staff at the University of Pittsburgh also deserves many thanks. Fran Nagy has helped me through many bureaucratic requirements. I would also like to apologize to her for her favorite football team’s sorry performances thus far this year. Jim McNerny and Chuck Fleishaker have been integral for repairing and maintaining the laser equipment. Tom Gasmire and Jeff Sicher have helped build, modify and maintain equipment.

My family has given me much through the years. I can never fully express how much they have given me and how much I appreciate them. However, I must mention my mother, because her guidance and support to continue my education beyond high school, making all of this possible.

Lastly and perhaps most fittingly I need to recognize Vanesa Vaquero-Vara, the other last member of the Pratt lab. Her help and companionship have been invaluable especially during the hectic last push of my graduate career.

Cheers,

Justin

## 1.0 INTRODUCTION

Photoinduced events surround and affect us. The range of events spans from simple examples such as the warm atmosphere on Earth caused by photo-absorption leading to heat, to the photo-induced molecular changes occurring within the eye which allowed you to read this sentence. Because life evolved with the presence of the sun, there is an abundance of naturally occurring and interesting photoinduced molecular events. How nature has developed to use and cope with light inspires to deepen understanding of photo-absorption and dynamics.

Electronic excitations cause particularly intriguing changes to molecular systems. These excitations promote a molecular system to an electronically excited state where the system possesses an abundance of energy, and also has a different electronic distribution relative to its normal ground state or any other electronic state. Thus, it is expected that an electronically excited molecule may behave differently and have access to numerous relaxation and energetic pathways not accessible to a molecule while in its ground state. While electronic excitations may be responsible for photoinduced events such as charge transfer, tautomerization and energy transfer, unambiguously identifying such phenomena is challenging.

Many spectroscopic methods have been developed to study excited state phenomena. One route which has been developed and employed to study excited state phenomena is jet-cooled gas phase spectroscopy. These methods allow for molecular systems to be isolated and cooled, reducing environmental perturbations and spectral congestion. This type of sample

preparation has been implemented in both vibrationally and time-resolved fluorescence excitation spectroscopy.<sup>1</sup>

The research presented here also implements a supersonic expansion (or jet-expansion) where a carrier gas, typically argon, is seeded with a fluorescent molecular sample of interest, and expanded through a small orifice into a vacuum chamber. During the expansion internal energy is removed from the seeded molecules through collisions with the carrier gas, and the translational energy of the gas is directed away from the source of the expansion. A benefit of a supersonic expansion's direction is that it may yield higher resolved spectroscopic measurements compared to gas cell or solution phase spectroscopic techniques.<sup>1</sup>

To achieve yet higher resolved measurements, such as those presented here, the supersonic expansion must be collimated to further reduce off axis velocity of molecules seeded into the carrier gas to lower the Doppler broadening. This is achieved with the use of a skimmer or a series of skimmers after the supersonic expansion, creating a molecular beam. Intersecting a collimated molecular beam with a narrow frequency ultraviolet laser has provided linewidths as narrow as 2.5 MHz at the full width half maximum (FWHM).<sup>2</sup> The results presented here typically have Doppler contributions of roughly 30 MHz.

The benefit of recording spectra with high resolution is that spectra of even relatively large molecules, ~30 atoms, are rotationally resolved,<sup>3</sup> which provides information describing the nuclear structure of molecular systems. This is due to the rotational energy level spacings which are dependent upon the system's inertial parameters, which in turn are dependent upon the geometry of the molecule. Any static molecular system can be described by three inertial parameters, which are found by diagonalizing its inertial tensor.<sup>4</sup> The three inertial parameters quantify the moment of inertia about one of three principal axes which are denoted as  $a$ ,  $b$  and  $c$ .

They are ordered from the axis with the least moment of inertia,  $a$ , to the greatest moment of inertia,  $c$ . The three inertial parameters are reported as rotational constants denoted A, B and C and are given in the units of MHz.

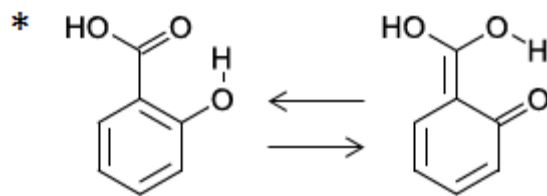
High resolution spectra can be reproduced with ground and excited state rigid rotor Hamiltonians, see Equation 1-1. Thus, careful analysis of high resolution spectra provides a

$$H = AP_a^2 + BP_b^2 + CP_c^2 \quad \text{Equation 1-1}$$

means to experimentally determine the rotational constants of molecular systems in the ground and excited states.<sup>4,5</sup> Thus, this technique is a powerful tool for determining structural information about molecular systems in both ground and electronically excited states.

In some instances, inertial parameters do not provide enough detail to thoroughly appreciate or interpret changes made by photo excitation. For instance, phenomena such as charge transfer may influence the inertial parameters, but cannot be determined quantitatively. Thus, instead of relying solely on inertial parameters, this work focuses on including the Stark-effect with the high resolution experiments,<sup>2,6</sup> allowing one to quantify the permanent electric dipole moment of molecular systems in the ground and excited states. This provides a means to follow changes of electronic distribution induced by photoexcitation. This proves to be sensitive tool for interpreting the effects of a variety of photoinduced phenomena.

The first example of such an effect are the results on 5-fluorosalicic acid (5FSA).<sup>7</sup> Similar systems have gained much interest owing to the possibility of excited state intramolecular proton transfer, see Scheme 1-1.



**Scheme 1-1**

These systems display red-shifted emission after excitation. This emission was attributed to a change in geometry upon excitation, a consequence of excited state intramolecular proton transfer.<sup>8-11</sup> However, time resolved results suggested that the red emission occurs on a time scale too slow to be proton transfer, and that a displacement of heavy atoms was responsible.<sup>12</sup> Our results demonstrate, that while the inertial parameters are not particularly sensitive to the position of the hydrogen atom (due to its relatively small mass), the excited state permanent electric dipole moment is sensitive to the position, yielding information on the position on the hydrogen atom.

This technique is particularly useful for deconvoluting molecular interactions. For example, a particularly interesting question arises when comparing the electronic origins of 7-azaindole and the 7-azaindole(H<sub>2</sub>O) complex. While these species only differ by the addition of a single water molecule, the excitation frequencies of these two systems are remarkably different, 1290 cm<sup>-1</sup>. Furthermore, the excited state's permanent electric dipole moment is seven times larger than the ground state's. Here, we use measurements of the permanent electric dipole moments to quantitatively account for the energetic difference.<sup>13</sup>

Another excited state phenomenon studied is the mixing of electronic states. When this phenomenon occurs, the prepared electronic state resembles higher electronic states, in this case also while remaining at a lower energy. We show this by measuring the permanent electric

dipole moment of an electronically mixed band of 7-azaindole. The results show that this band, which is only  $280\text{ cm}^{-1}$  above the origin, has a permanent electric dipole moment twice the size of the electronic origin. This serves as evidence that the energetically lower and less polar  $\pi\pi^*$  state (denoted as an  $L_b$  state), has mixed with an energetically higher and more polar  $\pi\pi^*$  state (denoted as an  $L_a$  state).<sup>14</sup>

Geometry is believed to play a large role in excited state charge transfer events.<sup>15</sup> In aromatic systems, removing conjugation is thought to have a large influence; however, this property is broken by a lack of planarity. We studied two phenyl substituted systems which possess different degrees of planarity, N-phenylcarbazole (PC) and 2-phenylindole (PI). PC possess a more twisted geometry compared to PI. Moreover, the results demonstrate that this causes the excitation of PC to be largely localized on the carbazole substituent, compared to PI.

## 1.1 WORKS CITED

1. D. H. Levy, *Ann. Rev. Phys. Chem.* **31**, 197 (1980).
2. W. A. Majewski, J. A. Pfanstiel, D. F. Plusquellic, and D. W. Pratt, in *Laser techniques in chemistry*, edited by A. B. Myers and T. R. Rizzo (Wiley, New York, 1995), p. 101.
3. L. Alvarez-Valtierra, J. W. Young, and D. W. Pratt. *Chem. Phys. Lett.* **509**, 96 (2011).
4. W. Gordy and R. L. Cook, in *Microwave Molecular Spectra* (Wiley-Interscience, New York, 1984).
5. D. F. Plusquellic, R. D. Suenram, B. Mate', J. O. Jensen, and A. C. Samuels, *J. Chem. Phys.* **115**, 3057 (2001).
6. T. M. Korter, D. R. Borst, C. J. Butler, and D. W. Pratt, *J. Am. Chem. Soc.* **123**, 96 (2001).
7. J. W. Young, A. J. Fleisher, and D. W. Pratt, *J. Chem. Phys.* **134**, 084310 (2011)
8. J. K. Marsh, *J. Chem. Soc., Trans.* **125**, 418 (1924).
9. A. Weller, *Z. Elektrochem.* **60**, 1144 (1956).
10. A. Weller, *Prog React Kinet.* **1**, 187 (1961).
11. P. B. Bisht, H. Petek, K. Yoshihara, and U. Nagashima, *J. Chem. Phys.* **103**, 5290 (1995).
12. J. L. Herek, S. Pedersen, L. Banares, and A. H. Zewail, *J. Chem. Phys.* **97**, 9046 (1992).
13. J. W. Young and D. W. Pratt, *J. Chem. Phys.* **135**, 084301 (2011).
14. J. R. Platt, *J. Chem. Phys.* **17**, 484 (1949).



15. K. Rotkiewicz, K. H. Grellmann, and Z. R. Grabowski, *Chem. Phys. Lett.* **19**, 315 (1973).

**2.0 EXPLORING SINGLE AND DOUBLE PROTON TRANSFER PROCESSES IN  
THE GAS PHASE. A HIGH RESOLUTION ELECTRONIC SPECTROSCOPY STUDY  
OF 5-FLUOROSALICYLIC ACID**

Reprinted with permission from *J. Chem. Phys.*

Justin W. Young, Adam J. Fleisher and David W. Pratt, *J. Chem. Phys.* **134**, 084310 (2011).

Copyright 2011 *American Institute of Physics.*

JWY and AJF developed a program to help with the analysis. JWY produced the experimental data, analyzed all experimental data, and performed theoretical calculations. JWY and DWP wrote the paper.

## 2.1 ABSTRACT

Two species that possess different absorption and emission properties have been observed in the low resolution fluorescence excitation spectrum of 5-fluorosalicylic acid (FSA) in the gas phase. The two species were identified as monomer and dimer species using high resolution techniques. Studies of these spectra in the presence of an applied electric field, together with *ab initio* quantum chemistry calculations, show that the monomer is a “closed” form of FSA exhibiting an *intramolecular* C=O...H-O-C hydrogen bond in the ground state. Absorption of light at ~ 344 nm transforms this species into the tautomeric form C-O-H...O=C *via* a barrierless proton transfer process. The large charge rearrangement that accompanies this process results in a significantly red-shifted emission spectrum. The (FSA)<sub>2</sub> dimer exhibits two *intermolecular* C=O...H-O-C hydrogen bonds but in this case the double proton transfer leads to a conical intersection with the ground state and rapid nonradiative decay. The onset of this process is revealed by a homogeneous broadening of the dimer’s high resolution spectrum.

## 2.2 INTRODUCTION.

Salicylic acid (SA), methyl salicylate (MS), and *o*-hydroxybenzaldehyde (OHBA) are highly investigated molecules.<sup>1-19</sup> Among chemical physicists, molecules of this type have gained notoriety owing to the possibility of excited state *intramolecular* proton transfer (ESIPT). This concept originated from studies of the electronic properties of MS and SA<sup>1-3</sup> that revealed a large Stokes-shifted emission in their solution phase spectra. This observation was originally

explained as arising from a double minimum potential on the excited state surface, owing to the formation of a zwitterion in the excited state following proton transfer from the –OH group to the –CO group. Later, Goodman and Brus<sup>5</sup> resolved vibronic structure in the excitation spectrum of MS suspended in a solid neon matrix, and argued that this structure was more characteristic of an excited state surface that resembles a distorted single minimum rather than a double minimum. An analogous conclusion was later made for SA.<sup>12</sup>

Not only has the form of the excited state surface been discussed, but the nature of the proton transfer has been debated as well. Nagaoka, *et al.*<sup>8</sup> created a model that used nodal planes to explain why the first excited state of OHBA is subject to tautomerization, but the second excited state is not.<sup>6</sup> However, in this model, the ES IPT process does not lead to a zwitterionic form; rather, the transformation in the excited state is better characterized as an enol to keto tautomerization. Their model also emphasized the importance of heavy atom motion. Similarly, more recent excited state *ab initio* calculations have suggested that, along with adjustments in the dimensions of the chelate ring, the hydrogen atom needs to move only slightly (0.1 - 0.2 Å) to explain the experimentally observed Stokes-shifted emission.<sup>15</sup>

The key role of heavy atom motion has been highlighted by time-resolved studies of MS; where the rise in Stokes-shifted emission occurs on a timescale that is consistent with heavy atom movement rather than a simple proton transfer.<sup>10</sup> But conclusive evidence for the hydrogen transfer has remained elusive. Jet-cooled gas phase spectra of MS and SA have been recorded in which two rotamers of both molecules were identified where only one undergoes excited state tautomerization.<sup>6,12,18,19</sup> Attempts to use deuterium substitution to identify the affected O-H stretching frequencies in MS, SA, and similar molecules using jet-cooled LIF and fluorescence dip IR spectroscopy have so far been unsuccessful, apparently because of the appearance of rapid

nonradiative decay channels in the electronically excited state.<sup>7,13,14</sup> The cyclic hydrogen bound dimer of SA has been observed in crystalline,<sup>4</sup> solution<sup>9,11</sup> and gas phases.<sup>12,13,16,17</sup> This work has largely focused on identifying the stable isomer of the dimer as well as searching for evidence of double proton transfer. Interpretations have differed between solution and gas phase results. Currently, it is believed that two different isomers are present in equilibrium with each other in solution through double proton transfer, while the gas phase results indicate that only one conformation is stable, and no double proton transfer occurs.

Recent studies of SA derivatives have revealed that selected substitutions of the benzene ring suppress the excited state tautomerization process, but that the intramolecular hydrogen bond strength is still remarkably increased.<sup>14,17</sup> An earlier attempt to obtain the high resolution spectrum of MS was unsuccessful.<sup>20</sup> In this work, we take advantage of these findings to analyze the electronic spectrum of one such molecule, 5-fluorosalicic acid (FSA) at both low and high resolution. Our findings shed light on the nature of ESIPT in both the monomeric and dimeric species.

## 2.3 EXPERIMENTAL

FSA (97%) was obtained from Sigma Aldrich and used without further purification. Low resolution fluorescence excitation spectra were acquired using a pulsed laser spectrometer described further elsewhere.<sup>21</sup> The sample was heated to ~120 °C, seeded into 2.8 kTorr of He gas and expanded through a 1 mm pulsed valve (General Valve Series 9) operating at 10 Hz into a vacuum chamber ( $10^{-5}$  Torr). The resulting expansion was intersected 2 cm downstream of the nozzle with the frequency-doubled output of an LDS 698 dye laser (Quanta Ray PDL-1). The dye laser was pumped at 10 Hz using the second harmonic of a Nd:YAG laser (Quanta Ray DCR-10). Signal was detected by a photomultiplier tube (PMT) mounted orthogonally to the direction of propagation of both the laser beam and jet expansion, with and without a visible filter (Corning Glass Works C.S. 3-71, cut 466-491 nm). The laser intensity was detected with a photodiode placed in the beam path beyond the vacuum chamber, and used for power normalization of the observed spectra. The data were processed by a boxcar integrator (Stanford Research Systems), and recorded digitally with QUICK DATA ACQUISITION software (Version 1.0.5).

High resolution experiments were performed using a molecular beam laser spectrometer.<sup>22</sup> FSA was placed in a quartz nozzle which was heated to ~160 °C. Argon gas at a pressure of 330 Torr was passed over the sample and expanded through a ~200  $\mu$ m orifice. The expansion was skimmed 2 cm downstream and intersected orthogonally by a UV laser beam 15 cm downstream of the nozzle. The UV beam was generated from the externally frequency doubled output of a continuous wave, Ar<sup>+</sup> pumped, single frequency tunable ring dye laser using

DCM laser dye. The resulting fluorescence signal was collected with spatially selective optics, detected by a photomultiplier tube and a photon counting system, and recorded by a data acquisition system (jba95). Relative frequencies in the spectra were calibrated using the fringes from a temperature-stabilized etalon having a free spectral range in the visible of  $299.7520 \pm 0.0005$  MHz. Absolute frequencies were calibrated using the iodine atlas.<sup>23</sup>

Spectra were simulated using the jb95 fitting program. This program utilizes a rigid rotor Hamiltonian for both electronic states and predicts a line spectrum using entered inertial parameters. Initial values of these parameters were extracted from quantum chemical calculations. Each transition is assigned a frequency, an intensity, and a transition type. Optimized parameters were then determined by first assigning quantum numbers to transitions observed in the experiment. After assignments have been made, the program utilizes a linear least-squares regression which optimizes the inertial parameters to minimize the standard deviation between the calculated and assigned transitions. Further details of the jb95 program have been described elsewhere.<sup>24</sup>

Stark spectra were measured by recording the spectra in the presence of an electric field. The electric field was created by applying voltages of opposite sign to two wire grids placed above and below the intersection of the laser and molecular beams. The distance between the wire grids was calibrated using the known dipole moments of aniline.<sup>25</sup>

Quantum chemical calculations were performed to aid in simulating and assigning conformations in the experimental spectra. Ground state geometries, inertial parameters, and dipole moments were obtained through these calculations at the M05-2X/6-31+G(d) level using the Gaussian 03 software package.<sup>26</sup> Excited state calculations have been performed with the CIS method. Geometry optimizations were carried out using the 6-31+G(d) basis set. To obtain

more accurate excited state dipole moments, single point calculations of the optimized structures were performed with the larger aug-pp-pvdz basis set.

## 2.4 RESULTS

The low resolution fluorescence excitation spectrum of FSA is shown in Figure 2-1a. The spectrum spans the energy region from 28900 to 29700  $\text{cm}^{-1}$ . It is dense with transitions; several Franck-Condon progressions crowd the spectrum at both low and high frequencies. The lowest frequency vibration that is active in the spectrum is at 49  $\text{cm}^{-1}$  mode. The first progression in this mode is built off the lowest energy transition at 28968  $\text{cm}^{-1}$ ; other progressions are built off “false origins” at higher energies.

A different low resolution spectrum was observed when a filter transmitting only visible radiation ( $> 466 \text{ nm}$ ) was placed in front of the PMT. This spectrum is shown in Figure 2-1b. The extensive progressions in the 49  $\text{cm}^{-1}$  have been significantly reduced in intensity. Instead, only seven relatively strong transitions remain; one at 29051  $\text{cm}^{-1}$ , and the rest shifted by at least 400  $\text{cm}^{-1}$  to higher energy.

High resolution spectra of several of these bands were recorded in order to determine the species responsible for them (see arrows in Fig. 2-1). Figure 2-2 shows the spectrum of the band located at 29147  $\text{cm}^{-1}$ . This spectrum was recorded with  $\sim 30 \mu\text{W}$  of UV radiation. It spans roughly 1  $\text{cm}^{-1}$ . Inertial parameters of this band were obtained from the jv95 fitting program utilizing a rigid rotor Hamiltonian for both electronic states. During the fitting process, most assignments were made close to the Q-branch where the spectral complexity and congestion is less. In this spectrum, spectral congestion is very high in the R and P branches, and thus reliable



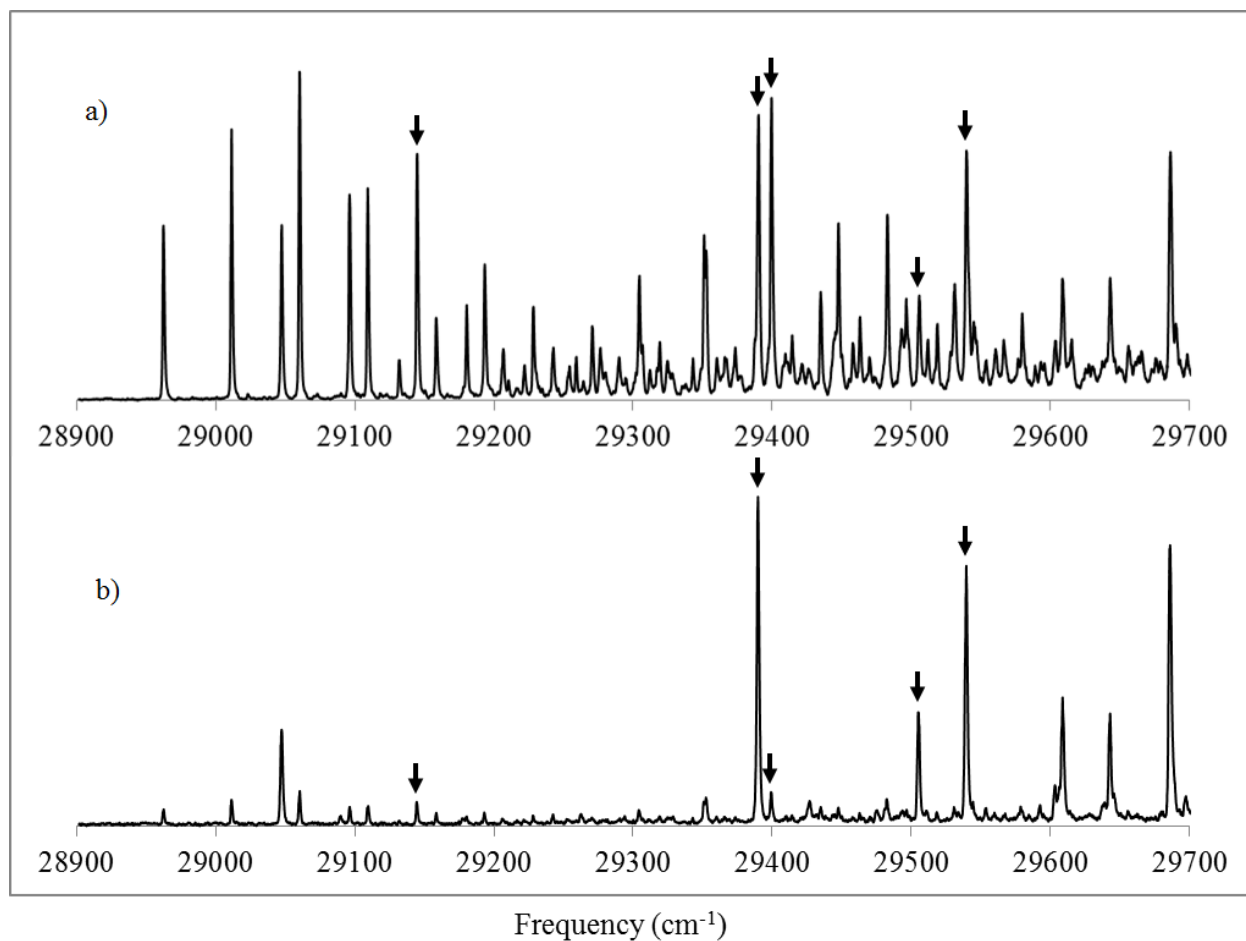


**Figure 2-1.  $S_1$ - $S_0$  fluorescence excitation spectrum of 5-fluorosalicic acid (FSA) viewing a.) total fluorescence (top) and b.) visible (> 480 nm) fluorescence only (bottom). Arrows denote transitions recorded in the high resolution apparatus. As will be shown, the strong lines in b.) belong to a FSA dimer species.**

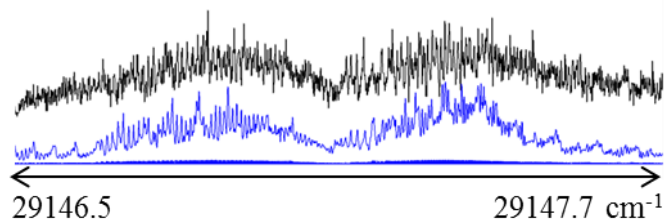


Figure 2-2 High resolution  $S_1$ - $S_0$  fluorescence excitation spectrum of the 29147  $\text{cm}^{-1}$  band of FSA with a simulated spectrum underneath.

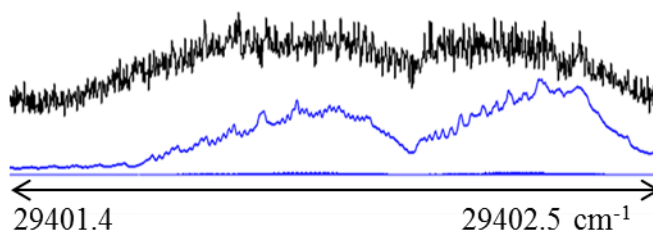


Figure 2-3. High resolution  $S_1$ - $S_0$  fluorescence excitation spectrum of the 29402  $\text{cm}^{-1}$  band of FSA with a simulated spectrum underneath. Note the significant increase in linewidth compared to Fig 2-2.

assignments were difficult to make. Adding distortion terms to the Hamiltonian improved the overall fit of the spectrum, particularly in the R-branch; however, these terms have been left out of the fit because individual transitions could not be resolved. The final fit utilized 32 assigned lines and resulted in an OMC (observed minus calculated) standard deviation of 13.9 MHz. Single rovibronic linewidths in the spectrum were reproduced using a Voigt profile composed of 30 MHz Gaussian and Lorentzian contributions of  $20 \pm 10$  MHz. The inertial parameters determined from the fit are listed in Table 2-I.

A similar spectrum was recorded of the band located at  $29402 \text{ cm}^{-1}$ . This spectrum was recorded with  $\sim 100 \text{ }\mu\text{W}$  of UV power and is shown in Figure 2-3. Again, the spectrum spans roughly  $1 \text{ cm}^{-1}$ . A dip in the center of the spectrum indicates the position of the Q-branch. However, peaks resulting from resolved rotational transitions or stacks were not identifiable in this spectrum, so its inertial parameters could not be determined. A simulation of this spectrum using the inertial parameters from the  $29147 \text{ cm}^{-1}$  band showed that its single rovibronic Lorentzian linewidth must be increased to at least 150 MHz so that the main features in the observed spectrum could be reproduced (see Fig. 2-3). Both bands are *ab*-hybrid bands.

The remaining three bands that were studied at high resolution, at 29393, 29508 and  $29542 \text{ cm}^{-1}$ , are quite different from the bands shown in Figures 2-2 and 2-3, as is evident from Figures 2-4, 2-5 and 2-6. Each of these bands is principally a *b*-type band, exhibits a larger overall width ( $\sim 1.7 \text{ cm}^{-1}$ ), and has a lower density of rovibronic lines. These were fit using a strategy similar to that for the band at  $29147 \text{ cm}^{-1}$ . In this case, inclusion of distortion terms did not visibly improve the fits. Also, the Lorentzian contribution to the linewidth is significantly smaller,  $10 \pm 5$  MHz for all three bands. The inertial parameters obtained from these fits also are listed in Table 2-I.

Table 2-I. Experimentally measured inertial parameters of four bands that appear in the gas phase  $S_1$ - $S_0$  fluorescence excitation spectrum of 5-fluorosalicicylic acid (FSA).

Parameter	29147 $\text{cm}^{-1}$	29393 $\text{cm}^{-1}$	29508 $\text{cm}^{-1}$	29542 $\text{cm}^{-1}$
<b><math>S_0</math></b>				
A''(MHz)	793(3) <sup>a</sup>	1816.0(4)	1815.5(6)	1816.4(1)
B''(MHz)	88.1(3)	891.3(2)	891.4(3)	891.5(1)
C''(MHz)	79.0(4)	597.9(2)	598.2(2)	598.2(1)
<b><math>S_1</math></b>				
A'(MHz)	816(3)	1869.3(5)	1876.9(6)	1874.2(1)
B'(MHz)	88.0(3)	870.3(2)	870.1(3)	870.6(1)
C'(MHz)	78.7 (5)	593.9(2)	594.9(2)	594.7(1)
OMC	13.9	9.8	13.2	4.5
a/b/c	45/55/0	18/82/0	18/82/0	18/82/0
Assignments	32	134	65	89

Table 2-II. Experimentally measured permanent electric dipole moments of FSA in its two electronic states.

Parameter	$S_0^c$	$S_1$
$\mu_a$ (D)	$\pm 0.30(3)^a$	$\mp 0.46(3)$
$\mu_b$ (D)	$\pm 1.03(3)$	$\pm 1.4(6)$
$\mu_c$ (D)	0.00	0.00
$\mu$ (D)	1.07(3)	1.22 (6)
$\theta_a, a/b$ (deg) <sup>b</sup>	$\pm 73.7$	$\mp 69.1$

<sup>a</sup> Experimental uncertainties in the last reported digits.

<sup>b</sup> Angle made by the dipole vector with the  $a$  inertial axis.

<sup>c</sup> The  $\pm$  and  $\mp$  symbols indicate if a change in sign occurs along that axes upon excitation

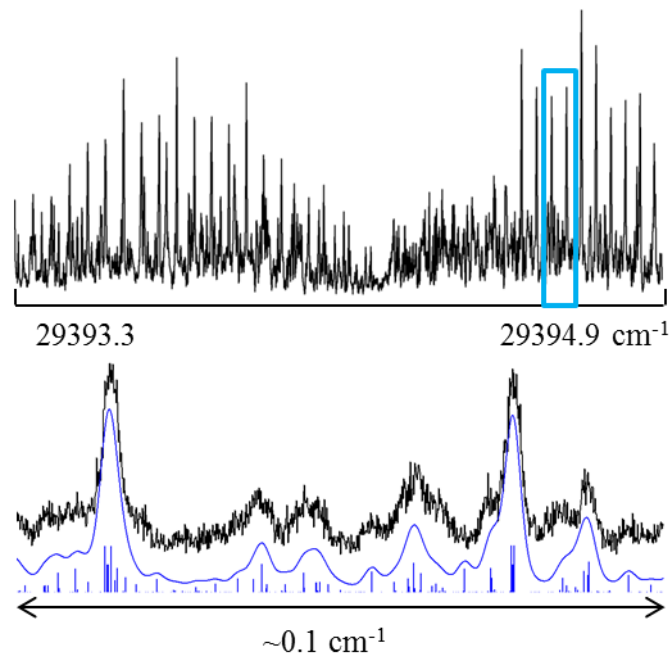


Figure 2-4. High resolution  $S_1$ - $S_0$  fluorescence excitation spectrum of three bands of FSA at  $29393\text{ cm}^{-1}$ . The lower panels show a small portion of the experimental spectrum (black), with two simulated spectra (blue), one with and one without a convoluted lineshape function.

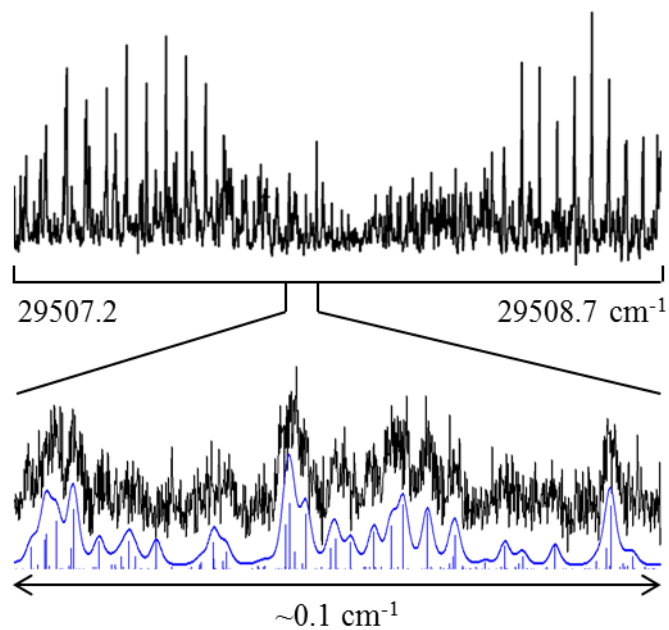


Figure 2-5. High resolution  $S_1$ - $S_0$  fluorescence excitation spectra of three bands of FSA at  $29508\text{ cm}^{-1}$ .

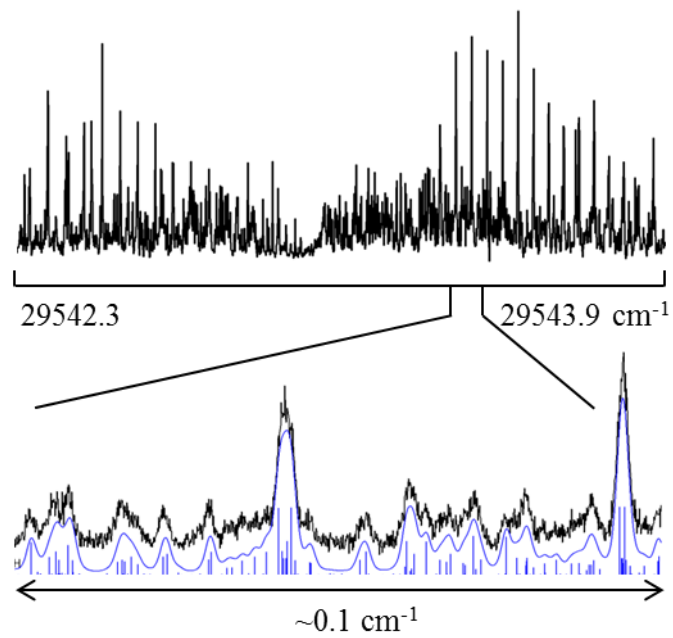
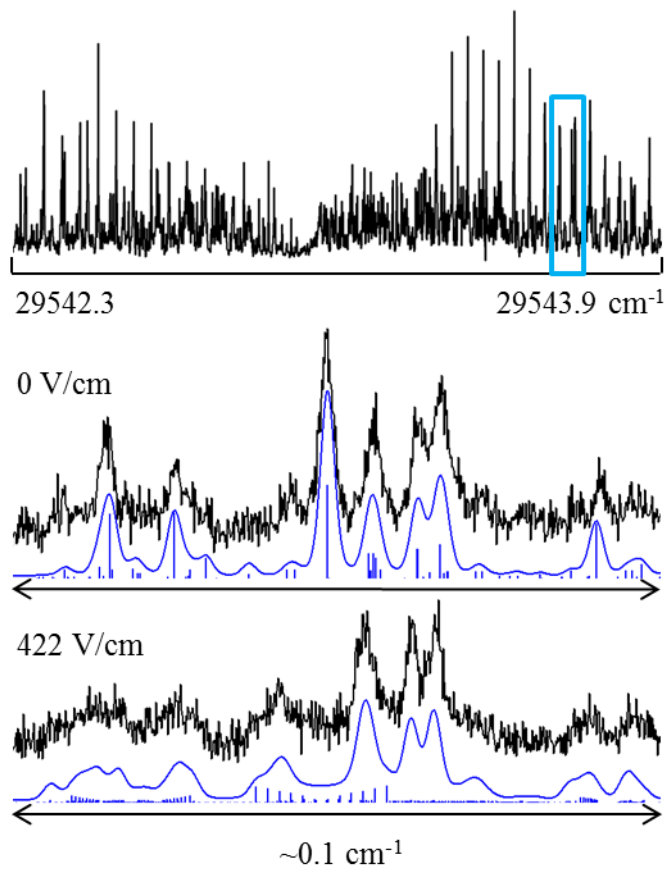


Figure 2-6. High resolution  $S_1$ - $S_0$  fluorescence excitation spectra of three bands of FSA at 29542  $\text{cm}^{-1}$ .

Finally, Stark effect measurements were performed on the band at  $29542\text{ cm}^{-1}$ . The data are shown in Figure 2-7. As is apparent, application of an applied electric field to the sample produces shifts and/or splittings of the rotationally resolved lines. Analyses of these, using the methodology described elsewhere,<sup>25</sup> yields the magnitudes and relative orientations of the permanent electric dipole moments of the species responsible for the spectrum, in both electronic states. These results are summarized in Table 2-II.



**Figure 2-7. Stark spectra of the 29393 cm<sup>-1</sup> band in FSA, at zero field (middle) and a 422 V/cm electric field (bottom). As before, the lower panels show a black experimental trace as well as blue simulated spectra with and without a lineshape function.**

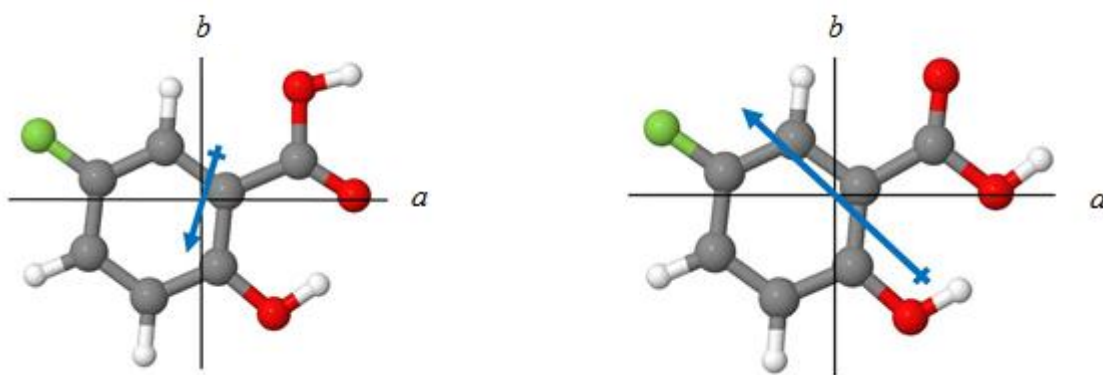


## 2.5 DISCUSSION

### Identification of the carriers of the spectra

While their different low resolution spectra (*cf.* Fig. 2-1) are suggestive, the high resolution spectra (*cf.* Figs. 2-(2-4)) provide conclusive evidence for the presence of two species in the sample. The clearest evidence is contained in the inertial parameters listed in Table 2-I. The 29147 and 29402  $\text{cm}^{-1}$  bands have rotational constants that are much smaller than those of the 29393, 29508, and 29542  $\text{cm}^{-1}$  bands. This indicates that the 29147 and 29402  $\text{cm}^{-1}$  bands result from a species that is much larger than the carrier of the three remaining bands. That the two different species differ significantly in size also is apparent from the overall widths of their spectra, which are much smaller for the 29147 and 29402  $\text{cm}^{-1}$  bands than for the 29393, 29508, and 29542  $\text{cm}^{-1}$  bands.

Quantum chemical calculations reveal that there are two reasonable structures for FSA in its ground electronic state, shown in Scheme 2-1 below. These differ in the orientation of their



Scheme 2-1

carboxyl (-COOH) functionalities with respect to the hydroxyl (-OH) group attached to the 2-position of the aromatic ring. This group is involved in hydrogen bonding with the carboxyl

group in both rotamers. In rotamer I (the “closed” form of FSA), the link is between the carbonyl ( $\text{-C=O}$ ) group and the  $\text{-OH}$  group attached to the aromatic ring, whereas in rotamer II (the “open” form of FSA) the link is between the two  $\text{-OH}$  groups, one serving as a donor and the other as an acceptor in the *intramolecular* hydrogen bond. Comparisons of the theoretical rotational constants of these two rotamers (see Table 2-II) with the experimentally measured ones suggests (with some ambiguity) that rotamer I is responsible for the observed bands at 29393, 29508, and 29542  $\text{cm}^{-1}$ .

A clear distinction between the two potential carriers of these bands can be made on the basis of a comparison of the calculated dipole moments of rotamers I and II with the measured ground state dipole moment ( $\mu$ ) of the band at 29542  $\text{cm}^{-1}$ , see Scheme 2-1 and Table 2-III. The measured dipole moment is in good agreement with the predicted value for rotamer I. Rotamer II is expected to have a significantly larger value of  $\mu$  in the ground state compared to the value for rotamer I. Thus, both the theoretical inertial parameters and dipole moments support the assignment of this rotamer as the carrier of the bands at 29393, 29508, and 29542  $\text{cm}^{-1}$ .

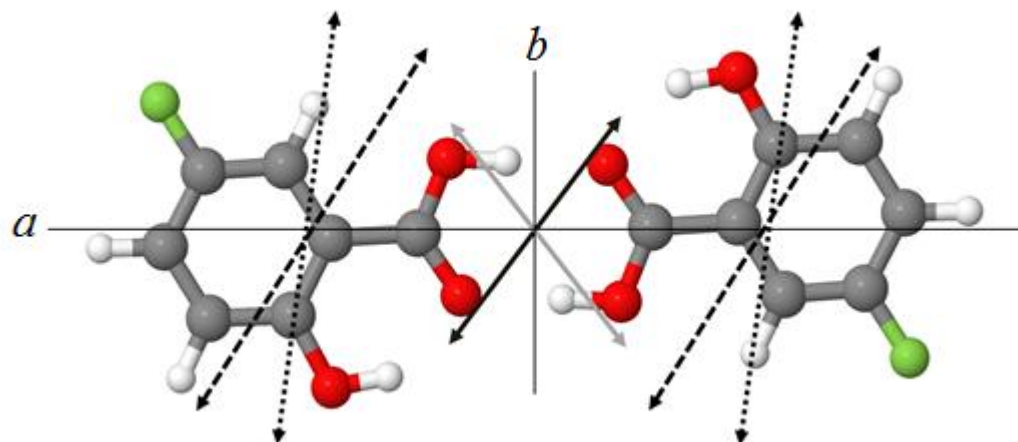
These two rotamers are further distinguished by their relative stabilities. Theoretical calculations (M05-2x/6-31g+(d)) predict rotamer I to be approximately 3500  $\text{cm}^{-1}$  lower in energy than rotamer II. Previous studies have drawn analogous conclusions for MS and SA, in which evidence suggests rotamer I as the favorable species. These conclusions have been supported by quantum calculations as well as from microwave spectra where only rotamer I transitions were observed.<sup>18,19</sup> The *intramolecular* hydrogen bonds unique to each rotamer are likely the prime source of the difference in their stabilities.

**Table 2-III. Theoretical inertial parameters and permanent electric dipole moments of two rotamers of FSA and the symmetric dimer, (FSA)<sub>2</sub>, in their ground electronic states.<sup>a</sup>**

<b>Parameter</b>	<b>Rotamer I</b>	<b>Rotamer II</b>	<b>Dimer</b>
<b>A'' (MHz)</b>	1817.0	1827.4	797
<b>B'' (MHz)</b>	893.4	884.3	87.2
<b>C'' (MHz)</b>	598.9	595.9	78.7
$\mu_a$ (D)	0.2747	1.618	
$\mu_b$ (D)	0.943	-1.492	
$\mu_c$ (D)	0.00	0.00	
<b><math>\mu</math> (D)</b>	0.982	2.20	

<sup>a</sup> Calculated using M05-2X/6-31+G(d).

A logical candidate for the carrier of the 29147 and 29402  $\text{cm}^{-1}$  bands is the doubly hydrogen bound dimer of FSA shown in Scheme 2-2 (see below). Its rotational constants would be expected to be much smaller than the monomer structures discussed above. Indeed, this proves to be true; a comparison of the predicted rotational constants of the dimer listed in Table 2-III with the measured values in Table 2-I shows excellent agreement. The two sides of the FSA dimer are linked by equivalent  $\text{C}=\text{O}\cdots\text{H}-\text{O}$  hydrogen bonds, as in the case of the structurally similar benzoic acid dimer.<sup>26-28</sup>



**Scheme 2-2**

While the dimer is symmetric, and has no permanent dipole moment, it has a non-zero transition dipole moment (TDM) that is uniquely oriented in the molecular frame. Scheme 2-2 displays the possible orientations of the monomer (broken) and dimer (solid) derived from the high resolution data, of which only one is correct. Examination of the possible TM's reveal that the dashed (monomers) and solid black (dimer) TM's are virtually parallel to each other. Since the dimer TDM can be thought of as an in-phase or out-of-phase combination of the monomer TDM's, the parallel lines must represent the in-phase TDM's. We do not know whether the

corresponding in-phase excitation lies at lower or higher energy, though simple exciton theory suggests that it is higher.<sup>30</sup> Isotopic substitution experiments could resolve this issue.<sup>29,31</sup>

### **Dynamics in the FSA monomer**

Rovibronic bands that were confirmed as belonging to the monomer (at 29393, 29508, and 29542  $\text{cm}^{-1}$ ) emit more red emission (are more Stokes shifted), and thus appear more intense in the filtered fluorescence excitation spectrum than those confirmed as belonging to the dimer species (29147 and 29402  $\text{cm}^{-1}$ ). Thus, relative to those of the monomer, the intensities of the dimer transitions decrease by a factor of roughly ten from the unfiltered to the filtered fluorescence excitation spectra. This information was used to distinguish which transitions belong to the monomer or dimer species, as listed in Tables 2-IV and 2-V. The assignments of the origin bands of both species are in agreement with previous work.<sup>17</sup>

Curiously, the origin band of the rotamer I species is likely overlapped with a vibrational band of the dimer species. This conclusion is drawn from two observations. First, this band is the only band that decreases in relative intensity by a factor of two, rather than ten or not at all, from the filtered to the unfiltered experiment. Second, this band is also a member of a 49  $\text{cm}^{-1}$  progression, which also includes the 29147  $\text{cm}^{-1}$  dimer band. Thus, due to the overlap, a more precise measure of the relative intensity of the monomer origin band is obtained from the filtered fluorescence excitation spectrum, in which the fluorescence from the other overlapping dimer band is blocked. This leads to the conclusion that the origin band is the least intense band observed of the rotamer I transitions.

In a previous study,<sup>17</sup> it was suggested that the excited state tautomerization process in FSA is highly suppressed. This conclusion was drawn from a dispersed fluorescence

**Table 2-IV. Relative frequencies and intensities of the monomer transitions in the S<sub>1</sub>-S<sub>0</sub> fluorescence excitation spectrum of 5-fluorosalicylic acid.**

<b>Frequencies (cm<sup>-1</sup>)</b>	<b>Relative Frequencies (cm<sup>-1</sup>)</b>	<b>UV Intensity</b>	<b>Visible Intensity</b>	<b>Assignments</b>
29050	0.0	21	10	0-0
29393	342.7	35	35	v <sub>1</sub> <sup>a</sup>
29508	458.5	12	12	v <sub>2</sub> <sup>a</sup>
29542	492.2	30	28	v <sub>3</sub> (ip ring stretching)
29611	561.5	15	13	v <sub>4</sub> (ip ring stretching)
29645	595.9	15	11	v <sub>5</sub> (op ring vibration)
29688	638.8	30	30	v <sub>6</sub> (op ring vibration)

<sup>a</sup> Maybe an in plane OH wag or in-plane carboxylic group wag.

**Table 2-V. Relative frequencies and intensities of the dimer transitions in the S<sub>1</sub>-S<sub>0</sub> fluorescence excitation spectrum of 5-fluorosalicic acid.**

Frequencies (cm <sup>-1</sup> )	Relative Frequencies (cm <sup>-1</sup> )	UV intensity	Visible intensity	Assignments	Calculated Frequency <sup>a</sup> (cm <sup>-1</sup> )
28965	0	21	2	0-0	
29015	48.9	34	3	v <sub>1</sub> (cogwheel rotation)	49.1
29050	84.9	21	10	Overlapped monomer 0-0, v <sub>2</sub> (unidirectional rotation)	87.8
29063	97.6	40	3	2v <sub>1</sub>	
29099	133.8	25	2	v <sub>1</sub> + v <sub>2</sub>	
29112	146.7	26	2	3v <sub>1</sub>	
29134	169.4	5		2v <sub>2</sub>	
29147	182.2	30	2	2v <sub>1</sub> + v <sub>2</sub>	
29161	196.1	10	1	4v <sub>1</sub>	
29183	217.9	11	1	v <sub>1</sub> + 2v <sub>2</sub>	
29196	231	17	1	3v <sub>1</sub> + v <sub>2</sub>	
29209	244.2	6		5v <sub>1</sub>	
29213	247.9	2		v <sub>3</sub> (C-COOH ip bend B <sub>u</sub> )	256.5
29225	259.9	4		v <sub>4</sub> (C-COOH ip bend A <sub>u</sub> )	259.3
29231	265.9	11		2v <sub>1</sub> + 2v <sub>2</sub>	
29245	280.2	6		4v <sub>1</sub> + v <sub>2</sub>	
29262	296.7	5		v <sub>1</sub> + v <sub>3</sub>	
29273	308.4	9		v <sub>1</sub> + v <sub>4</sub>	
29279	314	6		3v <sub>1</sub> + 2v <sub>2</sub>	
29307	342	15	1	2v <sub>1</sub> + v <sub>3</sub>	
29322	356.8	7		2v <sub>1</sub> + v <sub>4</sub>	
29354	388.5	20			
29355	390.2	19	2	3v <sub>1</sub> + v <sub>3</sub>	
29402	436.7	38	3	4v <sub>1</sub> + v <sub>3</sub>	
29437	472.3	13	2		
29450	485.2	21	2	5v <sub>1</sub> + v <sub>3</sub>	
29485	520.3	22	3		
29499	533.9	11	2	6v <sub>1</sub> + v <sub>3</sub>	
29521	556.2	9	1		
29534	568.6	14	2		

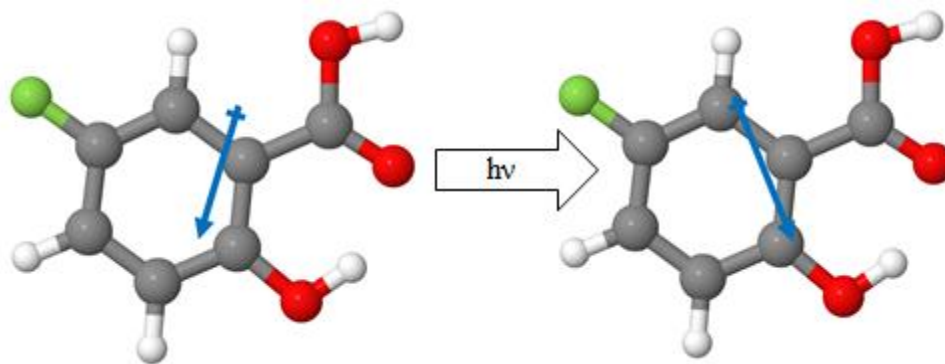
<sup>a</sup>Predicted by m052x/6-31g+(d).

measurement of the origin band of the monomer, which shows only a small amount of Stokes-shifted emission. It is uncertain if the authors accounted for the overlapping dimer band in their analysis. On the other hand, the authors did not observe any dimer transitions in their fluorescence dip infrared experiments, which suggests that the transition is not overlapped, and that the emission properties of the origin band of the monomer differ from those of its higher vibronic bands.

Our data show that the origin band of FSA is the least intense band observed of the rotamer I transitions (see Table 2-IV). Similarly, the origin bands of MS and SA seem to possess relatively low intensity.<sup>5,12</sup> This behavior implies that the minimum along the proton transfer coordinate is displaced in the excited state relative to the ground state, which causes the Franck-Condon overlap of the origin to be small, increasing only towards the higher vibronic bands. Moreover, no tunneling splittings or fluorescence broadenings were observed in the higher vibronic bands, which suggests that the excited state surface has a relatively deep single minimum, or at least involves relatively high barriers to other possible minima along other coordinates. Possible displacement coordinates are included in Table 2-IV.

New information about the excited state potential energy surface of FSA is provided by the measurement of its excited state dipole moment; see Table 2-II and Scheme 2-3 below. The change in both the orientation and the magnitude of  $\mu$  (0.15 D) is significantly smaller than that





**Scheme 2-3**

observed in other substituted benzoic acids.<sup>32</sup> In such cases, the carbonyl group typically gains electron density from the phenyl ring, which has a large effect on the molecule's electric dipole moment. However, the change in the permanent electric dipole moment in FSA is small.

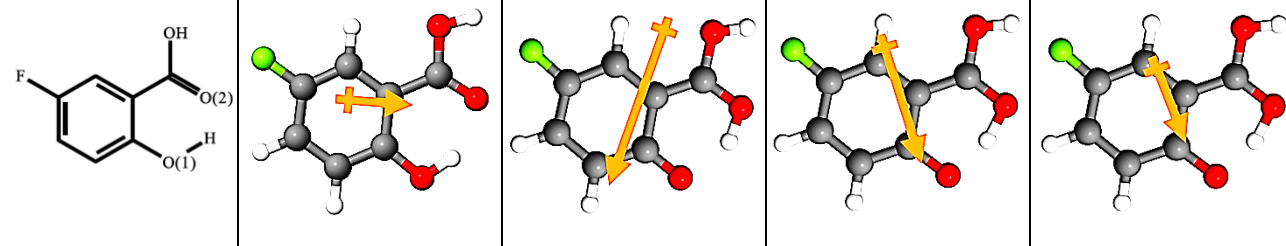
We have explored this issue further by optimizing the enol and keto structures of the excited  $S_1$  states of FSA at the CIS/6-31g (d,p) level of theory. These are shown in Table 2-VI. The rotational constants of both structures are different, but the differences are too small to shed light on the excited state structure. However, the calculations show that both the magnitude and the orientation of the dipole moment are very sensitive to the position of the enolic hydrogen relative to the chelate ring, as shown in Table 2-VI. The enol structure possesses a dipole moment which is oriented towards the carboxyl group, while the keto structure possesses a dipole moment that is larger in magnitude and oriented away from the carboxyl group. Curiously, the experimental dipole moment seems to lie between these two limits. Given this, and that Sobolewski and Domcke have reported a shallow potential energy surface in the  $S_1$  state of SA,<sup>15</sup> it follows that the excited state geometry may lay between these two limits as well.

We tested this hypothesis as follows. Sobolewski and Domcke<sup>33</sup> have recently described a study of the excited state reaction paths of salicylic acid. In this work they published Cartesian coordinates of a hydrogen transfer structure of salicylic acid optimized with CC2/cc-pVDZ.

Unlike the keto and enol structures mentioned above, this structure shown significant intramolecular hydrogen bond strength as well as chelate ring distortion.<sup>33</sup> We have modified these results by adding a fluorine atom to the 5-position of the phenyl ring, and predicted the excited state dipole moment at the CIS/aug-cc-pVDZ level of theory. Intriguingly, the dipole moment provided from this calculation best resembles the experimental dipole moment's orientation, Table 2-VI. What distinguishes this structure from the previous two is that the molecule has distorted itself by bringing the carboxyl oxygen and phenol oxygen closer to one another, thereby also minimizing their separation from the hydrogen. This structure is a hydrogen transferred species; however, the hydrogen is still very close to O(1) (1.44 Å) owing to the large strength of the hydrogen bond. Currently, this structure best reproduces the excited state dipole moment. It would be interesting to see if the dipole moment could be better reproduced from high level calculations with the fluorine atom attached.

Thus, this analysis confirms that the excited state structure of 5FSA is between the enol and keto limits, and is best described as the hydrogen transfer species. However, the difference in energy of the calculated  $S_1$  state and the optimized structure of rotamer I in the ground state predicts a maximum in emission fluorescence at ~550 nm (MP2/6-31+g(d)). This is a larger Stokes shift than has been observed. Further calculations on an optimized FSA structure will be needed to explore this discrepancy. Nonetheless, the data reported here clearly support a barrierless enol-to-keto hydrogen transfer in the excited state. It has been noted by Sobolewski and Domcke<sup>15</sup> that the excited state surface of SA possesses a broad minimum between the enol and keto form. Therefore, it seems plausible that the excited state structure of 5FSA also can be thought of as possessing character from both structures.

**Table 2-VI. Comparison of theoretical electric dipole moments (and O-O bond distances) of different possible excited state structures of FSA with experiment.**

Parameter	Enol <sup>a</sup>	Keto <sup>a</sup>	Hydrogen Transfer <sup>b</sup>	Experiment
$\mu_a$ (D)	1.07	-0.80	0.54	0.46
$\mu_b$ (D)	-0.09	-2.22	-1.71	-1.14
$\mu_c$ (D)	0.00	0.00	0.00	0.00
$\mu$ (D)	1.08	2.35	1.78	1.23
O(1)-H (Å)	0.98	1.70	1.44	N/A
O(2)-H (Å)	1.70	0.98	1.08	N/A
				

<sup>a</sup> Structure optimized with CIS/6-31g+(d), the dipole with CIS/aug-pp-pvdz.

<sup>b</sup> Structure optimized in Ref. 26, the dipole with CIS/aug-pp-pvdz.

## Dynamics in the FSA dimer

The origin band of the FSA dimer is red shifted by less than  $100\text{ cm}^{-1}$  compared to the corresponding band in the monomer. However, the two species exhibit quite different absorption and emission spectra. The dimer fluorescence excitation spectrum is dominated by extensive progressions in a  $49\text{ cm}^{-1}$  vibration whereas no such vibration appears in the spectrum of the monomer. We assign this vibration as a cogwheel rotation due to the resemblance with the calculated ground state frequency (Table 2-V). However, similar vibrations of  $(\text{SA})_2$  and the benzoic acid dimer have been assigned differently.<sup>12,28,29</sup> And, unlike the monomer, the dimer of FSA exhibits a “normal” fluorescence spectrum, with little red-shifted emission.

The abundant  $49\text{ cm}^{-1}$  progressions in the dimer spectrum indicate that upon excitation the molecule is displaced along this coordinate. Intriguingly, this vibration shows one hydrogen bond strengthening while one weakens, a likely precursor to double proton transfer. Similar progressions have been observed in the  $n\pi^*$  electronic state of benzoic acid dimer.<sup>29</sup> However, the data observed here show the electronic state observed in  $(\text{FSA})_2$  is  $\pi\pi^*$  type, since the electronic TDM lies in the molecular plane.

$(\text{FSA})_2$  is not void of other dynamic processes. Significant line broadening was observed in the high resolution spectrum of the dimer band at an energy of  $437\text{ cm}^{-1}$  above the origin. This band exhibits a Lorentzian linewidth of at least 150 MHz, yielding a lifetime no longer than 1.0 nsec, compared to 6.5 nsec for the origin band. Now, a characteristic property of the monomers of SA, MS, and related systems is the existence of a distinct energy threshold for efficient fluorescence quenching in the  $S_1$  state.<sup>33</sup> This threshold has been located at  $1100\text{ cm}^{-1}$  in SA and  $1300\text{ cm}^{-1}$  in MS.<sup>10,12</sup> This behavior was not observed in our spectra but we did not scan to such high excess energies. In the case of the monomer, it is believed that the quenching

is caused by a low-lying  $S_1$ - $S_0$  conical intersection, accessed *via* torsion and pyramidalization of the carboxyl group following the barrierless intramolecular hydrogen transfer. It is possible that the line broadening observed in our spectra signals the onset of a similar process in the FSA dimer. In that event, our data suggest that either cogwheel rotation (at  $49\text{ cm}^{-1}$ ), the C-COOH in-plane bend (at  $248\text{ cm}^{-1}$ ), or some combination of the two vibrations promote the process. Since both of these vibrations involve the hydrogen bonds between the two moieties, this is not an unlikely scenario. An alternative explanation is that  $(\text{FSA})_2$  is accessing a non-radiative  $n\pi^*$  state, similar to that observed in the benzoic acid dimer.<sup>29</sup>

## 2.6 CONCLUSIONS

Monomer and dimer species of FSA have been identified in the gas phase using high resolution electronic spectroscopy techniques, both in the absence and presence of an applied electric field. Only one monomer species was found; its measured ground state dipole moment clearly corresponds to that of the “closed” rotamer form of FSA. This rotamer exhibits a C=O...H-O intramolecular hydrogen bond between the carbonyl group of the acid functionality and the -OH group attached to the 2-position of the aromatic ring. This species is analogous to the ESIPT species of SA. However, measurements of the excited state dipole moment of FSA clearly show that in this case the ESIPT process occurs *via* a distorted single minimum potential rather than a double minimum one.

Comparison of the measured rotational constants of the dimer species show it to be a cyclic doubly hydrogen bound form of FSA. While the ESIPT process seems suppressed in this case, fluorescence line broadening was observed in a higher vibronic band, leading to the

conclusion that a vibrationally dependent dynamic process occurs in the excited state. A likely source of these dynamics is double proton transfer leading to a conical intersection with the ground state.

## 2.7 ACKNOWLEDGEMENTS

Discussions with Asuka Fujii, Andrzej Sobolewski, and Wolfgang Domcke are appreciated. This work has been supported by NSF (CHE-0911117). Computing time was provided by the Center for Molecular and Material Simulations at the University of Pittsburgh. We dedicate this paper to the memory of Bryan Kohler.

## 2.8 WORKS CITED

1. J. K. Marsh, *J. Chem. Soc., Trans.* **125**, 418 (1924).
2. A. Weller, *Z. Elektrochem.* **60**, 1144 (1956);
3. A. Weller, *Prog React Kinet.* **1**, 187 (1961).
4. G. E. Bacon and R. J. Jude, *Kristallogr.* **138**, 19 (1973).
5. J. Goodman and L. E. Brus, *J. Am. Chem. Soc.* **100**, 7472 (1978).
6. L. A. Heimbrook, J. E. Kenny, B. E. Kohler, and G. W. Scott, *J. Chem. Phys.* **75**, 5201 (1981).
7. L. Heimbrook, J. E. Kenny, B. E. Kohler, and G. W. Scott, *J. Phys. Chem.* **87**, 280 (1983).
8. S. Nagaoka, U. Nagashima, N. Ohta, M. Fujita, and T. Takemura, *J. Phys. Chem.* **92**, 166 (1988).
9. H. C. Joshi, H. B. Tripathi, T. C. Pant, and D. D. Pant, *Chem. Phys. Lett.* **173**, 83 (1990).
10. J. L. Herek, S. Pedersen, L. Banares, and A. H. Zewail, *J. Chem. Phys.* **97**, 9046 (1992).
11. D. D. Pant, H. C. Joshi, P. B. Bisht, and H. B. Tripathi, *Chem. Phys.* **185**, 137 (1994).
12. P. B. Bisht, H. Petek, K. Yoshihara, and U. Nagashima, *J. Chem. Phys.* **103**, 5290 (1995).
13. F. Lahmani and A. Zehnacker-Rentien, *Chem. Phys. Lett.* **271**, 6 (1997).
14. F. Lahmani and A. Zehnacker-Rentien, *J. Phys. Chem. A* **101**, 6141 (1997).
15. A. L. Sobolewski and W. Domcke, *Chem. Phys.* **232**, 257 (1998).
16. T. Yahagi, A. Fujii, T. Ebata, and N. Mikami, *J. Phys. Chem. A* **105**, 10673 (2001).

17. E. Abd El-Hakam Abou El-Nasr, A. Fujii, T. Ebata, and N. Mikami, *Mol. Phys.* **103**, 1561 (2005).
18. S. Melandri, B. M. Giuliano, A. Maris, L. B. Favero, P. Ottaviani, B. Velino, and W. Caminati, *J. Phys. Chem. A* **111**, 9076 (2007).
19. L. Evangelisti, S. Tang, B. Velino, and W. Caminati, *J. Mol. Struct.* **921**, 285 (2009).
20. J. W. Ribblett, Ph.D. Thesis, University of Pittsburgh (1999).
21. J. R. Johnson, K. D. Jordan, D. F. Plusquellic, and D. W. Pratt, *J. Chem. Phys.* **93**, 2258 (1990).
22. W. A. Majewski, J. A. Pfanstiel, D. F. Plusquellic, and D. W. Pratt, in *Laser techniques in chemistry*, edited by A. B. Myers and T. R. Rizzo (Wiley, New York, 1995), p. 101.
23. S. Gerstenkorn and P. Luc, (CNRS, Paris, 1978/1982).
24. D. F. Plusquellic, R. D. Suenram, B. Mate, J. O. Jensen, and A. C. Samuels, *J. Chem. Phys.* **115**, 3057 (2001).
25. T. M. Korter, D. R. Borst, C. J. Butler, and D. W. Pratt, *J. Am. Chem. Soc.* **123**, 96 (2001).
26. M. J. Frisch *et al.*, Gaussian 03, Revision E.01 (Gaussian, Inc., Wallingford CT, 2004).
27. G. M. Florio, E. L. Sibert, III, and T. S. Zwier, *Faraday Disc.* **118**, 315 (2001).
28. I. Kalkman, C. Vu, M. Schmitt, and W. L. Meerts, *ChemPhysChem* **9**, 1788 (2008).
29. Y. Tomioka, H. Abe, N. Mikami, and M. Ito, *J. Phys. Chem.* **88**, 2263 (1984).
30. A. S. Davydov, *Theory of molecular excitons*. (McGraw-Hill, New York, 1962).
31. A. Muller, F. Talbot, and S. Leutwyler, *J. Chem. Phys.* **116** (7), 2836 (2002).
32. A. J. Fleisher, P. J. Morgan, and D. W. Pratt, Non-symmetric push-pull molecules in the gas phase: High resolution Stark spectroscopy of *m*-aminobenzoic acid [online], *65th*



*OSU international symposium on molecular spectroscopy*. Columbus, OH, 2010; WF-08.

The Ohio State University, Dspace web site.

<https://kb.osu.edu/dspace/bitstream/1811/46140/29/WF08.pptx>

33. A. L. Sobolewski and W. Domcke, *Phys. Chem. Chem. Phys.* **8**, 3410 (2006).

**3.0 EXCITED STATE ELECTRON TRANSFER PRECEDES PROTON TRANSFER  
FOLLOWING IRRADIATION OF THE HYDROGEN-BONDED SINGLE WATER  
COMPLEX OF 7-AZAINDOLE WITH UV LIGHT**

Reprinted with permission from *J. Chem. Phys.*

Justin W. Young and David W. Pratt, *J. Chem. Phys.* **135**, 084301 (2011).

Copyright 2011 *American Institute of Physics.*

JWY produced the experimental results, analyzed the results and performed the theoretical calculations. JWY and DWP wrote the paper.

### 3.1 ABSTRACT

High resolution electronic spectra of the single water complex of 7-azaindole (7AIW) and of a deuterated analog (7AIW- $d_3$ ) have been recorded in a molecular beam, both in the absence and presence of an applied electric field. The obtained data include the rotational constants of both complexes in their ground ( $S_0$ ) and first excited ( $S_1$ ) electronic states, their  $S_1$ -  $S_0$  electronic transition moment and axis-tilting angles, and their permanent electric dipole moments (EDM's) in both electronic states. Analyses of these data show that the water molecule forms two hydrogen bonds with 7AI, a donor O-H...N<sub>7</sub> bond and an acceptor O...H-N<sub>1</sub> bond. The resulting structure has a small EDM in the  $S_0$  state ( $\mu = 0.54$  D) but a greatly enhanced EDM in the  $S_1$  state ( $\mu = 3.97$  D). We deduce from the EDM's of the component parts that 0.281 e<sup>-</sup> of charge is transferred from the acidic N<sub>1</sub>-H site to the basic N<sub>7</sub> site upon UV excitation of 7AIW, but that water-assisted proton transfer from N<sub>1</sub> to N<sub>7</sub> does not occur. A model of the resulting electrostatic interactions in the solute-solvent pair predicts a solvent-induced red-shift of 1260 cm<sup>-1</sup> which compares favorably to the experimental value of 1290 cm<sup>-1</sup>.

### 3.2 INTRODUCTION

Efforts to characterize the structure and dynamical behavior of 7-azaindole (7AI) in gas and solution phases have been rigorously pursued.<sup>1-28</sup> The earliest gas phase study in a free jet expansion was performed by Fuke, *et al.*<sup>2</sup> and was largely motivated by interest in the properties of doubly hydrogen-bonded base pairs. This and later studies have been very successful; a

variety of spectroscopies have identified numerous complexes including the 7AI dimer and solvated complexes of 7AI with argon, water, ammonia, and a variety of alcohols.<sup>2,4,9,14-16,18,20,22,24,25</sup> Of particular interest here are rotationally resolved experiments on the water complexes 7-azaindole-H<sub>2</sub>O (7AIW), 7-azaindole-(H<sub>2</sub>O)<sub>2</sub> (7AIW2), and 7-azaindole-(H<sub>2</sub>O)<sub>3</sub> (7AIW3); these studies have shown that the water molecule(s) bind with two hydrogen bonds to 7AI, to form a cyclic ring structure (see Figure 3-1).<sup>9,20</sup> While the placement of the water molecules in these structures could potentially lead them to act as a proton wire that mediates proton transfer, the rotationally resolved experiments have so far given no direct evidence for this reaction. However, proton transfer has been observed in gas phase femtosecond time-resolved experiments on the dimer,<sup>13</sup> and theoretical calculations suggest that the barrier to proton transfer is substantially lower in its photoexcited state.<sup>21</sup>

Excited state proton transfer (ESPT) in 7AI was first demonstrated by Kasha, El-Bayoumi and co-workers<sup>1</sup> in early steady-state solution phase experiments. These studies were largely motivated by the use of 7AI as a photo-probe since it is structurally similar to tryptophan, but possesses a much greater quantum yield as well as a longer lifetime in solution. Later experiments have shown that the photo-behavior of 7AI is solvent dependent, and depends on the concentration of water.<sup>6,7,10</sup> Currently, it is believed that the reaction rates in these systems are controlled by the fraction of solutes that are “correctly” solvated; *i.e.*, that form cyclic 1:1 solute-solvent complexes. Calculations show that the presence of one water molecule in the solvent “bridge” dramatically reduces the barrier to proton transfer in both electronic states,<sup>8</sup> and that the number of reactive complexes is small (< 2%), thereby accounting for the relatively slow reactions observed in neat solvents.<sup>11,12</sup> Later calculations<sup>23,26,27</sup> have further suggested that the

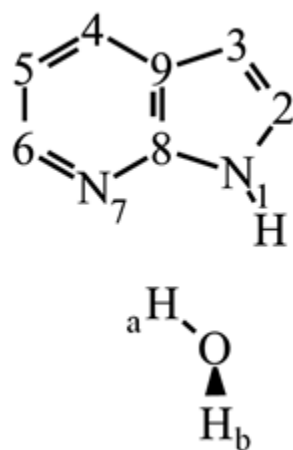


Figure 3-1. Structure of 7-azaindole-H<sub>2</sub>O (7AIW).

two protons in the excited state tautomerization of 7AIW are transferred concertedly, but asynchronously, breaking the underlying assumption of a geometric mean.

Movement of the positively charged proton in an ESPT reaction is likely to be accompanied by a significant rearrangement of negatively charged electrons, either within the molecule or in the surrounding environment. Such proton-coupled electron transfer (PCET) reactions are currently believed to play an important role in many important chemical processes, including much of the energy conversion that occurs within living cells.<sup>28</sup> Recent experimental<sup>29</sup> and theoretical<sup>30</sup> studies of PCET reactions have focused on the measurements of their rates in aqueous solution, and on the relative time scales of electron transfer, proton transfer, and solvent motion. In what follows, we describe high resolution electronic spectroscopy experiments on the single water complex 7AIW in the gas phase which demonstrate that electron transfer precedes proton transfer in its electronically excited state.

### 3.3 EXPERIMENTAL

7-Azaindole was purchased from Sigma-Aldrich (> 99%) and used without further purification. Rotationally resolved fluorescence excitation experiments were performed using a high resolution molecular beam spectrometer. In this setup, the molecular beam was prepared as follows. Argon carrier gas, at 500 Torr, was passed over a reservoir of water. The gas mixture was then flowed through a heated (400 K) quartz source containing 7AI and expanded through a 200  $\mu\text{m}$  quartz nozzle into the first of two differentially pumped vacuum chambers. The expansion was skimmed 2 cm downstream with a 1 mm skimmer leading to the second vacuum chamber, forming the molecular beam. Fifteen cm downstream from the source, the molecular

beam was intersected orthogonally with a tunable UV laser beam. Spherical mirrors, placed above and below the beam intersection point, were used to collect the fluorescence which was then recorded using a PMT and a photon counting system. Under these experimental conditions, a Doppler width of 30 MHz was exhibited by the rotationally resolved transitions; fits of the resulting spectra indicate that the 7AIW sample had been cooled to a rotational temperature of  $\sim 7$  K. For the isotopically labeled experiments, the reservoir of water was replaced with a reservoir of deuterium oxide.

Stark effect measurements were made using two stainless steel wire grids that were placed above and below the beam intersection point, within the spherical mirrors. Voltages were applied to both grids; one grid was kept at a positive voltage and the other at a negative voltage. In this arrangement, the electric field was perpendicular to the polarization of the laser beam, resulting in the selection rule  $\Delta M = \pm 1$ . The spacing between the two plates was calibrated using the known dipole moments of aniline.<sup>31,32</sup>

The UV beam was generated as follows. The 514 nm output from an Ar<sup>+</sup> laser (Spectra-Physics 171) was used to pump rhodamine 590 which served as the lasing medium of a tunable ring dye laser (Spectra-Physics 380D, modified as described by Majewski, *et al.*<sup>33</sup>). The output from the dye laser was doubled externally using a Spectra-Physics Wavetrain frequency doubler, generating a final output power of  $\sim 450$   $\mu$ W in the UV. This beam exhibits a FWHM of less than 1 MHz, was scanned over a few  $\text{cm}^{-1}$  by changing the cavity length with two rotatable quartz plates, and was directed to intersect the molecular beam as described above. Absolute frequency calibrations of the scans were made by comparison with a simultaneously recorded iodine spectrum.<sup>34</sup> Relative frequency calibrations were made with a near-confocal interferometer with a free spectral range of  $299.7520 \pm 0.0005$  MHz in the visible.

To aid with the analysis, quantum chemical calculations were performed using the Gaussian 03 software package.<sup>35</sup> Geometry optimizations were conducted at the MP2/aug-cc-pvdz and M05-2X/6-31+G\* levels of theory. Internal motion of the water molecule was modeled with a potential energy surface scan of the motion of interest at the M05-2X/6-31+G\* level of theory. Additionally, a CIS/6-31+G\* optimization was performed to aid in the characterization of the excited state.

### 3.4 RESULTS

Figure 3-2 shows the rotationally resolved fluorescence excitation spectrum of the origin band of the  $S_1 - S_0$  electronic transition of 7AIW at  $33,340.46 \text{ cm}^{-1}$ .<sup>2</sup> As is apparent, this band is a mainly *a*-type band with a significant amount of *b*-character. It exhibits no tunneling splittings from water motion, unlike the corresponding spectrum of indole-water.<sup>36</sup> Thus, the spectrum of 7AIW could be fit with rigid-rotor Hamiltonians for both states using the program JB95.<sup>37</sup> In the course of the fitting process, it was discovered that the spectrum exhibits axis tilting; several resolved transitions exhibit anomalous line intensities that result from an inertial axis reorientation which occurs on absorption of the photon.<sup>38,39</sup> Some examples of these are shown in Figure 3-3. Incorporating these into the fit, also using JB95, resulted in the inertial parameters listed in Table 3-I. The hybrid band character was determined to be  $87 \pm 2 \%$  *a*-type and  $13 \pm 2 \%$  *b*-type, resulting in an orientation of the electronic transition moment (ETM) vector that lies in the *ab*-plane and makes an angle of  $\theta = \pm 21 \pm 2^\circ$  with respect to the *a* axis. Importantly, it was also found from the fit that the ETM angle  $\theta$  and the axis tilting angle  $\beta$  have opposite signs;  $\beta = \mp 8 \pm 2^\circ$ .



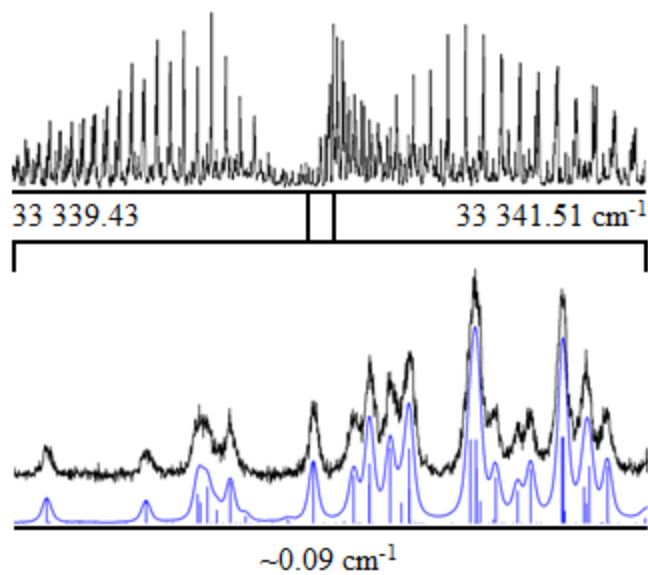


**Figure 3-2. High resolution  $S_1$ - $S_0$  fluorescence excitation spectrum of 7AIW in a molecular beam. Below is a close up view of the spectrum (black) with a simulated spectrum underneath (blue).**

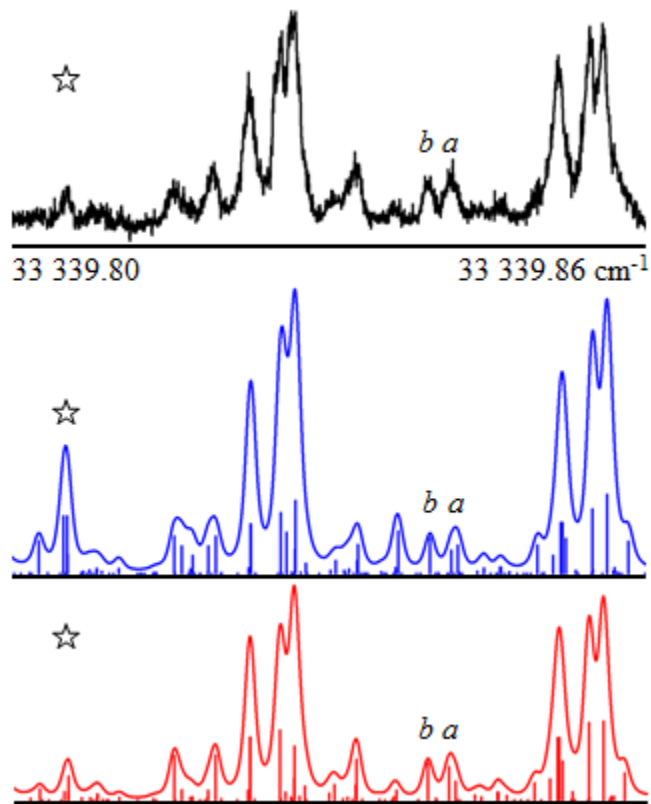


Figure 3-3. Portion of the  $S_1$ - $S_0$  fluorescence excitation spectrum of 7AIW, illustrating the axis tilting observed at full experimental resolution. The  $a/b$  character of the simulations in the bottom panels were normalized to the pure  $a$  and  $b$  transitions shown. The blue spectrum shows the result without including axis tilt, while the red spectrum includes an axis tilt of  $-8^\circ$ . The star highlights a particularly affected transition.

**Table 3-I. Measured inertial parameters of 7-azaindole-H<sub>2</sub>O (7AIW) and 1-deutero-7-azaindole-D<sub>2</sub>O (7-AIW-d<sub>3</sub>) in their S<sub>0</sub> and S<sub>1</sub> electronic states, compared to selected theoretical values.**

Parameter	Experimental 7AIW	Experimental 7-AIW-d <sub>3</sub>	Theoretical (M05-2X/6- 31+G*)	Theoretical (MP2/aug-cc- pvdz)
<b>S<sub>0</sub></b>				
A''(MHz)	1767.0(1)	1740.0(1)	1780.9	1753.53
B''(MHz)	1345.7(1)	1262.5(1)	1352.3	1342.64
C''(MHz)	764.4(1)	732.5(1)	769.5	761.26
ΔI'' (u·Å <sup>2</sup> )	-0.45(3)	-0.78(7)	-0.75	-0.74
<b>S<sub>1</sub></b>				
A'(MHz)	1803.1(1)	1766.2(1)	-	-
B'(MHz)	1360.7(1)	1281.5(1)	-	-
C'(MHz)	776.1(1)	743.7(1)	-	-
ΔI' (u·Å <sup>2</sup> )	-0.54(3)	-0.97(8)	-	-
Origin (cm <sup>-1</sup> )	33 340.46	33 352.11	-	-
<i>a/b/c</i>	87/13/0	75/25/0	-	-
ETM angle(θ)	±21°	±30°	-	-
Axes tilt (α/β/γ)°	0/±8/0	0/±5/0	-	-
Assignments	122	85	-	-
OMC	3.7	3.9	-	-

Individual rovibronic lines in the spectrum exhibit Voigt lineshape profiles with 30 MHz Lorentzian and 30 MHz Gaussian contributions; the calculated lifetime of the  $S_1$  state is 5.3 nsec. The standard deviation of the fit is 3.7 MHz, based on 122 assigned lines.

Similar results were obtained for a deuterated molecule ( $7AI-d$ ), isotopically labeled in position  $H_1$  (see Fig. 3-1) and complexed with  $D_2O$ . The electronic origin band of this species ( $7AIW-d_3$ ) is shifted by  $\sim 12\text{ cm}^{-1}$  to the blue of the corresponding band of  $7AIW$  and is shown at full rotational resolution in Figure 3-4. This spectrum shows all of the characteristics of the origin band of the normal species; it displays both hybrid-band character and axis tilting, and was fit in a similar manner. The inertial parameters resulting from this fit are also listed in Table 3-I. Substitution of deuterium makes a significant change in the hybrid band character ( $75 \pm 3\%$   $a$ -type and  $25 \pm 3\%$   $b$ -type), ETM orientation angle ( $\theta = \pm 30 \pm 3^\circ$ ), and axis tilting angle ( $\phi = \mp 5 \pm 2^\circ$ ). Notably, all rotational constants for  $7AIW-d_3$  are smaller than those for  $7AIW$  itself, as expected from the mass differences between H and D.

Comparisons of these data using Kraitchman's equations<sup>40</sup> make possible the determination of the center-of-mass (COM) positions of each of the substituted atoms in both electronic states. Two different comparisons were made; one between the rotational constants of  $7AI$  and  $7AIW$ , and another between the rotational constants of  $7AI-d_1$ , known from previous work,<sup>5,16</sup> and  $7AIW-d_3$ . What results from this comparison are two estimates (in both electronic states) of the COM positions of a hypothetical particle attached to the  $7AI$  frame that has the same mass as a water molecule. These are listed in Table 3-II. Note that there are significant differences in the derived values in the two electronic states, which suggests that the position of the hydrogen-bonded water molecule changes substantially when the photon is absorbed.

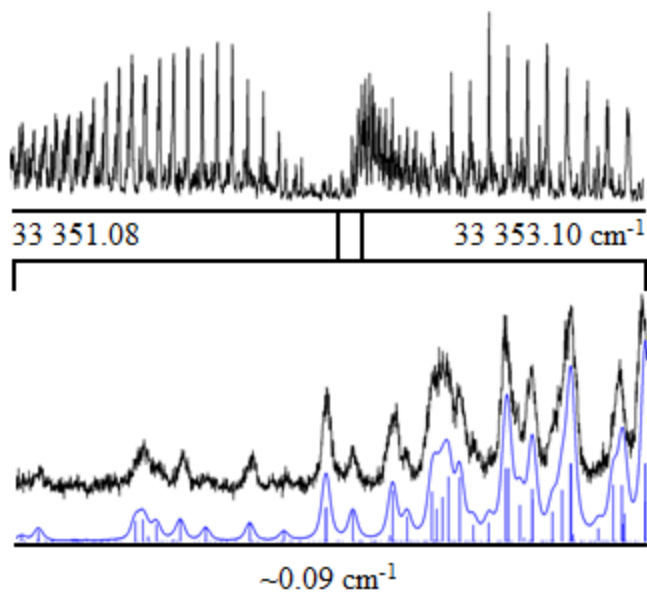


Figure 3-4.  $S_1$ - $S_0$  fluorescence excitation spectrum of 7AIW- $d_3$ . The lower panel shows a close up view of the spectrum (black) with a simulated spectrum underneath (blue).

Table 3-II. Absolute positions of  $H_2O$  (approximated as a point mass) in the single water complex of 7-azaindole in its  $S_0$  and  $S_1$  electronic states.

	7AI frame	7AIW frame
$S_0$		
a''	0.572(1)	3.230(1)
b''	3.839(1)	0.964(1)
c''	0.16(1)	0.050(4)
$S_1$		
a'	0.703(1)	3.045(1)
b'	3.677(1)	1.138(1)
c'	0.17(1)	0.057(4)
	7AI- $d_1$ frame	7AIW- $d_3$ frame
$S_0$		
a''	0.586(1)	3.223(1)
b''	3.825(1)	0.778(1)
c''	0.24(1)	0.070(4)
$S_1$		
a'	0.599(1)	3.186(1)
b'	3.775(1)	0.764(1)
c'	0.22(1)	0.068(4)

Stark-effect spectra of the electronic origin band of  $7\text{AIW}$  also were recorded, and used to deduce values of the magnitudes and orientations of the permanent electric dipole moments (EDM's) of the complex in its ground and excited electronic states. Representative data are shown in Figure 3-5. As is clear from these data, application of a DC electric field to the sample causes transitions observed in the field-free spectrum to split and shift in frequency. These effects were analyzed using a perturbed rigid rotor Hamiltonian for both states; the perturbation terms include the (properly calibrated) electric field strength, the EDM components along each of the inertial axes, and the direction cosines relating the laboratory and molecular frames.<sup>32,41</sup> The EDM's that were determined from these fits are reported in Table 3-III along with selected theoretical values. We find the permanent EDM in the excited state of  $7\text{AIW}$  to be much larger than the corresponding value in the ground state.

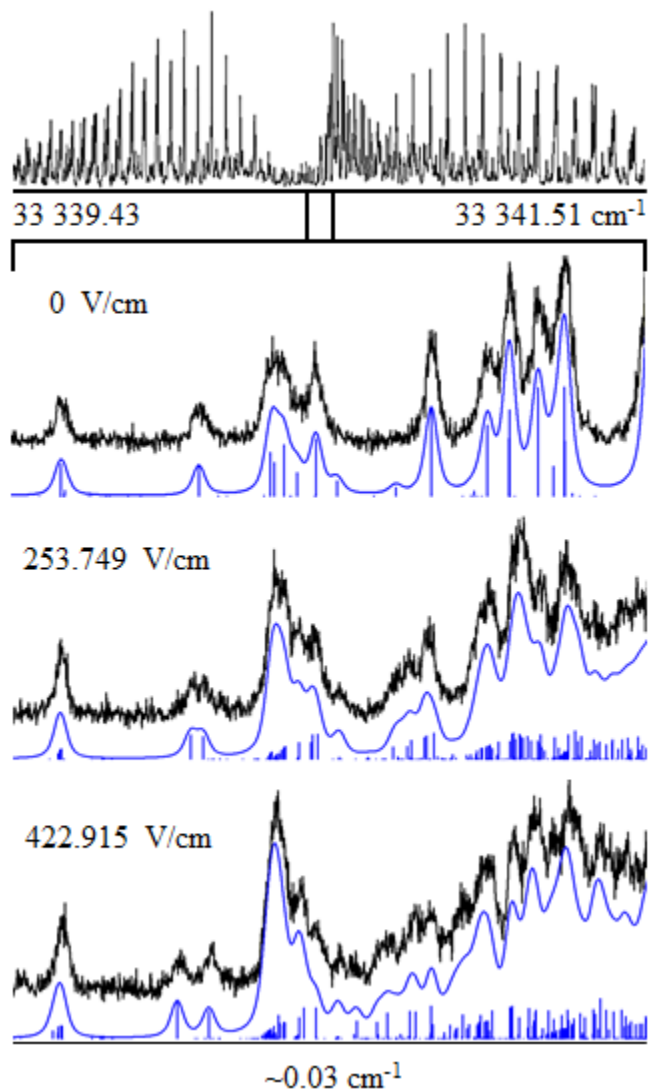
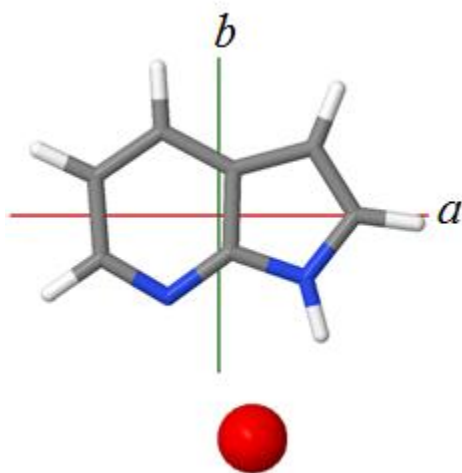


Figure 3-5. Stark spectra of 7AIW. The bottom panel shows a detailed view of the spectra (black) and simulations (blue) at various electric fields.

**Table 3-III. Experimental and theoretical permanent electric dipole moments of 7-azaindole-H<sub>2</sub>O in its S<sub>0</sub> and S<sub>1</sub> electronic states.**

	Experiment	Theoretical (M05-2X/6- 31+G*)	Theoretical (MP2/aug-cc- pvdz)	CIS/6-31+G*	Additive <sup>a</sup>
S <sub>0</sub>					
μ <sub>a</sub> (D)	0.53(6)	0.70	0.59	-	0.36
μ <sub>b</sub> (D)	0.1(3)	-0.10	-0.30	-	0.01
μ <sub>c</sub> (D)	-	1.18	1.01	-	-
μ (D)	0.54(7)	1.37	1.21	-	0.36
S <sub>1</sub>					
μ <sub>a</sub> (D)	-2.00(4)	-	-	-1.18	-0.21
μ <sub>b</sub> (D)	-3.43(8)	-	-	-1.95	-0.63
μ <sub>c</sub> (D)	-	-	-	0.97	-
μ (D)	3.97(5)	-	-	2.47	0.66

<sup>a</sup> Vector sum of the 7AI dipole components (Ref. 17) with  $\langle \mu_{H_2O} \rangle$  in a theoretical structure of 7AIW(M05-2X/6-31+G\*).



**Figure 3-6. Position of the water molecule (when treated as a point mass of 18 amu) determined from a Kraitchman's analysis of the ground state rotational constants of 7AI and 7AIW.**



## 3.5 DISCUSSION

### Structure of 7AIW in the ground and excited electronic states

Figure 3-6 shows the COM position of the water molecule that was derived from the Kraitchman analysis of the ground state rotational constants of 7AI and 7AIW, and 7AI- $d_1$  and 7AIW- $d_3$ , see Table 3-II. Both analyses place the water in close proximity to the two nitrogen atoms of the azaindole ring. Here, it is in a position where it can form two hydrogen bonds, a donor bond to N<sub>7</sub>, and an acceptor bond with the hydrogen atom attached to N<sub>1</sub>, see Fig. 3-1. Being linked to the substrate by two hydrogen bonds prevents the attached water from undergoing the kind of inversion/internal rotation tunneling motion that is exhibited by the (singly-attached) water in the indole-water complex.<sup>36</sup> This ground state geometry is confirmed by a comparison of its theoretical inertial constants with those deduced from the experiment, where good agreement is observed (see Table 3-I), and is consistent with the results of previous studies of this system.<sup>9,19</sup>

The excited state geometry of 7AIW is similar, see Table 3-II. However, a close inspection of these results reveals that the COM of the attached water molecule has moved upon excitation by  $\sim 0.2$  Å, and that this displacement is likely responsible for the observed axis tilt in the rotationally resolved spectrum. This idea was tested as follows. An optimized structure of 7AI was calculated (M05-2X/6-31+G\*),<sup>35</sup> and a point mass with the molecular weight of water was placed in the ground state position given by the Kraitchman analysis. The COM of the system was found, the inertial tensor was calculated and diagonalized, and then all the masses were moved into the 7AIW axis system. Next, the point mass was displaced to its excited state position, and the calculations were repeated. A comparison of the two inertial tensors, one for

the ground state and one for the excited state, showed that one could be transformed into the other by a rotation about the out-of-plane axis of  $-14^\circ$ . This angle has the same sign, but is slightly different in magnitude, from that which was determined from the experiment,  $\beta = -8^\circ$ . (As will be shown later, the sign of  $\theta$  in 7AIW is positive.) The small difference between the two values of  $\beta$  may have its origin in the assumption that the water molecule is a point mass in the Kraitchman's analysis, or in the use of the optimized ground state, rather than excited state, structure. However, the calculation does give evidence that the small photo-induced change of the water molecule's position is responsible for the observed axis tilt.

The experimental inertial defect in the ground state,  $-0.45 \text{ u \AA}^2$ , is smaller than that predicted by the theoretical optimization,  $-0.75 \text{ u \AA}^2$ , but still larger (in magnitude) than zero. The water molecule's out-of-plane hydrogen,  $H_b$ , is the probable source of the nonzero inertial defect; this value increases in magnitude in 7AIW- $d_3$  (see Table 3-I). Thus, a likely explanation for the difference in the observed and calculated values of  $\Delta I$  is that this hydrogen atom takes part in a large amplitude inversion-like motion in and out of the plane. To examine this further, a theoretical scan along the dihedral angle  $\tau$  ( $H_bO-H_aN_7$ ) was performed at the M05-2X/6-31+G\* level of theory. The results are shown in Figure 3-7. They predict a low barrier ( $\sim 40 \text{ cm}^{-1}$ ), suggesting that this hydrogen is indeed undergoing a large amplitude motion in and out of the plane.

A quantitative treatment of this problem was performed as follows. The calculated potential energy surface was represented by a sum of torsional terms of the form

$$V(\tau) = \sum_{n=1}^6 \frac{V_n}{2} (1 - \cos(n\tau)) \quad \text{Equation 3-1}$$

with excellent agreement. Energy levels were calculated using a particle-in-the-ring Hamiltonian and basis of the forms<sup>42</sup>

$$H = -F \frac{d^2}{d\tau^2} + V, \quad \psi(\tau) = \sqrt{\frac{1}{2\pi}} e^{im\tau} \text{ with } m = 0, \pm 1, \pm 2, \dots \quad \text{Equation 3-2}$$

where F is the internal rotor constant. In this case, the internal rotor constant represents the moment of inertia of rotating a water molecule about one of the hydrogen-oxygen bonds, 19.72 cm<sup>-1</sup>, and is similar to that found for the phenol-OH rotation.<sup>43</sup> Finally, the wavefunction,  $\Psi$ , of the zero point energy level was determined using the Rayleigh-Ritz method, where the sum of the squares of the coefficients was normalized to one (for more information see Appendix A). Using this wavefunction, the expectation value,

$$\sqrt{\langle \tau^2 \rangle} = \sqrt{\int_{-\pi}^{\pi} \Psi(\tau)^* \tau^2 \Psi(\tau) d\tau} \quad \text{Equation 3-3}$$

was found to be 38°, which corresponds to an inertial defect of - 0.64 u Å<sup>2</sup>. This expectation value is closer to the experimental value, - 0.45 u Å<sup>2</sup>, reported here. However, the experimental result is still significantly smaller in magnitude than the calculated value, which implies that the barrier for the hydrogen inversion may be even lower than 40 cm<sup>-1</sup>. The similar inertial defect of the excited state (- 0.54 u Å<sup>2</sup>) suggests that its barrier is similar.

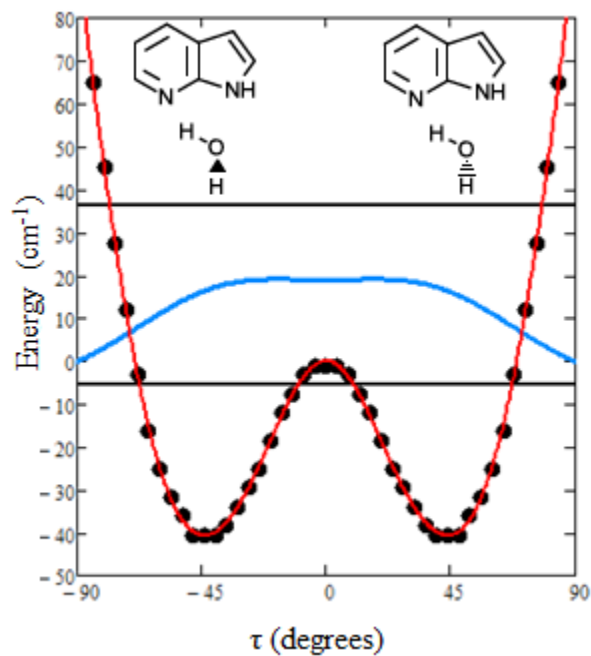


Figure 3-7. Potential energy for water motion. The points were calculated at the M05-2X/6-31+G\* level of theory. The red line shows a functional fit to the torsional terms, with  $V_1 = 7592$ ,  $V_2 = -5313$ ,  $V_3 = 2965$ ,  $V_4 = -1341$ ,  $V_5 = 410$ , and  $V_6 = -72$   $\text{cm}^{-1}$ . The blue curve is the real part of the ground state wavefunction along this coordinate.

## S<sub>1</sub>-S<sub>0</sub> ETM orientation in 7AI

Assignment of the orientation of the S<sub>1</sub>-S<sub>0</sub> electronic transition moment (ETM) in 7AI has been controversial. Most experimental determinations of this quantity using high resolution spectroscopy rely on the expression:<sup>44</sup>

$$\tan^2 \theta = I(b) / I(a) \quad \text{Equation 3-4}$$

where  $I(a)$  and  $I(b)$  are the percent  $a$  and  $b$  characters of an observed (in-plane)  $ab$ -hybrid band and  $\theta$  is the angle between the ETM vector and the  $a$ -inertial axis. Thus, an early study of the S<sub>1</sub>-S<sub>0</sub> rotational contour of the electronic origin band of 7AI by Hassan and Hollas<sup>3</sup> gave an  $ab$ -hybrid band with 93%  $a$ - and 7%  $b$ -type character, resulting in an angle of  $\theta = \pm 15^\circ$ . A later study of 7AIW complexes by Nakajima *et al.*<sup>9</sup> at higher resolution yielded both a magnitude and a sign for the orientation angle,  $\theta = -16 \pm 5^\circ$ . The sign determination was based on the assumption that the electronic distributions in the two electronic states are not significantly affected by complex formation. That the sign of  $\theta$  is negative in the bare molecule was confirmed in two more recent high resolution studies of 7AI and of several of its isotopomers; Schmitt *et al.*<sup>14</sup> found  $\theta = -21^\circ$ , and Kang *et al.*<sup>16</sup> found  $\theta = -14.2 \pm 1.3^\circ$ . But Vu *et al.*<sup>20</sup> state, based on theoretical arguments, that the sign of  $\theta$  should be positive; their DFT/MRCI calculations predict an angle of  $+35^\circ$ .

Three experimental observations made in this work confirm that  $\theta$  is negative in the bare molecule, and that the ETM vector is rotated in a clockwise direction with respect to the  $a$  axis, as shown in Figure 3-8, orientation II (left). First, the  $a$ -type hybrid band character in the S<sub>1</sub>-S<sub>0</sub> origin band of the complex is 87 %, implying that the ETM of 7AIW makes an angle of  $\theta = \pm 21^\circ$  with the  $a$  axis, orientations III and IV in Fig. 3-8 (right). The  $a$ -type band character in the

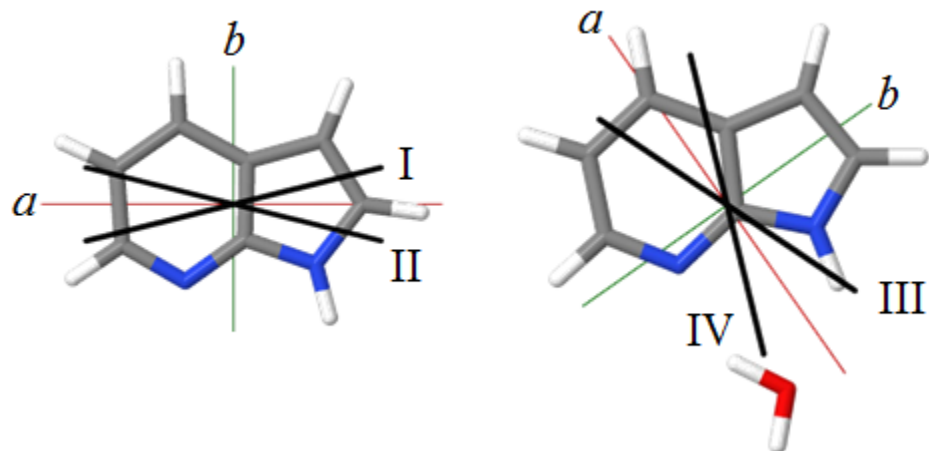


Figure 3-8. Possible  $S_1$ - $S_0$  ETM alignments of 7AI (left) and 7AIW (right).

corresponding spectrum of 7AIW- $d_3$  is 75%, implying  $\theta = \pm 30^\circ$ . Isotopically labeling a theoretical structure leads to the conclusion that the inertial frame of 7AIW- $d_3$  is rotated clockwise by  $8.4^\circ$  with respect to that of 7AIW, the expected result for the larger mass of  $D_2O$  compared to  $H_2O$ . Thus, since the absolute value of  $\theta$  is seen to increase on deuteration, it must be positive (Orientation III is preferred.) Second, our experiments show that the ETM angle and the axis tilting angle in 7AIW have opposite signs. The tilting angle predicted from the Kraitchman analysis (*vide supra*) is negative. Therefore, the ETM angle in the complex is again shown to be positive. And last, the  $a$ -type hybrid band character in the spectrum of the bare molecule is changed from 94 % to 87 % when the water is attached. Adding a water molecule to the theoretical structure of the bare molecule rotates the  $a$  axis in a clockwise direction by nearly  $60^\circ$ . Examination of this structure (see Fig. 3-8) shows that this would eliminate nearly all the  $a$ -character of the spectrum if the ETM angle in 7AI was positive. Thus,  $\theta$  is positive in the complex (Orientation III), and negative in the bare molecule (Orientation II in Fig. 3-8 (left)), in agreement with Vu *et al.*<sup>20</sup> for the complex, but not the bare molecule.

Describing the electronic character of the  $S_1$  state of 7AI can be difficult; however, previous work on indole provides significant insight. The orientations of the ETM's of 7AI and indole itself differ by  $53^\circ$ , when the chromophores are superimposed. This complicates the simple interpretation of their excited states as being pure  $L_a$  or  $L_b$  states, since in the canonical representations of such states the two ETM's make right angles with each other. However, similar ETM rotations of less than  $90^\circ$  have been reported in substituted benzenes<sup>45</sup> where placement of a polar group in the vicinity of the chromophore perturbs the MO's and causes the mixing of  $L_a$  and  $L_b$  states, a likely scenario here. Indole itself has an  $S_1$ - $S_0$  ETM that makes an angle of  $+39^\circ$  with respect to  $a$ .<sup>46</sup> But both indole and 7AI exhibit low lying  $S_1$  vibronic levels

with significantly differently oriented ETM's. The  $454\text{ cm}^{-1}$  band in indole has  $\theta = -32^\circ$ ,<sup>47,48</sup> whereas the  $280\text{ cm}^{-1}$  band in 7AI has  $\theta = +52.7^\circ$ .<sup>16</sup> So, the fact that the  $S_1$ - $S_0$  ETM orientations in indole and 7AI differ by  $\sim 53^\circ$  can only be interpreted to mean that one molecule (7AI) possesses more  $L_a$  character than the other. A change in the character of the prepared state could have significant impact on the rate of ESPT reactions.<sup>49</sup>

### **Charge redistribution in 7AI on complex formation**

As discussed above, the orientation of the  $S_1$ - $S_0$  ETMs of 7AI and 7AIW differ by a large angle,  $25^\circ$ , when the two chromophores are superimposed (see Fig. 3-8), suggesting large charge reorganization on complex formation. That attachment of a single water molecule to the 7AI frame might cause a significant rearrangement of electrons has been apparent since the early low resolution experiments, when it was first learned that the origin band of 7AIW is shifted by  $1290\text{ cm}^{-1}$  to the red of the origin band of the bare molecule.<sup>2</sup> Here, we use the measured dipole moments of the bare molecule and the complex in its two electronic states to explore the reasons for this behavior in greater detail.

Figure 3-9 shows the measured permanent EDM's of 7AIW in its two electronic states and their orientations in the principal axis system of the complex. Also shown in the same coordinate system are the permanent EDM's of 7AI<sup>17</sup> and water,<sup>50</sup> the component parts. As is apparent, the two bare molecules have relatively large EDM's in their ground states, but vector addition of the two components results in a relatively small predicted dipole moment for the complex in its ground state, since they are oriented in opposite directions (Fig. 3-9, left). (This sum is similar in magnitude to the measured dipole moment; its orientation is less well



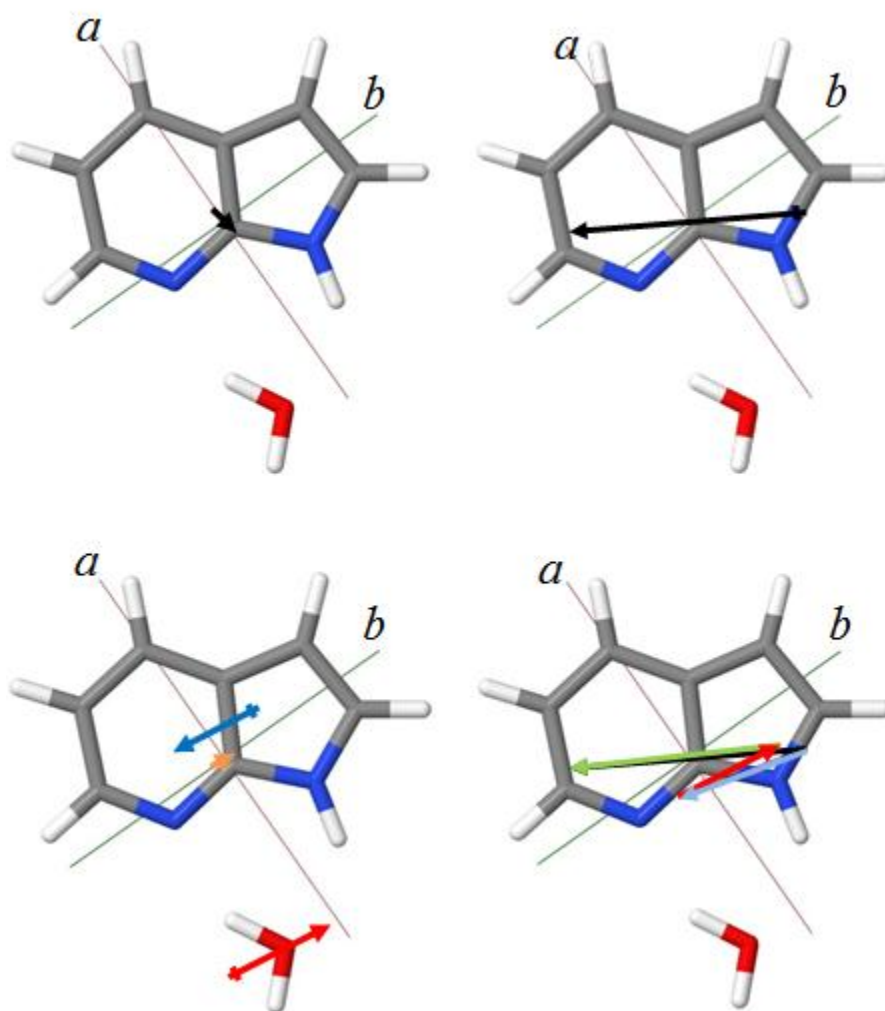


Figure 3-9. The top panels show the experimentally measured EDMs, in the ground (left) and excited states (right). The bottom left panel shows the ground state EDM's of water (red), 7AI (blue) and their sum (orange),  $\mu_{7AI} + \langle \mu_{H_2O} \rangle$ . The bottom right panel shows the component EDMs of water (red) and 7AI\* (blue), as well as a difference dipole (green) between the measured EDM and the vector sum of its components.

determined by the experiment, see Table 3-III.) Systems like these also may have an induced dipole component.<sup>51</sup> However, in this case the induced component of the total dipole moment is likely to be small because the EDM vector of the water molecule is directed nearly orthogonal to the 7AI moiety.

An interesting conclusion is reached when this same vector model is applied to the electronically excited state of 7AIW (Fig. 3-9, right). There, we also show the permanent EDM's of 7AIW and its component parts. The dipole moment of 7AI is substantially increased by excitation, from 1.59 to 2.30 D,<sup>17</sup> but it points in essentially the same direction. So, again, the EDM's of water and 7AI are essentially anti-parallel, and they should largely cancel. A large induced dipole moment is not expected in this case, either. *But the experimentally determined value of the EDM of 7AIW in its electronically excited state is more than seven times larger than that of its ground state, 3.97 vs. 0.54 D.* Clearly, the simple vector model, based on the widely accepted idea that the total dipole moment of a complex is equal to the sum of its component parts, does not apply in the S<sub>1</sub> state of 7AIW.

There are two possible explanations for this result. One is a “cooperative” ESPT reaction. If absorption of light in the UV resulted in the transfer of a proton from N<sub>1</sub> to the water molecule, and from the water molecule to N<sub>7</sub>, then the dipole of the water would be reversed, and the two (now largely parallel) EDM's of water and 7AI would add to produce a significantly larger EDM of the complex, as large as  $1.85 + 3.97 = 5.82$  D if they were exactly aligned. The second possible explanation is that the ESPT reaction does not occur, but that there is substantial charge reorganization within the 7AI molecule itself, a reorganization that results in a separation of charge and a large increase in its permanent EDM. In this case, the water molecule plays the important role of stabilizing the developing “ion-pair” character of the S<sub>1</sub> state. Of the two

explanations, the latter is preferred, since only the enhanced attraction of the two oppositely directed dipoles can explain the observed red shift in the electronic spectrum. If this is correct, then these experiments demonstrate for the first time that electron transfer precedes proton transfer in a PCET reaction.<sup>28-30</sup>

Our quantitative model of this effect is as follows. First, vector addition of the EDM's of the excited state 7AI and the vibrationally-averaged ground state water molecules results in a predicted dipole of 0.66 D for 7AIW in its  $S_1$  state, oriented as shown in Fig. 3-9 (right). Then, this vector was subtracted from the observed EDM vector of the complex, yielding a "difference" dipole (also shown in Fig. 9) that could be attributed to charge transfer. Next, it was assumed that this transfer occurs between the prime acidic and basic sites in the 7AI molecule,  $N_1$  and  $N_7$ . Then, the distance between these two atoms was determined from the M05-2X/6-31+G\* geometry to be 2.40 Å. Finally, taking the projection of the difference dipole onto the  $\overrightarrow{N_1N_7}$  vector and dividing by the distance between these two points, it was found that 0.281 electrons transferred from  $N_1$  to  $N_7$ . Interestingly, this amount of charge transfer is substantially larger than the intermolecular charge transfer deduced from a similar treatment of the acid-base reactions in the photoexcited complexes of 2-naphthol-ammonia ( $0.15e$ )<sup>52</sup> and 2-naphthol-water ( $0.05e$ ).<sup>53</sup>

We next explore whether or not an electrostatic model based on this idea satisfactorily accounts for the observed red shift in the electronic spectrum. The relative energy of the ground state of the complex can be calculated from the dipole-dipole interaction,<sup>54</sup>

$$\Delta U_{S0} = E_{\mu H_2O}^{\mu 7AI} \quad \text{Equation 3-5}$$

The excited state is characterized by two charge-dipole interactions and a dipole-dipole interaction,

$$\Delta U_{S1} = E_{\mu H2O}^{N7^-} + E_{\mu H2O}^{N1^+} + E_{\mu H2O}^{\mu 7AI^*} \quad \text{Equation 3-6}$$

These equations allow a calculation of the difference in the  $S_1 \leftarrow S_0$  excitation energies of 7AI and 7AIW,

$$\Delta U_{excitation} = \Delta U_{S1} - \Delta U_{S0} \quad \text{Equation 3-7}$$

If the dipole of water is then allowed to interact with a charge of  $+ 0.281 e^-$  at the position of  $N_1$ , with a charge of  $- 0.281 e^-$  at the position of  $N_7$ , and with the dipole of 7AI in both states, according to Eqs. (3-5) and (3-6), then Eq. (3-7) yields for the stabilization energy  $\Delta U_{excitation} = -1440 \text{ cm}^{-1}$ . This is comparable to the experimental red-shift,<sup>2</sup>  $1290 \text{ cm}^{-1}$ , confirming the model.

The model may be refined to take into account the large amplitude motion of the attached water molecule in the following way. First, the electrostatic contributions were calculated at selected values of the inversion angle  $\tau$  using M05-2X/6-31+G\* optimized geometries. The results of these calculations are shown in Figure 3-10. Then, the angular dependence of each interaction was reproduced using functions of the form

$$E_{H2O}^{7AI}(\tau) = \sum_{j=1}^3 (u_j \times \cos(j\tau)) + \sum_{k=1}^3 (t_k \times \cos^2(k\tau)) + C \quad \text{Equation 3-8}$$

Finally, expectation values of the dipole-dipole and charge-dipole interactions were calculated using Eqs. (3-9) and (3-10), yielding  $\langle \Delta U_{excitation} \rangle = -1260 \text{ cm}^{-1}$ , in good agreement with experiment:

$$\langle \Delta U_{S0} \rangle = \int_{-\pi}^{\pi} \Psi(\tau)^* E_{\mu H2O}^{\mu 7AI}(\tau) \Psi(\tau) d\gamma \quad \text{Equation 3-9}$$

$$\langle \Delta U_{S1} \rangle = \int_{-\pi}^{\pi} \Psi(\tau)^* (E_{\mu H2O}^{N7-}(\tau) + E_{\mu H2O}^{N1+}(\tau) + E_{\mu H2O}^{\mu 7AI*}(\tau)) \Psi(\tau) d\tau \quad \text{Equation 3-10}$$

The largest sources of error in this calculation are likely to be the use of the ground state geometries to predict the excited state electrostatic interactions as well as the potential energy surface, which may possess too high of a barrier for this motion.

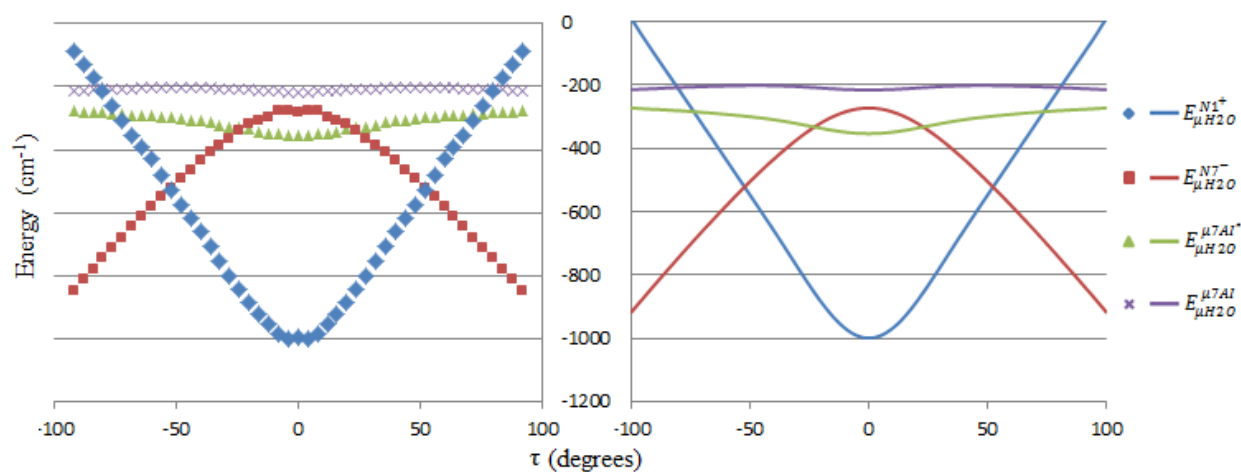


**Figure 3-10.** Calculated electrostatic interactions between ground and excited state 7AI and the water molecule at different values of the inversion angle  $\tau$ , left. On the right are shown functions that were fit to each of the calculated curves.

### 3.6 SUMMARY

Detailed analyses of the high resolution  $S_1$ - $S_0$  electronic spectra of the single water complex of 7-azaindole (7AIW) and a deuterated isotopologue in both the absence and presence of an applied electric field show that irradiation of the complex with UV light results in a significant charge reorganization in its electronically excited state. As a result, the ETM orientation of the complex is rotated by  $25^\circ$  relative to the bare molecule, and the permanent EDM of the complex is increased by nearly an order of magnitude. A simple electrostatic model of these effects suggests that 0.281 electrons are transferred from the acidic  $N_1$  to the basic  $N_7$  sites in 7AIW, thereby quantitatively accounting for the observed red shift ( $-1290\text{ cm}^{-1}$ ) of the electronic spectrum on complex formation. This accord between theory and experiment also shows that no proton transfer occurs within the lifetime of the  $S_1$  state; thus, electron transfer precedes proton transfer in 7AIW.

Recent theoretical work suggests that the proton transfer reaction in this system occurs at a rate of order  $10^{-6}\text{ s}^{-1}$ ,<sup>26</sup> a time scale that is significantly longer than that of our experiments. A plausible explanation for this effect is that properly placed additional solvent molecules are needed to stabilize the charge separation that results from the primary photochemical event. That ESPT reactions might be impeded in the absence of solvent, or in the presence of “improperly” placed solvent molecules, was suggested many years ago by several authors,<sup>55-57</sup> and recently confirmed in analogous high resolution experiments on a similar system.<sup>58</sup>

### 3.7 ACKNOWLEDGEMENTS

We appreciate frequent discussions of this work with A. J. Fleisher and other current group members. Computing time was provided by the Center for Molecular Material Simulations at the University of Pittsburgh. Our research program is supported by NSF (Grant No. CHE-0911117).



### 3.8 WORKS CITED

1. C. A. Taylor, M. A. El-Bayoumi, and M. Kasha, *Proc. Nat. Acad. Sci.* **63**, 253 (1969).
2. K. Fuke, H. Yoshiuchi, and K. Kaya, *J. Phys. Chem.* **88**, 5840 (1984).
3. K. H. Hassan and J. M. Hollas, *J. Mol. Spectrosc.* **138**, 398 (1989).
4. S. K. Kim and E. R. Bernstein, *J. Phys. Chem.* **94**, 3531 (1990).
5. W. Caminati, S. Di Bernardo, and A. Trombetti, *J. Mol. Struct.* **223**, 415 (1990).
6. Y. Chen, R. L. Rich, F. Gai, and J. W. Petrich, *J. Phys. Chem.* **97**, 1770 (1993).
7. Y. Chen, F. Gai, and J. W. Petrich, *Chem. Phys. Lett.* **222**, 329 (1994).
8. M. S. Gordon, *J. Phys. Chem.* **100**, 3974 (1996).
9. A. Nakajima, M. Hirano, R. Hasumi, K. Kaya, H. Watanabe, C. C. Carter, J. M. Williamson, and T. A. Miller, *J. Phys. Chem. A* **101**, 392 (1997).
10. A. S. Smirnov, D. S. English, R. L. Rich, J. Lane, L. Teyton, A. W. Schwabacher, S. Luo, R. W. Thornburg, and J. W. Petrich, *J. Phys. Chem. B* **101**, 2758 (1997).
11. S. Mente and M. Maroncelli, *J. Phys. Chem. A* **102**, 3860 (1998).
12. G. M. Chaban and M. S. Gordon, *J. Phys. Chem. A* **103**, 185 (1999).
13. D. E. Folmer, E. S. Wisniewski, and A. W. Castleman, *Chem. Phys. Lett.* **318**, 637 (2000) and references contained therein.
14. M. Schmitt, C. Ratzer, K. Kleinermanns, and W. L. Meerts, *Mol. Phys.* **102**, 1605 (2004).
15. A. Hara, K. Sakota, M. Nakagaki, and H. Sekiya, *Chem. Phys. Lett.* **407**, 30 (2005).
16. C. Kang, J. T. Yi, and D. W. Pratt, *J. Chem. Phys.* **123**, 094306 (2005).
17. C. Kang, J. T. Yi, and D. W. Pratt, *Chem. Phys. Lett.* **423**, 7 (2006).
18. K. Sakota, N. Inoue, Y. Komoto, and H. Sekiya, *J. Phys. Chem. A* **111**, 4596 (2007).
19. Y. N. Svartsov and M. Schmitt, *J. Chem. Phys.* **128**, 214310 (2008).

20. T. B. C. Vu, I. Kalkman, W. L. Meerts, Y. N. Svartsov, C. Jacoby, and M. Schmitt, *J. Chem. Phys.* **128**, 214311 (2008).
21. H. Sekiya and K. Sakota, *J. Photochem. Photobiol. C* **9**, 81 (2008) and references therein.
22. K. Sakota, Y. Kageura, and H. Sekiya, *J. Chem. Phys.* **129**, 054303 (2008).
23. D. Kina, A. Nakayama, T. Noro, T. Taketsugu, and M. S. Gordon, *J. Phys. Chem. A* **112**, 9675 (2008).
24. K. Sakota, N. Komure, W. Ishikawa, and H. Sekiya, *J. Chem. Phys.* **130**, 224307 (2009).
25. Y. Kageura, K. Sakota, and H. Sekiya, *J. Phys. Chem. A* **113**, 6880 (2009).
26. M. P. T. Duong and Y. Kim, *J. Phys. Chem. A* **114**, 3403 (2010).
27. M. P. T. Duong, K. Park, and Y. Kim, *J. Photochem. Photobiol. A* **214**, 100 (2010).
28. R. I. Cukier and D. G. Nocera, *Annu. Rev. Phys. Chem.* **49**, 337 (1998).
29. C.-C. Hsieh, C.-M. Jiang, and P.-T. Chou, *Accounts Chem. Res.* **43**, 1364 (2010).
30. A. Sirjoosingh and S. Hammes-Schiffer, *J. Phys. Chem. A* **115**, 2367 (2011).
31. D. G. Lister, J. K. Tyler, J. H. Høq, and N. W. Larsen, *J. Mol. Struct.* **23**, 253 (1974).
32. T. M. Korter, D. R. Borst, C. J. Butler, and D. W. Pratt, *J. Am. Chem. Soc.* **123**, 96 (2001).
33. W. A. Majewski, J. F. Pfanstiel, D. F. Plusquellic, and D. W. Pratt, in *Laser Techniques in Chemistry*, A. B. Myers and T. R. Rizzo, Eds. (Wiley, New York, 1995), p. 101.
34. S. Gerstenkorn and P. Luc, *Atlas du spectre d'absorption de la molécule d'iode 14800-20000  $cm^{-1}$*  (CNRS, Paris, 1986).
35. M. J. Frisch, G. W. Trucks, H. B. Schlegel, *et al.*, *Gaussian 03, Revision E.01* (Gaussian, Inc., Wallingford CT, 2004).
36. T. M. Korter, D. W. Pratt, and J. Kuepper, *J. Phys. Chem. A* **102**, 7211 (1998).

37. D. F. Plusquellic, R. D. Suenram, B. Mate', J. O. Jensen, and A. C. Samuels, *J. Chem. Phys.* **115**, 3057 (2001).
38. J. T. Hougen and J. K. G. Watson, *Can. J. Phys.* **43**, 298 (1965).
39. A. Held, B. B. Champagne, and D. W. Pratt, *J. Chem. Phys.* **95**, 8732 (1991).
40. W. Gordy and R. L. Cook, in *Microwave Molecular Spectra* (Wiley-Interscience, New York, 1984).
41. D. M. Miller, P. J. Morgan, and D. W. Pratt, *J. Phys. Chem. A* **113**, 6964 (2009).
42. W. H. Flygare, *Molecular Structure and Dynamics*. (Prentice-Hall, Englewood Cliffs, N.J., 1978).
43. G. Berden, W. L. Meerts, M. Schmitt, and K. Kleinermanns, *J. Chem. Phys.* **104**, 972 (1996).
44. J. M. Hollas, *High Resolution Spectroscopy* (Butterworths, London ; Boston, 1982).
45. R. T. Kroemer, K. R. Liedl, J. A. Dickinson, E. G. Robertson, J. P. Simons, D. R. Borst, and D. W. Pratt, *J. Am. Chem. Soc.* **120**, 12573 (1998).
46. T. M. Korter, J. Kuepper, and D. W. Pratt, *J. Chem. Phys.* **111**, 3946 (1999).
47. C. Brand, J. Kuepper, D. W. Pratt, W. L. Meerts, D. Kruegler, J. Tatchen, and M. Schmitt, *Phys. Chem. Chem. Phys.* **12**, 4968 (2010).
48. J. Kuepper, D. W. Pratt, W. L. Meerts, C. Brand, J. Tatchen, and M. Schmitt, *Phys. Chem. Chem. Phys.* **12**, 4980 (2010).
49. K. Sakota and H. Sekiya, *J. Phys. Chem. A* **113**, 2663 (2009).
50. S. A. Clough, Y. Beers, G. P. Klein, and L. S. Rothman, *J. Chem. Phys.* **59**, 2254 (1973).
51. C.-H. Kang, T. M. Korter, and D. W. Pratt, *J. Chem. Phys.* **122**, 174301 (2005).
52. A. J. Fleisher, P. J. Morgan, and D. W. Pratt, *J. Chem. Phys.* **131**, 211101 (2009).

53. A. J. Fleisher, J. W. Young, D. W. Pratt, A. Cembran, and J. Gao, *J. Chem. Phys.* **134**, 114304 (2011).
54. G. C. Maitland, *Intermolecular Forces: Their Origin and Determination* (Clarendon Press, Oxford, 1981).
55. P.-T. Chou, M. L. Martinez, and J. H. Clements, *J. Phys. Chem.* **97**, 2618 (1993).
56. T. C. Swinney and D. F. Kelley, *J. Chem. Phys.* **99**, 211 (1993).
57. A. Sytnik, D. Gormin, and M. Kasha, *Proc. Natl. Acad. Sci.* **91**, 11968 (1994).
58. P. J. Morgan, A. J. Fleisher, V. Vaquero-Vara, D. W. Pratt, R. P. Thummel, M. Kijak, and J. Waluk, submitted.

**4.0 EXCITED ELECTRONIC STATE MIXING IN 7-AZAINDOLE.  
QUANTITATIVE MEASUREMENTS USING THE STARK EFFECT**

Justin W. Young and David W. Pratt

To be submitted to *Chemical Physics Letters*

JWY produced the experimental results, analyzed the results and performed the theoretical calculations. JWY and DWP wrote the paper.

## 4.1 ABSTRACT

Stark effect measurements of the +280  $\text{cm}^{-1}$  vibronic band in the high resolution  $S_1$ - $S_0$  fluorescence excitation spectrum of 7-azaindole in a molecular beam show that the excited state permanent electric dipole moment (EDM) of the upper vibrational level is 4.6 D, twice as large as the EDM of the zero-point level of the  $S_1$  state. This large difference is attributed to state mixing with the more polar  $S_2$  state. A classical polarizability model was implemented to estimate how much energy is required to polarize the electronic origin's EDM to resemble the +280  $\text{cm}^{-1}$  band's. The energy predicted from this analysis is 258  $\text{cm}^{-1}$ , suggesting that the higher vibronic band terminates in a level that contains substantial  $S_2$  character, and perhaps is the origin of this state.

## 4.2 INTRODUCTION

The presence of rapid relaxation pathways in biological chromophores is thought to be a consequence of an evolutionary means to protect cells, DNA and proteins from radiative damage. Numerous investigators have focused research on the mechanism of such processes. For instance, research on the amino acids tryptophan and tyrosine has found that these chromophores may relax to the ground state through conical intersections along a hydrogen atom dissociation coordinate.<sup>1,2,3</sup> Having this knowledge, it may not be surprising to learn that many of the electronic transitions of indole, the chromophore of tryptophan, show electronic state mixing as much as  $\sim 1000 \text{ cm}^{-1}$  below the second excited state.<sup>4</sup>

As a result of tryptophan's low quantum yield, the 7-azaindole chromophore has been used as a fluorescent tag as an alternative to tryptophan.<sup>5</sup> While structurally similar to indole, this molecule possess a longer lifetime and a higher quantum yield than tryptophan. This use has initiated much of the spectroscopic research on 7-azaindole.<sup>6-16</sup> Its lowest electronically excited singlet state is the  $L_b$  state, analogous to indole. But early high resolution experiments showed that the  $S_1$ - $S_0$  electronic transition moment (ETM) of the  $+280\text{ cm}^{-1}$  vibronic band is oriented very differently from that of the origin band, indicating a significantly different electronic distribution.<sup>8</sup> Later IR experiments showed that the N-H bond strength of the  $+280\text{ cm}^{-1}$  vibrational level in the  $S_1$  state is significantly less than in other vibrational levels of this state.<sup>17</sup> Two explanations were proposed to explain these results. One is that  $S_1$  excitation leads to proton transfer from the pyrrole to the pyridine ring. The second explanation is that this band is a mixed band with more  $L_a$  character than the rest of the bands.

Here, we will examine the properties of the  $+280\text{ cm}^{-1}$  vibrational level in the  $S_1$  state of 7-azaindole, using high resolution electronic spectroscopy coupled with the Stark effect. Information on the structure will be inferred through the rotational constants. Furthermore, the excited state dipole moment will be measured through the use of the Stark effect, and compared to previous measurements on the electronic origin band.<sup>9</sup>

### 4.3 EXPERIMENTAL

Spectroscopic measurements were made with a molecular beam laser spectrometer. Here, the sample, 7AI (> 99%) purchased from Sigma-Aldrich and used without further purification, was placed in the first of three chambers inside a quartz source. The chambers were divided by a layer of quartz with a ~ 5 mm hole connecting the chambers. Each chamber was held at increasingly higher temperatures to prevent condensation. The final chamber of the source terminated in a ~ 200  $\mu\text{m}$  diameter nozzle. Then, when the sample was heated to ~ 100° C and argon carrier gas (at 300 Torr) was passed over it, the seeded carrier gas was expanded through the nozzle into the first chamber of the differentially pumped vacuum system creating a supersonic jet. This expansion was skimmed 2 cm downstream, forming a molecular beam leading into the second vacuum chamber. The molecular beam was then intersected orthogonally by a focused ultraviolet laser beam tuned in wavelength to a particular band in the absorption spectrum of 7-azaindole. Resonant fluorescence was collected with spherical optics, detected with a photomultiplier tube and recorded using jba acquisition software.

The exciting laser beam was generated from all lines of a continuous wave  $\text{Ar}^+$  laser (Spectra-Physics 171) pumping rhodamine 590 laser dye which served as the lasing medium of a tunable ring dye laser (Spectra-Physics 380D).<sup>18</sup> The visible output of the ring dye laser was coupled into an external frequency doubler (Spectra-Physics Wavetrain) generating ultraviolet light. This set up yielded ~ 400  $\mu\text{W}$  of power and a ~ 1 MHz linewidth. During scans, an iodine spectrum was recorded simultaneously to perform an absolute frequency calibration. Similarly, relative frequency calibrations were made using frequency markers from a near-confocal etalon having a free spectral range of  $299.7520 \pm 0.0005$  MHz.



Stark-effect measurements were performed by recording spectra in the presence of an applied homogenous electric field. The electric field was generated by applying opposite voltages to two stainless steel flat wire mesh grids placed within the spherical mirrors above and below the intersection of the molecular and laser beams. In this arrangement, the electric field and polarization of the laser beam are perpendicular, resulting in the selection rule  $\Delta M = \pm 1$ . The spacing between the plates was calibrated using the known dipole moments of aniline.<sup>19,20</sup>

*Ab initio* calculations for comparison to the experimental measurements were performed using the Gaussian 03 software package.<sup>21</sup>

#### 4.4 RESULTS

Figure 4-1 shows the rotationally resolved fluorescence excitation spectrum of the 0,0 +280  $\text{cm}^{-1}$  band of 7-azaindole, at 34910.5  $\text{cm}^{-1}$  ( $\sim 286$  nm). The spectrum consists of roughly 8,000 rovibrational transitions spanning  $\sim$  three wavenumbers. The observed transitions exhibit *a* and *b* type selection rules; the presence of *a*-type transitions is discernible from the central Q-branch. Similar to the origin band, the spectrum was simulated using ground and excited state rigid rotor Hamiltonians included in the JB95 fitting program.<sup>22</sup> The spectrum was fit with 90 assigned lines, resulting in a standard deviation of 3.00 MHz and a rotational temperature of  $\sim 6.5$  K. The fitting parameters are listed in Table 4-I. The *a/b* hybrid band character was determined to be 27.1 / 72.9 %, corresponding to an in-plane electronic transition moment (ETM) that makes an angle of 58.6 degrees or -58.6 degrees with the *a*-inertial axis. A Voigt profile of 60 MHz Lorentzian and Gaussian contributions were used to simulate the lineshapes of individual rovibronic lines in the spectrum.

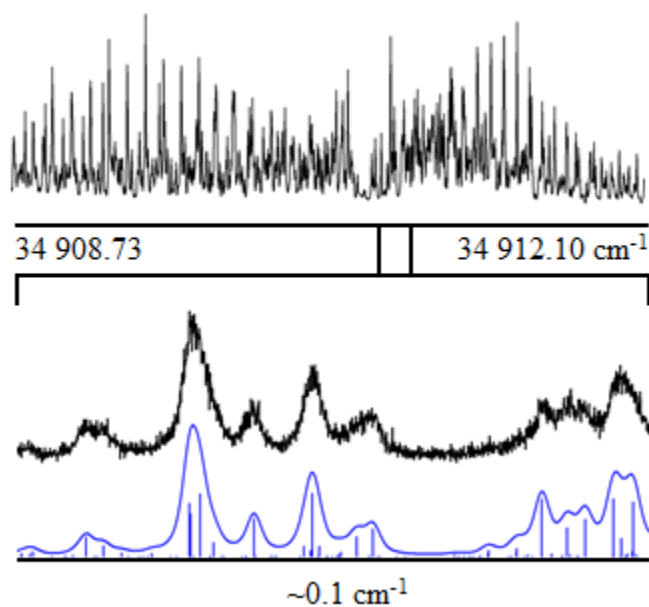


Figure 4-1. Rotationally resolved fluorescence excitation spectrum of the +280 cm<sup>-1</sup> band in the S<sub>1</sub>-S<sub>0</sub> electronic transition of 7-azaindole in a molecular beam. The upper panel shows an over view of the entire spectrum. The lower panel shows a portion of the spectrum at full resolution (black) with the simulated spectrum underneath, with and without a Voigt profile.

Table 4-I. Experimental inertial parameters of the 7AI  $S_1 \leftarrow S_0$  origin band and the +280  $\text{cm}^{-1}$  band.

Parameter	Experimental 7AI origin band <sup>a</sup>	Experimental 7-AI +280 $\text{cm}^{-1}$
$S_0$		
$A''$ (MHz)	3928.3(2)	3928.6(1)
$B''$ (MHz)	1702.5(1)	1702.45(6)
$C''$ (MHz)	1188.2(1)	1188.13(4)
$\Delta I''$ ( $\text{u} \cdot \text{\AA}^2$ )	-0.16(3)	-0.14(2)
$S_1$		
$A'$ (MHz)	3744.4(1)	3818.5(1)
$B'$ (MHz)	1701.7(1)	1687.90(6)
$C'$ (MHz)	1170.5(1)	1171.17(5)
$\Delta I'$ ( $\text{u} \cdot \text{\AA}^2$ )	-0.20(3)	-0.25(2)
Origin ( $\text{cm}^{-1}$ )	~34 630	34 970.40 (1)
$a/b/c$	87/13/0	27.1/72.9/0
ETM angle( $\theta$ )	$\pm 21^\circ$	$\pm 58.6^\circ$
Assignments	-	90
OMC	-	3.00

<sup>a</sup>Ref. 9.

Stark-effect spectra of the  $+280\text{ cm}^{-1}$  band are shown in Figure 4-2. The electric field's effect on the spectra is clearly exhibited there; shifts and splittings of several of the rovibrational lines are observed due to the interaction of the electric field with the permanent electric dipole moment (EDM) of the isolated molecule in the two electronic states. Several spectra were recorded in the presence of fields ranging from 85 to 592 V/cm; these were analyzed and fit using perturbed rigid-rotor Hamiltonians. The perturbation terms included the calibrated electric field strength, the EDM component along each of the inertial axes in the both the ground and excited states, and the direction cosines relating the laboratory and inertial frames. Fitting procedures focused on adjusting the EDM contributions to reproduce the Stark-effect spectra. The results of this analysis are listed in Table 4-II.

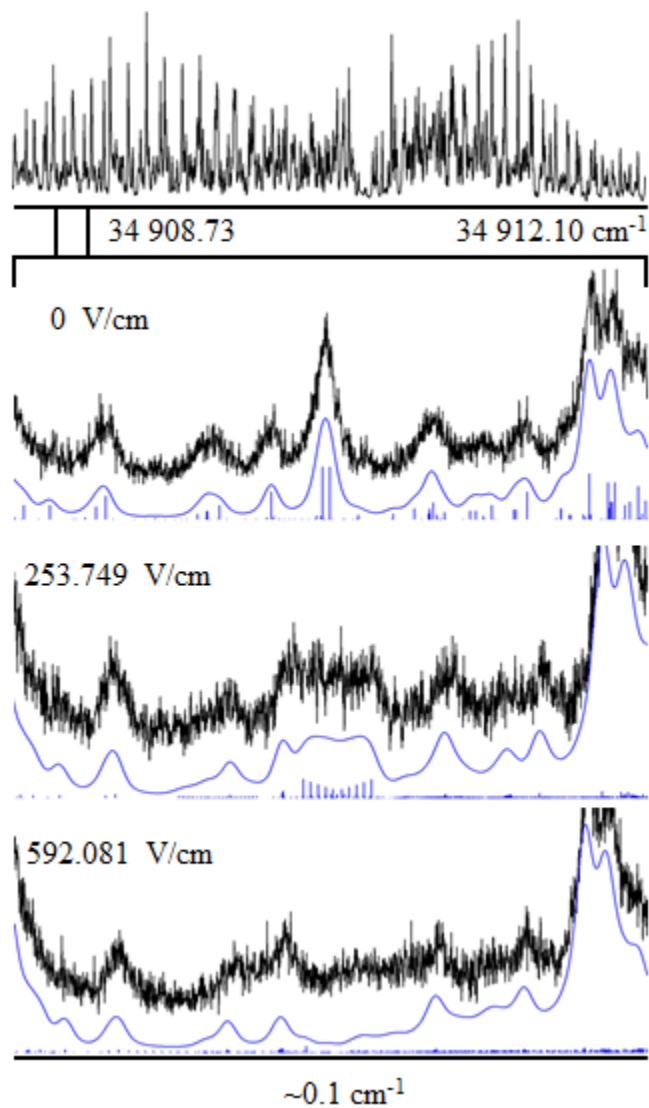


Figure 4-2. Stark-effect spectra of the  $+280 \text{ cm}^{-1}$  band in the  $S_1$ - $S_0$  electronic transition of 7Al, measured at the designated electric field values.

**Table 4-II. Measured and calculated permanent electric dipole moments of 7AI in its ground and excited electronic states.**

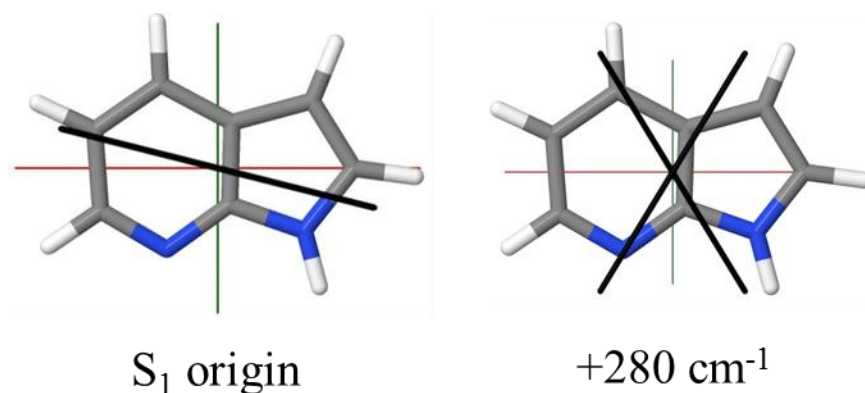
	Experiment $S_1 \leftarrow S_0$ 7AI <sup>a</sup>	Experiment +280 cm <sup>-1</sup> 7AI	Theoretical <sup>b</sup> $\pi\pi^*$ $S_1$	Theoretical <sup>b</sup> $\pi\sigma^*$	Theoretical <sup>b</sup> $\pi\pi^*$	Theoretical <sup>b</sup> 7H- Tautomer
Ground						
$\mu_a$ (D)	1.45(1)	1.45(1) <sup>a</sup>	-	-	-	
$\mu_b$ (D)	0.65(6)	0.65(6) <sup>a</sup>	-	-	-	
$\mu_c$ (D)	-	-	-	-	-	
$\mu$ (D)	1.59(3)	1.59(3) <sup>a</sup>	-	-	-	
Excited						
$\mu_a$ (D)	2.23(4)	4.29(2)	3.45	-7.26	2.73	-0.04
$\mu_b$ (D)	0.55(8)	-1.6(3)	0.42	-3.80	-0.77	0.16
$\mu_c$ (D)	-	-	-	-	-	0
$\mu$ (D)	2.30(3)	4.6(1)	3.47	8.19	2.84	0.16

<sup>a</sup>Ref. 9.

<sup>b</sup>Calculated using CIS/6-31+G\*.

## 4.5 DISCUSSION

Examination of the data in Table 4-I shows that both the origin band and the  $+280\text{ cm}^{-1}$  band of 7-azaindole originate from the same conformation of the ground state since their  $S_0$  inertial parameters are indistinguishable, within experimental error. However, the nature of the two bands is very different. One distinguishing feature is the orientation of their ETM's; see Scheme 4-I.<sup>8,10</sup> The ETM angle in the origin band is  $-14.2^\circ$  whereas the ETM angle in the vibronic band is  $\pm 58.6^\circ$ . The difference in the two orientations is large, either  $44.4$  or  $72.8^\circ$ , and must be a consequence of a difference in the electronic structure of the two upper states of these vibronic transitions.



**Scheme 4-1**

The second important difference is in the value of the rotational constants of the vibrational levels that are accessed in the two transitions, see Table 4-I. The A value of the level reached in the  $+280\text{ cm}^{-1}$  band is 74 MHz larger than that of the state reached in the origin band, whereas the B value is 14 MHz smaller and the C value is nearly the same. Consequently, the

magnitude of the inertial defect in the higher vibrational level is larger than that in the lower vibrational level, suggesting some significant out-of-plane distortion when exciting the +280  $\text{cm}^{-1}$  band.

The third important difference is in the value of the excited state EDM's of the vibrational levels that are accessed in the two transitions, 2.30 D for the origin band and 4.6 D for the +280  $\text{cm}^{-1}$  band, see Table 4-II. Both values are larger than that of the ground state, 1.59 D. But the EDM of the upper state vibrational level accessed in the +280  $\text{cm}^{-1}$  band is twice as large as the EDM of the zero-point vibrational level of the  $S_1$  state, see Appendix B for an image.

One possible explanation for these effects is that the +280  $\text{cm}^{-1}$  band induces excited state intramolecular proton transfer from the pyrrole nitrogen to the pyridine nitrogen, resulting in a proton-transferred structure. Similar phenomena have been observed in a number of indole-related species.<sup>2,3,12</sup> A proton-transferred structure should have different rotational constants, since the process should be accompanied by a significant rearrangement of electrons and could result in changes in many bond angles and distances. However, it is not clear why this would lead to a significant out-of-plane distortion of the isolated molecule. Proton transfer could affect the electron density of the chromophore enough to change the orientation of its  $S_1$ - $S_0$  ETM. Similarly, one would expect proton transfer to drastically affect the permanent EDM of the electronically excited state. However, theoretical calculations predict that the proton-transferred structure would possess a small EDM moment ( $\sim 0.2$  D), clearly distinguishable from the observed 4.6 D EDM of the +280  $\text{cm}^{-1}$  band (see Table 4-II). Thus, the observed effects do not support the idea that the minimum energy structure reached on absorption of the photon in the +280  $\text{cm}^{-1}$  band is a proton-transferred species.



Two other possible explanations for these effects are that the +280 cm<sup>-1</sup> band is the origin of the S<sub>2</sub> state, or is a mixed state containing both S<sub>1</sub> and S<sub>2</sub> character. CIS/6-31+G\* calculations suggest that the S<sub>1</sub>/S<sub>2</sub> gap in 7-azaindole is at least 1000 cm<sup>-1</sup>.<sup>13</sup> Thus, it is doubtful that the +280 cm<sup>-1</sup> transition is the origin of the S<sub>2</sub> state. However, indole, a similar molecule, also exhibits large fluctuations in its rotational constants and ETM orientations among several of the S<sub>1</sub>-S<sub>0</sub> vibronic bands that have been studied at high resolution.<sup>4</sup> A DFT/MRCI theoretical study<sup>2,3</sup> of these effects revealed that a conical intersection connecting the S<sub>1</sub> and S<sub>2</sub> states lies approximately 2000 cm<sup>-1</sup> above the S<sub>1</sub> minimum, and that this intersection can be accessed to varying degrees *via* different Herzberg-Teller (HT) active modes, affecting their spectroscopic properties. The differences in the rotational constants and ETM orientation observed in 7-azaindole are comparable in magnitude to those observed in the previous work on indole. Thus, we believe that the “anomalous” properties of the +280 cm<sup>-1</sup> band in 7-azaindole are the result of S<sub>1</sub>/S<sub>2</sub> state mixing. As in indole, the two lowest ππ\* states are believed to undergo HT coupling; however, additional mixing with a low lying σπ\* state also is a possibility. One intriguing difference between the two molecules is that an out-of-plane mode appears to be involved in 7-azaindole, whereas the HT-active modes in indole are in-plane modes.

Unfortunately, the CIS/6-31+G\* calculations performed to date are unable to reproduce the observed large increase in the EDM of the excited state +280 cm<sup>-1</sup> vibrational level; see Table 2. But such an increase is expected from previous condensed phase studies of similar molecules. Thus, both experiment and theory suggest that the S<sub>1</sub> state of indolic systems is the <sup>1</sup>L<sub>b</sub> state, and that the S<sub>2</sub> state is the <sup>1</sup>L<sub>a</sub> state. Solvatochromic studies have shown that <sup>1</sup>L<sub>a</sub> states are significantly more polar than <sup>1</sup>L<sub>b</sub> states.<sup>23-26</sup> “Pure” <sup>1</sup>L<sub>b</sub> states have negatively oriented ETM’s, whereas “pure” <sup>1</sup>L<sub>a</sub> states have positively oriented ETM’s. Thus, the observed

difference in the orientation of the ETM's of the two bands, and the observed large increase in the EDM of the upper vibronic level in the +280 cm<sup>-1</sup> band, compared to the origin band, is also believed to be a consequence of state mixing, since this level has more <sup>1</sup>L<sub>a</sub> character than the zero-point level of the S<sub>1</sub> state. The factor of two increase in **μ** provides a quantitative estimate of the degree of this mixing in the isolated molecule.

It was intriguing to see if the 280 cm<sup>-1</sup> energy difference between the two bands is quantifiable through classical means. To test this idea, a simple novel approach was implemented. First, the polarizability ( $\alpha$ ) of the S<sub>1</sub> state was calculated using the CIS/6-31+G\* level of theory and basis set. Then, using the measured difference in the S<sub>1</sub> and S<sub>2</sub> EDM's ( $\Delta\mu$ ), the hypothetical electric field ( $\epsilon$ ) that would be required to polarize the zero-point level so that its EDM was equal to that of the +280 cm<sup>-1</sup> level was found using Eq. (4-1):

$$\epsilon = \alpha^{-1} \Delta\mu \quad \text{Equation 4-1}$$

The difference in energy of the two states, with and without the field, is then given by Eq. (4-2),

$$\Delta E = \frac{1}{2} \alpha \epsilon^2 \quad \text{Equation 4-2}$$

yielding an energy difference of  $\Delta E = 258 \text{ cm}^{-1}$ , relatively close to the experimentally observed value of 280 cm<sup>-1</sup>.

## 4.6 SUMMARY

High resolution electronic spectroscopy in a molecular beam, both in the absence and presence of an applied electric field, has been used to show that the permanent electric dipole

moment (EDM) of the upper state level in the  $0,0 +280 \text{ cm}^{-1}$  band in the  $S_1$ - $S_0$  transition of 7-azaindole is larger by a factor of two than the EDM of the zero-point level of the  $S_1$  state. Both EDM's are significantly larger than that of the ground state. These differences, as well as previously measured differences in rotational constants, N-H stretching frequencies, and electronic transition moment orientations, have been attributed to state mixing of the zero-order  $S_1$  ( $^1L_b$ ) and  $S_2$  ( $^1L_a$ ) states by Herzberg-Teller coupling *via* an out-of-plane vibrational mode. A classical electrostatics model shows that the energy difference between the two states is similar to the energy that would be required to polarize the electronic origin band so that the two bands in question have the same dipole moments.

#### 4.7 ACKNOWLEDGEMENTS

We would like to thank the Center for Molecular and Material Simulations at the University of Pittsburgh for computing time. Our research program is supported by NSF (Grant No. CHE-0911117).

## 4.8 WORKS CITED

1. A. L. Sobolewski, W. Domcke, C. Dedonder-Lardeux, and C. Jouvet, *Phys. Chem. Chem. Phys.* **4**, 1093 (2002).
2. M. N. R. Ashfold, B. Cronin, A. L. Devine, R. N. Dixon, and M. G. D. Nix, *Science* **312**, 1637 (2006).
3. M. N. R. Ashfold, A. L. Devine, R. N. Dixon, G. A. King, M. G. D. Nix, and T. A. A. Oliver, *Proc. Natl. Acad. Sci.* **105**, 12701 (2008).
4. C. Brand, J. Küpper, D.W. Pratt, W. L. Meerts, D. Krugler, J. Tatchen, and M. Schmitt, *Phys. Chem. Chem. Phys.* **12**, 4968 (2010); J. Küpper, D. W. Pratt, W. Leo Meerts, C. Brand, J. Tatchen, and M. Schmitt, *Phys. Chem. Chem. Phys.* **12**, 4980 (2010).
5. C. A. Taylor, M. A. El-Bayoumi, and M. Kasha, *Proc. Nat. Acad. Sci. U. S. A.* **63**, 253 (1969).
6. Y. Chen, R. L. Rich, F. Gai, and J. W. Petrich, *J. Phys. Chem.* **97**, 1770 (1993).
7. W. Caminati, S. Di Bernardo, and A. Trombetti, *J. Mol. Struct.* **223**, 415 (1990).
8. C. Kang, J. T. Yi, and D. W. Pratt, *J. Chem. Phys.* **123**, 094306 (2005).
9. C. Kang, J. T. Yi, and D. W. Pratt, *Chem. Phys. Lett.* **423**, 7 (2006).
10. M. Schmitt, C. Ratzer, K. Kleinermanns, and W. L. Meerts, *Mol. Phys.* **102**, 1605 (2004).
11. K. Fuke and K. Kaya, *J. Phys. Chem.* **93**, 614 (1989).
12. K. Fuke, H. Yoshiuchi, and K. Kaya, *J. Phys. Chem.* **88**, 5840 (1984).
13. Y. N. Svartsov and M. Schmitt, *J. Chem. Phys.* **128**, 214310 (2008).
14. C. Vu Thi Bao, I. Kalkman, W. L. Meerts, Y. N. Svartsov, C. Jacoby, and M. Schmitt, *J. Chem. Phys.* **128**, 214311 (2008).
15. J. W. Young and D. W. Pratt, *J. Chem. Phys.* **135**, 084301 (2011).

16. R. S. Moog and M. Maroncelli, *J. Phys. Chem.* **95**, 10359 (1991).
17. K. Sakota and H. Sekiya, *J. Phys. Chem. A* **113**, 2663 (2009).
18. W. A. Majewski, J. F. Pfanstiel, D. F. Plusquellic, and D. W. Pratt, in *Laser Techniques in Chemistry*, A. B. Myers and T. R. Rizzo, Eds. (Wiley, New York, 1995), 101.
19. D. G. Lister, J. K. Tyler, J. H. Høq, and N. W. Larsen, *J. Mol. Struct.* **23**, 253 (1974).
20. T. M. Korter, D. R. Borst, C. J. Butler, and D. W. Pratt, *J. Am. Chem. Soc.* **123**, 96 (2001).
21. M. J. Frisch, G. W. Trucks, H. B. Schlegel, et al. Gaussian 03, Gaussian, Inc., Wallingford CT, 2004.
22. D. F. Plusquellic, R. D. Suenram, B. Mate', J. O. Jensen, and A. C. Samuels, *J. Chem. Phys.* **115**, 3057 (2001).
23. E.H. Strickland, J. Horowitz, and C. Billups, *Biochemistry* **9**, 4924 (1970).
24. E.H. Strickland, J. Horowitz, and C. Billups, *Biochemistry* **11**, 3657 (1972).
25. E.H. Strickland, and J. Horowitz, *Biopolymers* **12**, 1989 (1973).
26. M. Martinaud, and A. Kadiri, *Chem. Phys.* **28**, 473 (1978).

**5.0 USING HIGH RESOLUTION ELECTRONIC SPECTROSCOPY TO PROBE  
THE EFFECTS OF RING TWIST ON CONJUGATION AND ELECTRON TRANSFER  
IN 2-PHENYLINDOLE AND N-PHENYLCARBAZOLE**

Justin W. Young, Vanesa Vaquero-Vara, John T. Yi, Leonardo Alvarez-Valtierra,  
and David W. Pratt

To be submitted to *Nature Chemistry*.

VVV recorded and analyzed the microwave spectrum of 2-phenylindole. JTY and JWY recorded the spectrum of N-phenylcarbazole. LAV helped in the laboratory. JWY recorded and analyzed the fluorescence excitation spectra of 2-phenylindole and carbazole, and stark spectra of N-phenylcarbazole. JWY and DWP wrote the paper.

## 5.1 ABSTRACT

High resolution electronic spectra of 2-phenylindole (PI) and N-phenylcarbazole (PC) have been recorded in the collision-free environment of a molecular beam. Inertial defects determined from fits of the spectra were used to determine the twist angles between the two chromophores and their attached phenyl groups in the ground ( $S_0$ ) and excited ( $S_1$ ) electronic states. PI was found to be significantly more planar than PC, especially in the  $S_1$  state. Stark-effect measurements of their permanent electric dipole moments show that  $S_1$ - $S_0$  excitation of PC is largely localized on the carbazole portion of the molecule. The corresponding excitation of PI involves both parts of the molecule, thereby explaining its more planar nature in the  $S_1$  state.

## 5.2 INTRODUCTION

The conjugation present in aromatic molecules provides a class of species with intriguing properties, making possible numerous applications which present themselves naturally in biological systems and deliberately in engineered chemical systems. Particularly useful and intriguing are the photo-absorption properties of conjugated  $\pi$  systems and their ability to transport electric charge, allowing conjugated  $\pi$  systems to be implemented as antennae and molecular wires. Recent applications of these ideas include the use of oligo (phenylethynyl) bridges,<sup>1</sup> conjugated polymers,<sup>2</sup> and nano-sized graphene sheets<sup>3</sup> as molecular wires to improve electron transfer to attached electrodes.

Similar research has focused on photo-induced charge transfer events occurring within relatively small conjugated systems. In such a scheme, a molecule possessing an aromatic ring is

photo-excited, and then donates or accepts an electron to or from other parts of the molecule, or to neighboring species. Perhaps the most widely cited example of this behavior is found in 4,4'-dimethylaminobenzonitrile (DMABN), where it is believed that photo-excitation causes an electron to transfer from the DMA group to the BN portion of the molecule. The DMA group then appears to twist relative to the plane of the phenyl ring, removing conjugation between the two component parts and preventing back transfer of the electron.<sup>4,5</sup>

The role of twisting in charge transfer events, and the formation of electronically excited states called twisted intramolecular charge transfer (TICT) states, is an often debated topic.<sup>6,7</sup> In this report, we describe a comparative study of the properties of two molecules, N-phenylcarbazole (PC), which shows no noticeable torsional activity in its vibrationally resolved electronic spectrum,<sup>8</sup> and 2-phenylindole (PI), which shows extensive torsional activity in its vibrationally resolved electronic spectrum.<sup>9</sup> Both molecules could be classified as donor-acceptor type systems, in which the phenyl groups act as donors and the carbazole or indole groups act as acceptors. But, if twisting is essential to the process, we hypothesize that only PI will exhibit significant CT on excitation by light. We test this hypothesis here by measuring the structures and permanent electric dipole moments of both species in their ground and electronically excited states, using high resolution laser techniques.

### 5.3 METHODS

Carbazole, PC and PI were purchased from Sigma Aldrich and used without further purification. Low resolution fluorescence excitation spectra (FES) of PI were recorded using a pulsed jet spectrometer. The sample was prepared by passing helium gas (2.8 kTorr) over the heated



nozzle ( $\sim 120^\circ\text{C}$ ) containing PI, and then expanding the seeded gas through a 1 mm pulsed valve (General Valve Series 9) operating at 10 Hz into a vacuum chamber ( $10^{-5}$  Torr). The expansion was intersected at right angles 2 cm downstream of the nozzle with a pulsed ultraviolet (UV) laser beam. Resonance fluorescence was detected with a photomultiplier tube (PMT), processed with a boxcar integrator (Stanford Research Systems), and recorded digitally with QUICK DATA ACQUISITION software (version 1.0.5). A frequency-doubled DCM laser (Quanta-Ray PDL-1) pumped by the second harmonic of a  $\text{Nd}^{3+}$ :YAG laser (Quanta-Ray DCR 1A), operating at 10 Hz, was used as the UV excitation source. This setup yields a linewidth of  $\sim 1\text{ cm}^{-1}$  and is described in greater detail elsewhere.<sup>10</sup>

Microwave spectra of PI were recorded using a chirped-pulse Fourier transform microwave (CP-FTMW) spectrometer. In this experiment, the sample was heated in a nozzle to  $120^\circ\text{C}$ , seeded into helium, and expanded through a 1 mm pulsed valve operating at 10 Hz into a perpendicularly aligned microwave cavity held under vacuum ( $\sim 10^{-5}$  Torr). The sample was excited and polarized using chirped microwave pulses having maximum frequency widths of  $\sim 500$  MHz. Then, the free induction decay of the sample was detected using an antenna and recorded with a digital oscilloscope (Tektronix DPO 7054). A detailed description of this experiment is given elsewhere.<sup>11,12</sup>

High resolution FES spectra were recorded using our laser-molecular beam spectrometer.<sup>13</sup> Argon carrier gas at  $\sim 1$  kTorr was seeded by passing it over the solid sample, heated to its melting point, and then expanded through a  $200\ \mu\text{m}$  quartz nozzle into a vacuum chamber. The expansion was skimmed 2 cm downstream of the nozzle, forming a molecular beam, and then intersected at right angles with the UV laser beam about 10 cm further downstream. When tuned to an absorption band of the probed molecule, fluorescence was

produced and collected with spherical mirrors placed above and below the point of intersection of the two beams, and then detected by a PMT. The signal was processed by a photon counting system and recorded digitally using jba95 acquisition software. The UV laser beam was produced by pumping a tunable ring dye laser (Spectra-Physics 380D) with the 514 nm output of a continuous wave Ar<sup>+</sup> laser, and frequency doubled using an external doubler (Spectra-Physics Wavetrain). While recording spectra, etalon frequency markers, with a free spectral range of 299.7520 ±0.0005 MHz, and iodine spectra were recorded simultaneously for linearization and frequency calibration. Spectra were simulated and fit using the JB95 fitting program, which utilizes rigid rotor Hamiltonians for the ground and electronically excited states to predict line spectra, and to fit the experimental spectra using a least-squares procedure. Further information about this program is given elsewhere.<sup>14</sup>

Stark spectra were produced in a similar fashion, except that the sample was additionally exposed to a homogenous electric field produced by applying a voltage between two wire mesh plates placed above and below the intersection point of the molecular and laser beams. The separation between the plates was calibrated using the known dipole moments of aniline.<sup>15,16</sup> Analyses of these spectra also utilized JB95, by adding terms to the rigid-rotor Hamiltonians that describe the effect of the applied field on the energies of the two states, and their dependence on both the magnitude and orientations of the permanent electric dipole moments (EDM's).

*Ab-initio* calculations were performed using the Gaussian 03 suite of programs.<sup>17</sup> Particularly the ground state structures, torsional coordinates, and EDM's were scanned using the M05-2X/6-31+(G)\* level of theory.

## 5.4 RESULTS

Figure 5-1 shows the vibrationally resolved fluorescence excitation spectrum (FES) of PI. As is evident, this spectrum exhibits extensive vibrational activity, suggesting that the molecule undergoes a large geometry change when it absorbs light. One mode dominates the observed Franck-Condon progression of at least ten vibronic bands; the  $\sim 64 \text{ cm}^{-1}$  spacing of these bands is nearly harmonic. The low frequency of this vibration suggests a large amplitude motion, denoted  $T$  in what follows. Other modes appear in combination with this mode, and appear to mix with it at higher energies.

More information about the nature of these modes was provided by high resolution experiments. Figure 5-2 shows the high resolution FES of band  $T_0^5$  at  $31\,664 \text{ cm}^{-1}$ . The spectrum spans  $\sim 2 \text{ cm}^{-1}$ , and exhibits  $a$ -type rotational selection rules. To fit this spectrum, a CP-FTMW spectrum of PI was first recorded, to determine the ground state inertial parameters. Then, these parameters were held constant, and the high resolution FES of PI was fit by varying the excited state parameters in a least-squares fashion, using JB95.<sup>14</sup> The spectrum was simulated using a Voigt profile with Gaussian and Lorentzian contributions of 30 and 40 MHz, respectively. The reported values of the ground and excited state parameters are listed in Table 5-I.

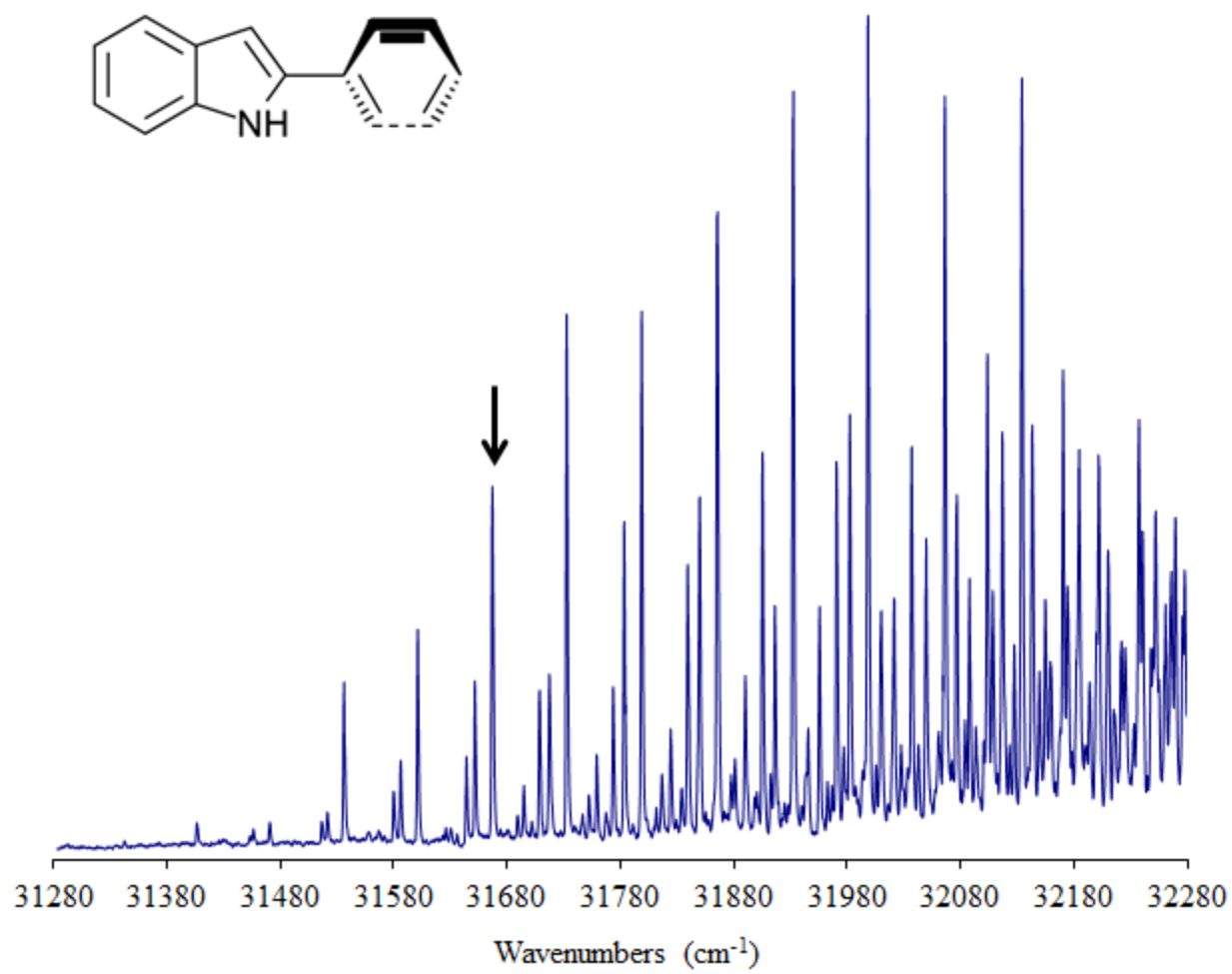


**Figure 5-1. Jet-cooled fluorescence excitation spectrum of 2-phenylindole (PI). An arrow denotes the band recorded at high resolution.**

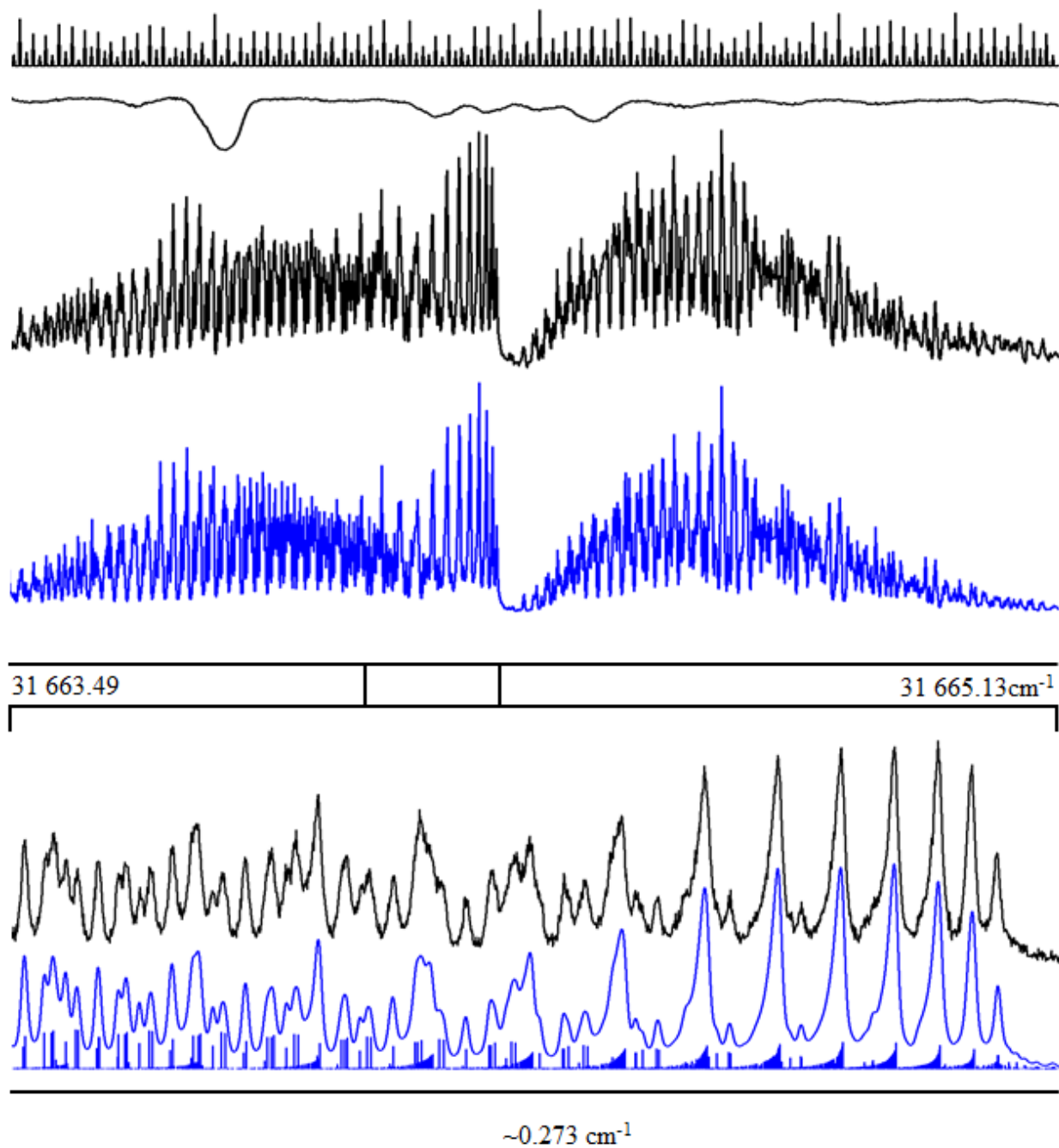


Figure 5-2. Rotationally resolved electronic spectrum of PI. The upper panel shows (from top to bottom) the frequency markers, the iodine spectrum, the experimental spectrum (black) and the simulated spectrum.

**Table 5-I. Inertial parameters of PI, carbazole and PC in their ground and excited electronic states.**

Parameter	PI	Carbazole <sup>a</sup>	PC
<b>S<sub>0</sub></b>			
A''(MHz)	2306.12(2)	2253.2(1)	539.8(2)
B''(MHz)	297.1728(2)	594.16(3)	351.76(2)
C''(MHz)	266.3035(2)	470.35(8)	224.084(9)
$\Delta I''$ (u·Å <sup>2</sup> )	-22.014(3)	-0.39(3)	-117.6(3)
<b>S<sub>1</sub></b>			
A'(MHz)	2269.29(7)	2250.8(1)	533.4(2)
B'(MHz)	297.949(5)	586.29(3)	356.07(3)
C'(MHz)	264.484(5)	465.26(3)	224.206(9)
$\Delta I'$ (u·Å <sup>2</sup> )	-8.17(4)	-0.29(3)	-112.8(3)
Origin (cm <sup>-1</sup> )	31 664.27	30 808.14	30 065.63
<i>a/b/c</i>	100/0/0	0/100/0	100/0/0
Assignments	96	106	159
OMC	4.68	3.96	3.02

<sup>a</sup> Ref. 18

Low resolution FES spectra of carbazole and N-phenylcarbazole have been previously recorded.<sup>22</sup> Neither shows any torsional vibrational activity. In this work, we also recorded high resolution spectra of the electronic origin bands of both molecules; these are shown in Figure 5-3. In agreement with earlier work, the  $S_1$ - $S_0$  origin of carbazole was found to exhibit *b*-type selection rules. This band was simulated using a Voigt profile having 30 MHz Gaussian and 5 MHz Lorentzian contributions, yielding the inertial parameters listed in Table 5-I. (These results are in agreement with previous measurements.<sup>18</sup>) The corresponding origin band of PC was found to show an intense Q-branch, clearly indicating *a*-type selection rules. Furthermore, the spectrum exhibits a high density of states, typical of systems this size, or other systems with relatively small rotational constants. The spectrum was simulated using a Voigt profile of 30 and 10 MHz Gaussian and Lorentzian contributions, respectively. The inertial parameters used to fit the spectrum are again listed in Table 5-I.

Each of the three high resolution spectra was recorded again in the presence of an electric field, see the bottom panels in Figure 5-3. The presence of the field causes different rovibrational transitions in the spectrum to shift and/or split, by an amount that depends on the magnitude of the field and the permanent electric dipole moments (EDM's) of the molecule in both electronic states. Detailed analyses of these effects have appeared elsewhere.<sup>16</sup> In the present instance, this behavior was fit by including in the Hamiltonians of the two states both first- and second-order Stark perturbation terms. However, a correlation was found between the ground and excited state EDM values of PC and PI, making it difficult to determine them independently from the experimental data. Since *ab initio* calculations have been shown to predict ground state EDMs reasonably well,<sup>19</sup> we chose to fit the spectra by varying the excited

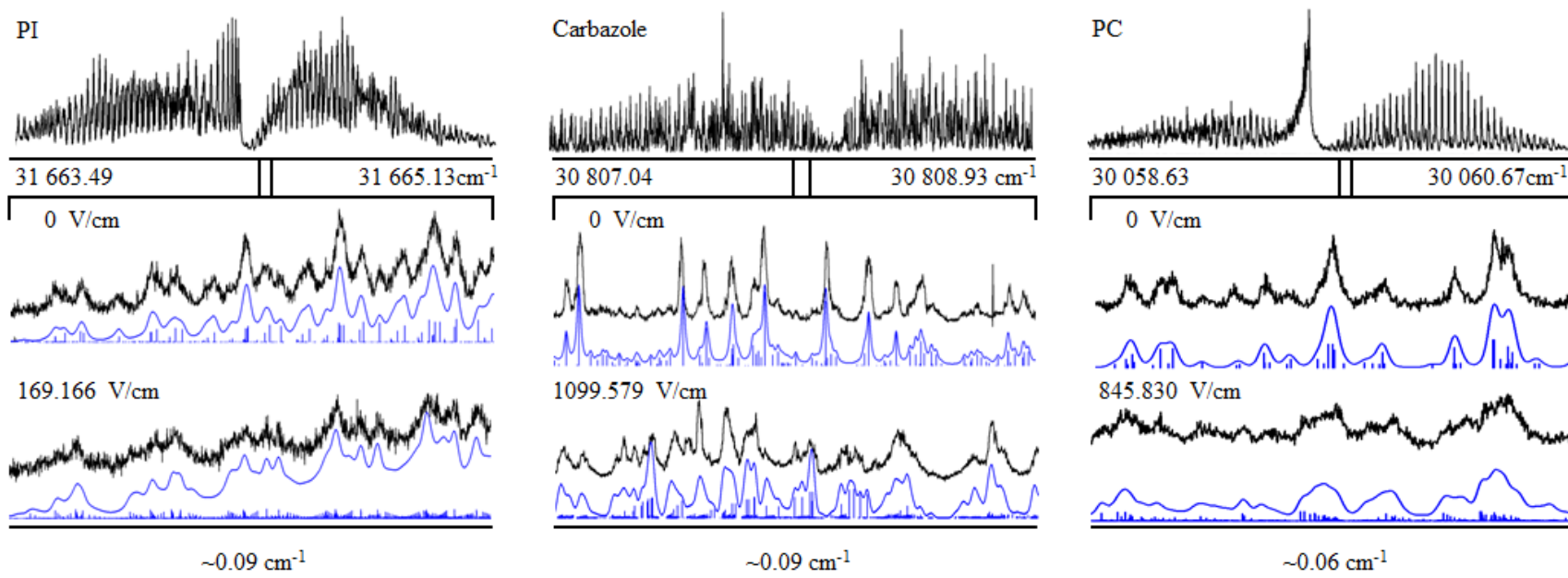


Figure 5-3. Stark effect on the rotationally resolved spectra of carbazole, PC and PI, from left to right, showing both the experimental (black) and simulated (blue) spectra. The bottom panels show expanded views of portions of the spectra, in the absence and presence of an applied electric field.



**Table 5-II. Permanent electric dipole moments of indole, PI, carbazole, and PC in their ground and electronically excited states.**

	Indole <sup>a</sup>	PI <sup>b</sup>	Carbazole	PC <sup>b</sup>
S <sub>0</sub>				
μ <sub>a</sub> (D)	1.376(8)	1.659	-	1.825
μ <sub>b</sub> (D)	1.40(1)	1.170	1.54(3)	-
μ <sub>c</sub> (D)	-	-	-	-
μ (D)	1.963(1)	2.030	1.54(3)	1.825
S <sub>1</sub>				
μ <sub>a</sub> (D)	1.556(8)	4.97(7)	-	3.47(1)
μ <sub>b</sub> (D)	1.01(1)	-0.7(6)	1.90(2)	-
μ <sub>c</sub> (D)	-	-	-	-
μ (D)	1.856(1)	5.0(1)	1.90(2)	3.47(1)

<sup>a</sup> Taken from Ref 20.

<sup>b</sup> Ground state EDM components were set to those calculated by M05-2x/6-31+G\*

state EDMs, keeping the ground state values constant, and equal to their theoretical values. The results of these fits are collected in Table 5-II.

## 5.5 DISCUSSION

### Structures of PI and PC in the $S_1$ state

The distinctive  $\sim 64 \text{ cm}^{-1}$  Franck-Condon progression observed in the vibrationally resolved FES of PI, Figure 5-1, is likely due to a torsional vibration. The small force constant and large reduced mass of this type of vibration would explain its low frequency. Further, the extensive progression along this coordinate clearly shows that there is a significant displacement along this coordinate in excited state PI, compared to the ground state.

Since the inertial defect is especially sensitive to out-of-plane distortions of the molecule, the angle between phenyl and indole planes can be determined from the experimental data, notwithstanding the possible contributions of vibrational averaging. Examining the data in Table 5-I, we see that the excited state inertial defect of PI is less negative,  $-8 \text{ u}\text{\AA}^2$ , than the corresponding parameter in the ground state,  $-22 \text{ u}\text{\AA}^2$ . This shows that excited state PI is significantly more planar than the ground state. To quantify the dependence of the inertial defect on torsional angle, a scan of the changes in rotational constants along this coordinate was calculated by optimizing the (ground-state) structure of 2PI at selected angles using M05-2X/6-31+(G)\*. Inertial defects were determined from these data, and plotted as a function of torsional angle, see Figure 5-4. Examination of this plot reveals that, within the approximations made,

ground state 2PI is found to have a torsional angle of  $24^\circ$ , and excited state 2PI is found to have a torsional angle of  $13^\circ$ , a reduction of more than  $10^\circ$ .

Previously, it was shown by Phillips<sup>22</sup> that the jet-cooled vibrational spectrum of PC closely resembles that of carbazole, and unlike PI, does not possess a clear torsional progression. The ground state inertial defect of PC is large,  $-118 \text{ u}\text{\AA}^2$ , suggesting that there is significant out-of-plane character. The excited state inertial defect is only slightly smaller in magnitude,  $-113 \text{ u}\text{\AA}^2$ , suggesting that the excited state is only slightly more planar. Using the method described above, the torsional angles between the two planes of PC were determined to be  $56^\circ$  and  $54^\circ$  in the ground and excited electronic states, respectively.

Another result of the phenyl addition to carbazole is that the inertial axis of PC rotate relative to the carbazole frame, see Scheme 5-1. However, since the  $S_1$ - $S_0$  electronic transition moment (ETM) of carbazole is aligned along the  $b$ -axis, and along the  $a$ -axis in PC, then relative to carbazole frame, the two ETM orientations are identical. Similarly, the  $S_1$ - $S_0$  ETM in PI is aligned along the phenyl-indole bond, just as the corresponding ETM in PC is aligned along the phenyl-carbazole bond.

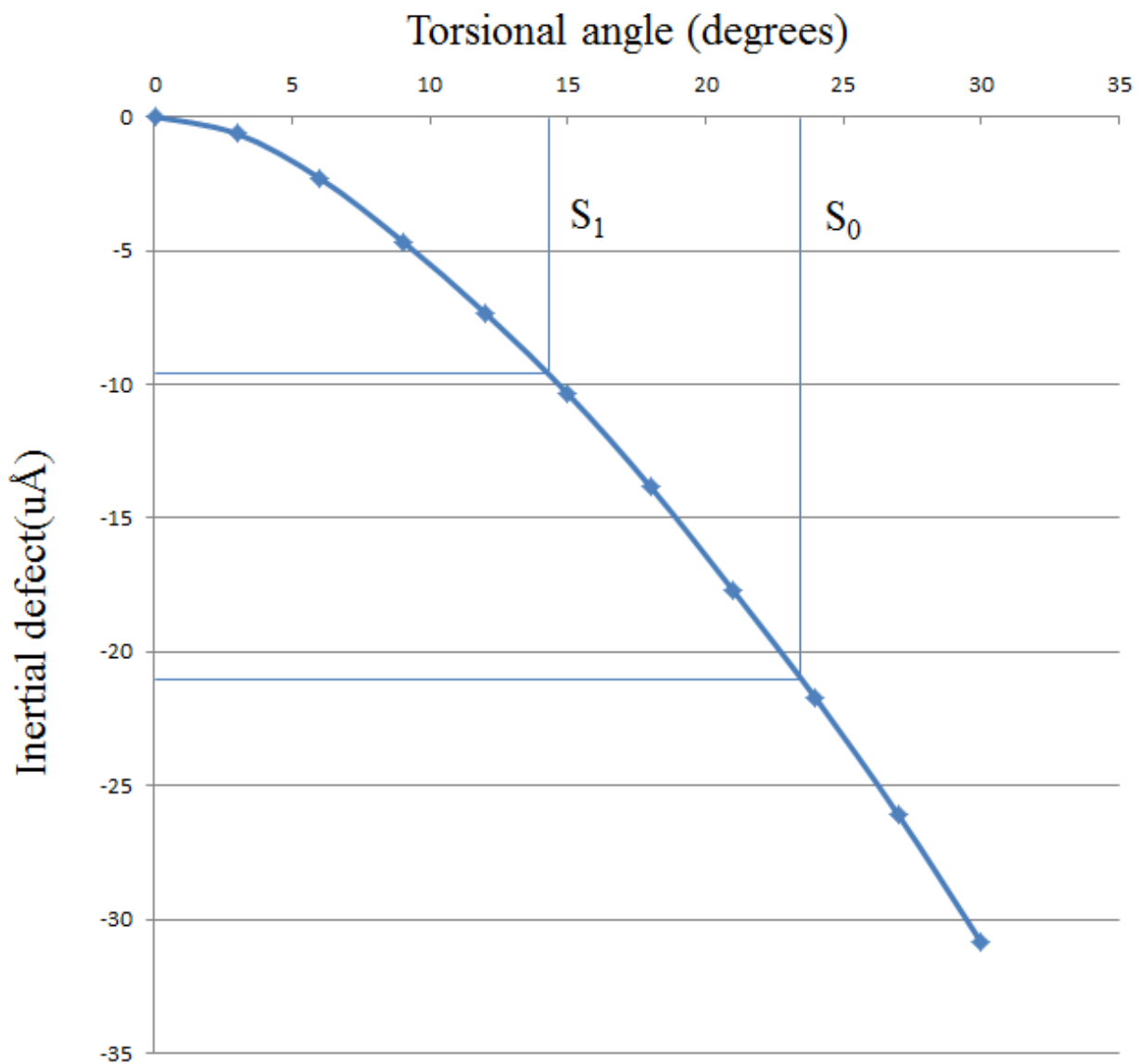
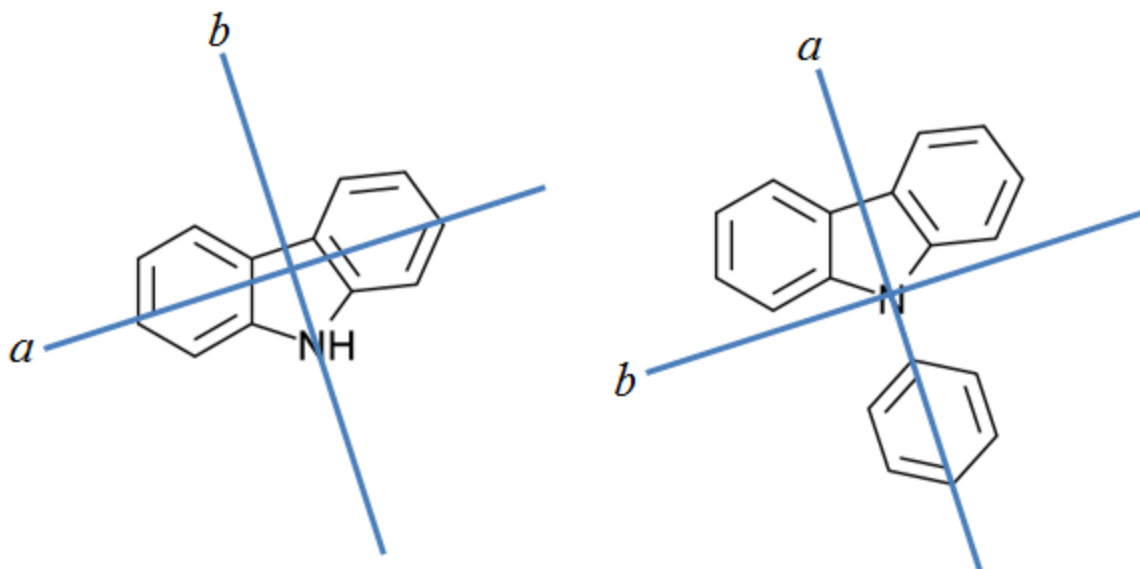


Figure 5-4. A plot showing the inertial defect of PI as a function of the torsional angle.. Data points were calculated using M05-2X/6-31+G\*. Tie lines indicated likely values of the vibrationally averaged value of the torsional angle in the S<sub>0</sub> and S<sub>1</sub> electronic states.



Scheme 5-1

The spectroscopic results discussed here show a clear contrast between PI and PC. Specifically, PI exhibits an extensive torsional progression in its  $S_1$ - $S_0$  spectrum, whereas PC does not. Our analyses of these results shows that both PI and PC are twisted molecules in their electronic ground states, but that only PI exhibits a large change in its vibrationally averaged torsional angle when it is excited by light. Excited state PI is significantly more planar in its  $S_1$  state. Since decreasing the angle between the parent and attached phenyl group likely increases the overlap of each moiety's  $\pi$  molecular orbitals, it may be expected that PI will demonstrate the effects of conjugation more so than PC.

### Effects of ring substitution

While phenyl groups are not particularly polar, their conjugation with the molecule to which they are attached can have a major impact on its electronic properties. Generally, the larger a conjugated system becomes, the smaller the spacings between its allowed energy states. The results described here provide a nice example of this effect. The  $S_1$  electronic origins of both

indole and carbazole are both shifted to the red by phenyl substitution, but the shift in PI (3567  $\text{cm}^{-1}$ ) is much larger than that in PC (742  $\text{cm}^{-1}$ ), a clear consequence of the more planar nature of PI in its  $S_1$  state.

Phenyl substitution has a clear effect on the EDMs as well. Particularly, the excited state EDM of the phenyl substituted compounds are larger than the non-substituted compounds, whereas their ground state EDMs are relatively similar (see Table 5-II). A likely explanation of this effect is that photo-excitation of both molecules leads to charge transfer from the phenyl rings to the parent molecules. Assuming that the change in EDM along the bond joining the two rings upon excitation ( $\Delta\mu$ ) is due to charge transfer, the amount of electron transfer from one molecule to the other can be quantified using Eq. (5-1):

$$q(e^-) = \frac{\Delta\mu(D) * 0.2082}{d(\text{\AA})} \quad \text{Equation 5-1}$$

In PC, the distance (d) between the centers of mass of the phenyl ring and carbazole is 4.5  $\text{\AA}$ ,  $\Delta\mu$  is 1.65 D and thus we calculate from Eq. (1) that 0.076  $e^-$  has been transferred from the phenyl ring to the carbazole ring. In PI, the distance between the rings is 5.3  $\text{\AA}$ ,  $\Delta\mu$  along the a axis is 3.3 D, and the amount of charge transfer is 0.13  $e^-$ . Thus, this analysis indicates that almost twice as much charge is transferred in PI relative to PC. This confirms the hypothesis that CT and ring twisting are intimately linked.

PI seems to behave remarkably similar to 1-phenylpyrrole.<sup>21</sup> Both molecules exhibit a clear Franck-Condon progressions in their jet-cooled fluorescence excitation spectra. Furthermore, both systems seem to exhibit similar charge transfers between ring systems upon excitation, 0.15  $e^-$  in 1-phenylpyrrole.<sup>21</sup> And the change in the torsional angles in the two systems are similar.

## 5.6 ACKNOWLEDGEMENTS

This work has been supported by NSF (CHE-0911117), to whom we are grateful.

## 5.7 WORKS CITED

1. S. Creager, C. J. Yu, C. Bamdad, S. O'Connor, T. MacLean, E. Lam, Y. Chong, G. T. Olsen, J. Luo, M. Gozin, and J. F. Kayyem, *J. Am. Chem. Soc.* **121**, 1059 (1999).
2. S. Boussaad and N. J. Tao, *Nano Lett.* **3**, 1173 (2003).
3. J. Lahiri, Y. Lin, P. Bozkurt, I. I. Oleynik, and M. Batzill, *Nat. Nano.* **5**, 326 (2010).
4. K. Rotkiewicz, K. H. Grellmann, and Z. R. Grabowski, *Chem. Phys. Lett.* **19**, 315 (1973).
5. A. E. Nikolaev, G. Myszkiewicz, G. Berden, W. L. Meerts, J. F. Pfanstiel, and D. W. Pratt, *J. Chem. Phys.* **122**, 084309 (2005).
6. T. Yoshihara, S. I. Druzhinin, and K. A. Zachariasse, *J. Am. Chem. Soc.* **126**, 8535 (2004).
7. I. Fdez. Galván, M. E. Martín, A. Muñoz-Losa, M. L. Sánchez, and M. A. Aguilar, *J. Chem. Theory Comput.* **7**, 1850 (2011).
8. P. David, *J. Photochem. Photobio. A* **105**, 307 (1997).
9. W. E. Sinclair, H. P. Yu, D. Phillips, and J. M. Hollas, *J. Chem. Phys.* **106**, 5797 (1997).
10. S. J. Humphrey and D. W. Pratt, *J. Chem. Phys.* **99**, 5078 (1993).
11. G. G. Brown, B. C. Dian, K. O. Douglass, S. M. Geyer, S. T. Shipman, and B. H. Pate, *Rev. Sci. Instrum.* **79**, 053103 (2008).
12. R. G. Bird, J. L. Neill, V. J. Alstadt, J. W. Young, B. H. Pate, and D. W. Pratt, *J. Phys. Chem. A.* **115**, 9392 (2011).
13. W. A. Majewski, J. F. Pfanstiel, D. F. Plusquellic, and D. W. Pratt, in *Laser Techniques in Chemistry*, A. B. Myers and T. R. Rizzo, Eds. (Wiley, New York, 1995), 101.



14. D. F. Plusquellic, R. D. Suenram, B. Mate, J. O. Jensen, and A. C. Samuels, *J. Chem. Phys.* **115**, 3057 (2001).
15. D. G. Lister, J. K. Tyler, J. H. Høq, and N. W. Larsen, *J. Mol. Struct.* **23**, 253 (1974).
16. T. M. Korter, D. R. Borst, C. J. Butler, and D. W. Pratt, *J. Am. Chem. Soc.* **123**, 96 (2001); D.M. Mitchell, P.J. Morgan, and D. W. Pratt, *J. Phys. Chem. A.* **112**, 12597 (2008).
17. M. J. Frisch, G. W. Trucks, H. B. Schlegel, *et al.* GAUSSIAN 03, Revision E.01, Gaussian, Inc., Wallingford, CT, 2004.
18. J. T. Yi, L. Alvarez-Valtierra, and D. W. Pratt, *J. Chem. Phys.* **124**, 244302 (2006).
19. J. W. Young, A. J. Fleisher, and D. W. Pratt, *J. Chem. Phys.* **134**, 084310 (2011).
20. C.-H. Kang, T. M. Korter, and D. W. Pratt, *J. Chem. Phys.* **122**, 174301 (2005).
21. J. A. Thomas, J. W. Young, A. J. Fleisher, L. Alvarez-Valtierra, and D. W. Pratt, *J. Phys. Chem. Lett.* **1**, 2017 (2010).
22. D. Phillips, *J. Photochem. Photobiol. A.* **105**, 307 (1997).

## 6.0 SUMMARY

High resolution spectra of several systems were presented, and analysis of these results revealed aspects of several intriguing photoinduced phenomena. Measurement of the excited state dipole moment (EDM) suggests that the excited state is a convolution of the enol and keto forms of the molecule, and the proton lies between these two structures. Solvent-induced charge redistribution was observed in the excited state of 7-azaindole( $\text{H}_2\text{O}$ ). In this complex, the excited state EDM was roughly seven times larger than the ground state EDM. This behavior was attributed to the presence of the water molecule, which promotes electron transfer from the acidic to the basic nitrogen when the molecule is excited by light. The effect of electronic state mixing on the electronic distribution was observed in an electronically mixed band of 7-azaindole, which possessed an EDM roughly twice as large as that of the electronic origin band. Finally, the effects of ring planarity were investigated in 2-phenylindole and N-phenylcarbazole; the results demonstrated that conjugation and electron transfer is more present in the 2-phenylindole, which is more planar than N-phenylcarbazole.

Although the events mentioned above undoubtedly affect the molecular structure and vibrations, the geometry changes from these events are small. Measuring vibrations and/or inertial parameters does not provide a complete description of the events occurring in an excited state. Demonstrated here is that coupling the high resolution spectroscopic technique with the Stark-effect allows for a more thorough characterization of the molecular system's charge

distribution prior to and after photo-excitation. Because the electronic distribution is related to a molecule's reactivity and dependent on both nuclear and electronic structure, it is remarkably useful to describe changes that occur in a molecular system upon photo-excitation. Many of the results observed and discussed here would largely have been undetected or underappreciated if not for implementing Stark-effect measurements.

## **APPENDIX A**

### **ENERGY LEVELS AND WAVEFUNCTIONS FROM INTERNAL ROTATION**

The method for solving energy levels for internal rotation has been documented by Flygare.<sup>1</sup> This appendix demonstrates how to implement this method in an easy-to-use Mathcad spreadsheet. The Hamiltonian being solved is shown in Equations 3-1 and 3-2. The derivation for the matrix elements are given in Ref 1. The spreadsheet is shown below as entered into Mathcad.<sup>2</sup> It is divided into four main sections, input, setting up the Hamiltonian matrix, solving the wavefunction coefficients, and graphing the results.

## Energy levels for internal rotation

### input

a := (19.72)      f := 50

Enter into the variable 'a' the internal rotor constant  
( called F in equation 3-1)

The variable f is half the size of the basis

v6 := -71.921      v3 := 2965

These set of variables represent the V terms in  
equation 3-1

v2 := -5313      v5 := 410.339

v1 := 7592      v4 := -1341

### Matrix set up

This portion of the program begins to make arrays to build the matrix

j := 0..f      i := 0..f

x<sub>j</sub> := j      y<sub>i</sub> := -i

p := 0..(2f)

r := 0..(2f)

$$s1_p := \begin{cases} \frac{p}{2} & \text{if } \text{mod}(p,2) = 0 \\ p - \frac{p-1}{2} & \text{if } \text{mod}(p,2) \neq 0 \end{cases} \quad s2_r := \begin{cases} \frac{r}{2} & \text{if } \text{mod}(r,2) = 0 \\ r - \frac{r-1}{2} & \text{if } \text{mod}(r,2) \neq 0 \end{cases}$$

$$m1_p := \begin{cases} y_{s1_p} & \text{if } \text{mod}(p,2) = 0 \\ x_{s1_p} & \text{otherwise} \end{cases} \quad m2_r := \begin{cases} y_{s2_r} & \text{if } \text{mod}(r,2) = 0 \\ x_{s2_r} & \text{otherwise} \end{cases}$$

m1 and m2 create a  
0, -1, 1, -2, pattern to  
represent the positive and  
negative quantum levels

$$H_{op,r} := (m1_p)^2 \cdot a \cdot \delta(m2_r, m1_p)$$

$$H_{pp,r} := \frac{v1}{2} \cdot \delta(m2_r, m1_p) - \frac{v1}{4} \cdot \delta(m1_p, m2_r - 1) - \frac{v1}{4} \cdot \delta(m1_p, m2_r + 1) + \frac{v2}{2} \cdot \delta(m2_r, m1_p) - \frac{v2}{4} \cdot \delta(m1_p, m2_r + 2) - \frac{v2}{4} \cdot \delta(m1_p, m2_r - 2) +$$

$$\frac{v3}{2} \cdot \delta(m2_r, m1_p) - \frac{v3}{4} \cdot \delta(m1_p, m2_r + 3) - \frac{v3}{4} \cdot \delta(m1_p, m2_r - 3) + \frac{v6}{2} \cdot \delta(m2_r, m1_p) - \frac{v6}{4} \cdot \delta(m1_p, m2_r - 6) - \frac{v6}{4} \cdot \delta(m1_p, m2_r + 6) +$$

$$\frac{v4}{2} \cdot \delta(m1_p, m2_r) - \frac{v4}{4} \cdot \delta(m1_p, m2_r - 4) - \frac{v4}{4} \cdot \delta(m1_p, m2_r + 4) + \frac{v5}{2} \cdot \delta(m1_p, m2_r) - \frac{v5}{4} \cdot \delta(m1_p, m2_r - 5) - \frac{v5}{4} \cdot \delta(m1_p, m2_r + 5)$$

$$M_{p,r} := H_{op,r} + H_{pp,r}$$

Ho and Hp are matrices representing the kinetic and potential energy matrix elements. M is the sum of these two matrices

$$\text{Lines} := \text{eigenvals}(M)$$

Using a solve eigenvalues function, built into mathcad, the energy levels are found. Using a sort function they are arranged lowest to highest in Lines 2

$$\text{Lines2} := \text{sort}(\text{Lines})$$

Lines2 =

	0
0	-5.374
1	36.26
2	122.921
3	213.944
4	322.78
5	446.732
6	587.943
7	745.145
8	917.308
9	1.103·10 <sup>3</sup>
10	1.303·10 <sup>3</sup>
11	1.515·10 <sup>3</sup>
12	1.739·10 <sup>3</sup>
13	1.975·10 <sup>3</sup>
14	2.222·10 <sup>3</sup>
15	...

Using the Ritz method to solve for the coefficients of a particular energy level

Enter the energy level you are interested in

energylevel := 0

boom<sub>p,r</sub> := M<sub>p,r</sub> - Lines<sub>2energylevel-δ</sub>(m<sub>1p</sub>, m<sub>2r</sub>)

boom2 := boom<sup>T</sup>

hat := 0..2f coeff<sub>hat</sub> := .1

Given

$$\text{boom2} \cdot \text{coeff} = 0 \quad \sum_{x=0}^{2f} (\text{coeff}_x)^2 = 1$$

number := Find(coeff)



Mathcad solves this system of equations to determine the coefficients of the wavefunction For the designated energy level

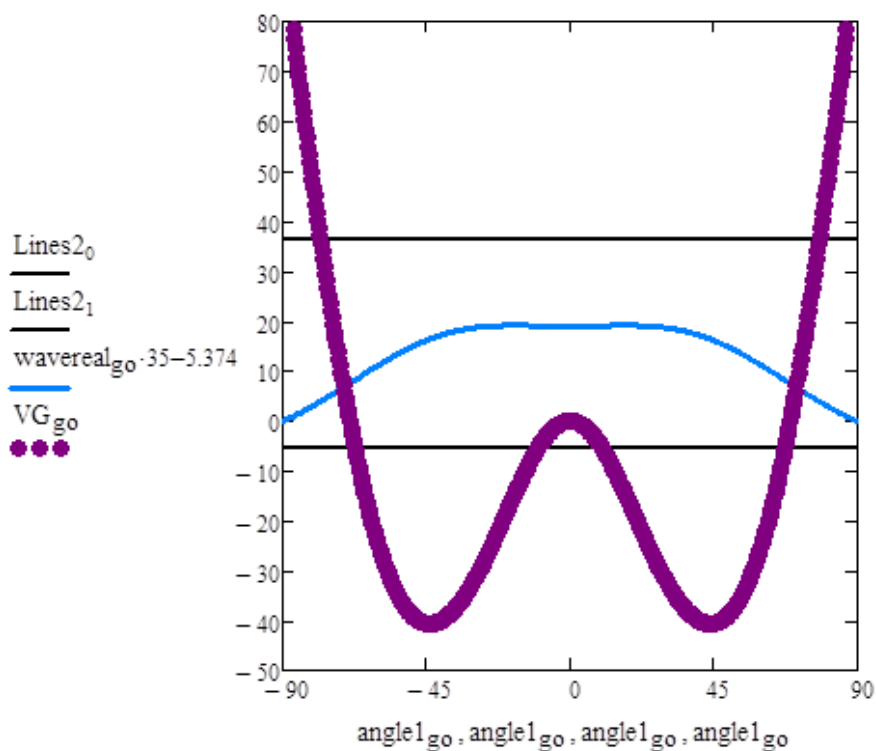
**Graphing the data**

$$go := 0..560 \quad ang_{go} := -1.7 + \frac{go}{560} \cdot 3.4 \quad angle1_{go} := \frac{ang_{go}}{2\pi} \cdot 360$$

$$waverf_{go} := \left[ \sum_{x=0}^{2f} \left( number_x \cdot \frac{1}{\sqrt{2\pi}} \cdot e^{im1_x \cdot ang_{go}} \right) \right]$$

$$wavereal := (Re(waverf))$$

$$VG_{go} := \frac{v1}{2} \cdot (1 - \cos(1 \cdot ang_{go})) + \frac{v3}{2} \cdot (1 - \cos(3 \cdot ang_{go})) + \frac{v6}{2} \cdot [1 - \cos((6 \cdot ang_{go}))] + \frac{v2}{2} \cdot (1 - \cos(ang_{go}^2)) + \frac{v4}{2} \cdot (1 - \cos(4 \cdot ang_{go})) + \frac{v5}{2} \cdot (1 - \cos(ang_{go}^3))$$



**Works Cited**

1. W. H. Flygare, *Molecular Structure and Dynamics*. (Prentice-Hall, Englewood Cliffs, N.J., 1978).
2. Mathcad 15.0, *Parametric Technology Corporation* (2010).



## APPENDIX B

### PERMANENT ELECTRIC DIPOLE MOMENTS OF 7-AZAINDOLE

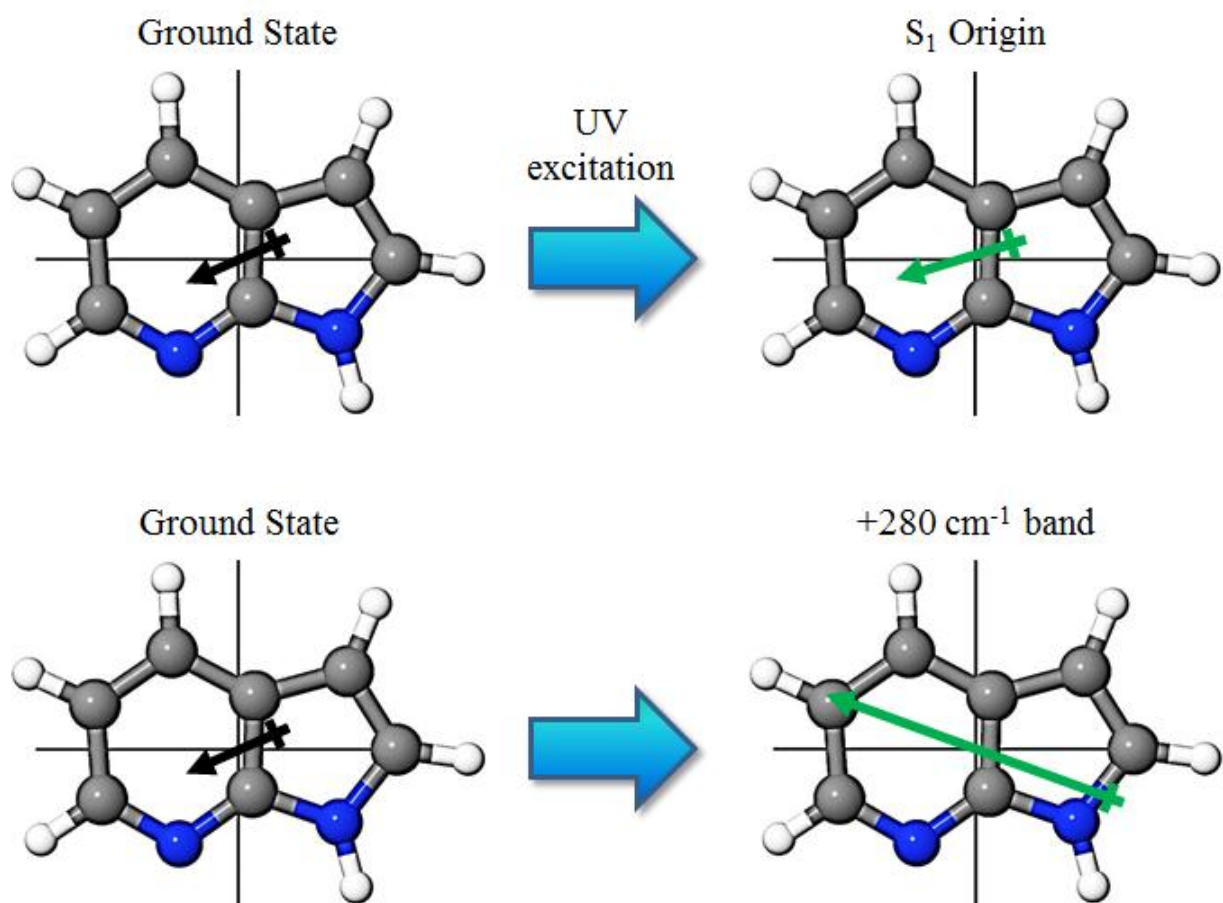


Figure 6-1. Permanent electric dipole moments of 7-azaindole in the ground state, S<sub>1</sub> origin and the +280 cm<sup>-1</sup> vibronic band. The ground state and S<sub>1</sub> dipole moment were taken from Ref 1.

## Works Cited

1. C. Kang, J. T. Yi, and D. W. Pratt, Chem. Phys. Lett. **423**, 7 (2006).

## APPENDIX C

### LIST OF JUSTIN W. YOUNG'S PUBLICATIONS

STARK-EFFECT STUDIES OF 1-PHENYLPYRROLE IN THE GAS PHASE. DIPOLE REVERSAL UPON ELECTRONIC EXCITATION.

J.A. Thomas, J. W. Young, A. J. Fleisher, L. Alvarez-Valtierra, and D. W. Pratt, *J. Phys. Chem. Lett.* **1**, 2017 (2010).

HIGH RESOLUTION ELECTRONIC SPECTROSCOPY OF 9-FLUORENEMETHANOL IN THE GAS PHASE: NEW INSIGHTS INTO THE PROPERTIES OF  $\pi$ -HYDROGEN BONDS.

D. M. Miller, J. W. Young, P. J. Morgan, and D. W. Pratt, *J. Chem. Phys.* **133**, 124312 (2010).

ROTATIONALLY RESOLVED S(1)-S(0) ELECTRONIC SPECTRA OF 2,6-DIAMINOPYRIDINE: A FOUR-FOLD BARRIER PROBLEM.

C. L. Clements, J. W. Young, and D. W. Pratt, *J. Phys. Chem. A.* **114**, 12005 (2010).

GROUND STATE 14(N) QUADRUPOLE COUPLINGS IN THE MICROWAVE SPECTRA OF N,N'-DIMETHYLANILINE AND 4,4'-DIMETHYLAMINOBENZOTRILE.

R. G. Bird, J. L. Neil, V. J. Alstadt, J. W. Young, B. H. Pate, and D. W. Pratt, *J. Phys. Chem. A*. **115**, 9392 (2011).

EXPLORING SINGLE AND DOUBLE PROTON TRANSFER PROCESS IN THE GAS PHASE: A HIGH RESOLUTION ELECTRONIC SPECTROSCOPY STUDY OF 5-FLUOROSALICYLIC ACID.

J. W. Young, A. J. Fleisher, and D. W. Pratt, *Chem. Phys. Lett.* **134**, 084310 (2011).

FLICKERING DIPOLES IN THE GAS PHASE: STRUCTURES, INTERNAL DYNAMICS AND DIPOLE MOMENTS OF  $\beta$ -NAPHTHOL-H<sub>2</sub>O IN ITS GROUND AND EXCITED ELECTRONIC STATES.

A. J. Fleisher, J. W. Young, D. W. Pratt, A. Cembran, and J. Gao. *J. Chem. Phys.* **134**, 114304 (2011).

HIGH RESOLUTION FLUORESCENCE EXCITATION SPECTRA OF BOTH ENANTIOMERS OF NAPROXEN IN THE GAS PHASE: ARE THEY EQUIVALENT OR NOT?

L. Alvarez-Valtierra, J. W. Young, and D. W. Pratt. *Chem. Phys. Lett.* **509**, 96 (2011).

EXCITED STATE ELECTRON TRANSFER PRECEDES PROTON TRANSFER  
FOLLOWING IRRADIATION OF THE HYDROGEN-BONDED SINGLE WATER  
COMPLEX OF 7-AZAINDOLE WITH UV LIGHT.

J. W Young, and D. W. Pratt, *J. Chem Phys.* **135**, 084301 (2011).

INTERNAL AND EXTERNAL PERTURBATIONS IN ELECTRONIC SPECTROSCOPY.  
THE STARK SPECTRUM OF INDOLE-NH<sub>3</sub>.

A. J. Fleisher, J. W. Young, and D. W. Pratt, *Phys. Chem. Chem. Phys.* submitted (2011).